Imaging spectroscopy: Earth and planetary remote sensing with the USGS Tetracorder and expert systems

Roger N. Clark, Gregg A. Swayze, K. Eric Livo, Raymond F. Kokaly, Steve J. Sutley, J. Brad Dalton, Robert R. McDougal, and Carol A. Gent
U.S. Geological Survey, Denver, Colorado, USA

Received 17 January 2002; revised 9 August 2002; accepted 3 October 2002; published 6 December 2003.

[1] Imaging spectroscopy is a tool that can be used to spectrally identify and spatially map materials based on their specific chemical bonds. Spectroscopic analysis requires significantly more sophistication than has been employed in conventional broadband remote sensing analysis. We describe a new system that is effective at material identification and mapping: a set of algorithms within an expert system decision-making framework that we call Tetracorder. The expertise in the system has been derived from scientific knowledge of spectral identification. The expert system rules are implemented in a decision tree where multiple algorithms are applied to spectral analysis, additional expert rules and algorithms can be applied based on initial results, and more decisions are made until spectral analysis is complete. Because certain spectral features are indicative of specific chemical bonds in materials, the system can accurately identify and map those materials. In this paper we describe the framework of the decision making process used for spectral identification, describe specific spectral feature analysis algorithms, and give examples of what analyses and types of maps are possible with imaging spectroscopy data. We also present the expert system rules that describe which diagnostic spectral features are used in the decision making process for a set of spectra of minerals and other common materials. We demonstrate the applications of Tetracorder to identify and map surface minerals, to detect sources of acid rock drainage, and to map vegetation species, ice, melting snow, water, and water pollution, all with one set of expert system rules. Mineral mapping can aid in geologic mapping and fault detection and can provide a better understanding of weathering, mineralization, hydrothermal alteration, and other geologic processes. Environmental site assessment, such as mapping source areas of acid mine drainage, has resulted in the acceleration of site cleanup, saving millions of dollars and years in cleanup time. Imaging spectroscopy data and Tetracorder analysis can be used to study both terrestrial and planetary science problems. Imaging spectroscopy can be used to probe planetary systems, including their atmospheres, oceans, and land surfaces.

INDEX TERMS: 5464 Planetology: Solid Surface Planets: Remote sensing; 5470 Planetology: Solid Surface Planets: Surface materials and properties; 5410 Planetology: Solid Surface Planets: Composition; 5405 Planetology: Solid Surface Planets: Atmospheres—composition and chemistry; 5494 Planetology: Solid Surface Planets: Instruments and techniques; *KEYWORDS:* imaging spectroscopy, reflectance spectroscopy, planetary mapping, expert system, Tetracorder, mineral map

Citation: Clark, R. N., G. A. Swayze, K. E. Livo, R. F. Kokaly, S. J. Sutley, J. B. Dalton, R. R. McDougal, and C. A. Gent, Imaging spectroscopy: Earth and planetary remote sensing with the USGS Tetracorder and expert systems, *J. Geophys. Res.*, *108*(E12), 5131, doi:10.1029/2002JE001847, 2003.

1. Introduction

[2] Spectroscopy is a tool that has been used for decades to identify, understand, and quantify solid, liquid, or gaseous materials, especially in the laboratory. In disciplines ranging from astronomy to chemistry, spectroscopic measurements are used to detect absorption features due to specific chemical bonds, and detailed analyses are used to determine the abundance and physical state of the detected absorbing species. Spectroscopic measurements have a long history in the study of the Earth and planets [e.g., *Hunt*, 1977; *Clark et al.*, 1990a; *Pieters and Englert*, 1993; *Clark*, 1999]. Up to the 1990s, remote spectroscopic measurements of Earth and planets have been dominated by multispectral imaging experiments that collect high quality images in a few, usually broad, spectral bands. However, a new generation of sensors is now available that combines imaging with spectroscopy to create the new discipline of imaging spectroscopy [e.g., see *Goetz et al.*, 1985; *Rencz*, 1999 and

references therein]. (Imaging spectroscopy has many names in the remote sensing community, including imaging spectrometry, hyperspectral, and ultraspectral imaging. *Ball* [1995] argues that spectrometry be limited to measurement not including photons, as in mass spectrometry, leading *Clark* [1999] to argue for ''imaging spectroscopy'' as the appropriate term.) Imaging spectrometers acquire data with enough spectral range, resolution, and sampling at every pixel in a raster image so that individual absorption features can be identified and spatially mapped [*Goetz et al.*, 1985].

[3] Some traditional approaches to remote sensing analysis born in the era of multispectral imaging are based on statistical methods exploiting the large number of samples (pixels) in the remotely sensed data. The demonstrated power of these approaches is vastly multiplied by the large increase in information content inherent when the number of spectral bands increases from the order of 10 to the order of 100. Such scene statistical results are by their nature scene-dependent, cannot be applied globally, and the statistical approaches do not exploit the information inherent in each individual spectrum concerning the chemical and nature of the remotely sensed surface. Analysis tools from another discipline, signal processing, have had good success at detection of specific spectral signatures across data sets using vector filter approaches. However, this approach requires that the signature be stable from lab to field. Most geologic and many biologic materials do not meet this criterion.

[4] Our team emerged from a spectroscopic discipline, which focuses on the information inherent in each spectrum. Over the past decade we have developed a software system that takes an explicitly spectroscopic approach to ''hyperspectral'' analysis. That is, the objective driving our system is to determine the chemical, mineralogical, or biological nature of each spectrum as an individual, independent of the rest of the hundreds to millions of companion spectra in the data set. The analysis must also be done with such efficiency that this automated analysis can be performed on very large data sets in short periods of time. A central task we have focused on is robust detection of geologic and biologic materials from visible and near-infrared (IR) spectroscopic measurements. Our software system includes many other capabilities and is being continually expanded, but our material identification concept is our unique contribution and is the subject of this paper.

[5] The spectral analysis system described here is called Tetracorder, paying homage to the ''Tricorder''© remote analyzer of the Paramount Pictures Star Trek series. This paper will describe the Tetracorder material detection concept and we will throughout use the term ''Tetracorder'' synonymously with the detection system. However, it should be understood that the Tetracorder software system encompasses more than spectral detection: Tetracorder is a generalized application system where multiple algorithms and analyses can be commanded through an expert system rule set and decisions about the analyses performed to steer analyses in certain directions. All these capabilities are beyond the scope of this paper; therefore we will focus on material identification and mapping.

[6] This paper will describe the concepts behind our Tetracorder material detection scheme with illustrative examples, then delve into aspects of the implementation of Tetracorder. We will then discuss verification of Tetracorder performance, which is accomplished with a combination of human verification of Tetracorder spectral analyses, field checking Tetracorder maps in situ, and through laboratory analysis of collected samples. We will present examples of Tetracorder analyses of terrestrial data sets, and close with implications for planetary science.

[7] Tetracorder: a software program containing multiple algorithms which can be commanded as an expert system. This paper describes the software and expert system rule set for Tetracorder version 3.5. When we refer to ''Tetracorder'' in the text, we mean the Tetracorder software and the expert system driving the analysis.

[8] Expert System: In this paper, for spectroscopic analysis and identification of materials, an expert system is a set of rules used to instruct algorithms to analyze spectral data to attain a certain result, such as the identification of minerals in a spectrum, including the influences of mixtures. The expert system rules presented here are the collective result of a team of spectroscopists, physicists, geologists, and botanists who analyzed spectra and imaging spectroscopy data sets at multiple sites and geologic environments for over a decade.

2. Tetracorder Materials Detection Concept

2.1. Overview

[9] At its highest level, Tetracorder identifies materials by comparing a remotely sensed observed spectrum (the unknown) to a large library of spectra of well-characterized materials, but we do so using several innovations to maximize accuracy and performance. The first of our innovations is that in the comparison of a specific reference to the unknown, only the portions of the spectrum that are known to be diagnostic of the reference material are used. Every spectral feature is due to an interaction of photons of particular energies with the atoms and electrons within the chemical under study, and the nature of the absorption is largely unique to the specific chemical structure. At other wavelengths, photon interactions do not give rise to absorption; mostly transmission or scattering occurs. Taken together, the presence of spectrally ''active'' and ''inactive'' spectral regions for a material gives rise to the central concept of a ''diagnostic absorption feature.'' Diagnostic absorption features are unique to particular materials in shape (variation in intensity with wavelength over a narrow interval) and usually are concentrated in limited ranges of wavelength by type of absorption. Between diagnostic features are portions of the spectrum which contain little information specific to the material of interest. The focus on diagnostic features in analysis of natural scenes is critical because mixtures which obey nonlinear systematics (e.g., coatings, intimate mixtures, solutions) are common in the natural environment and frustrate simple matching of spectra.

[10] In Tetracorder, each comparison of an unknown to a reference spectrum is highly tailored to the chemistry of the reference material by focusing on diagnostic spectral features (Figures 1a and 1b). The tailoring is based on specific expert knowledge of our team of spectroscopists, geologists, and biologists. By neglecting portions of the spectrum that are irrelevant to the chemistry of the reference material, we reduce noise or clutter induced by these ''inactive'' wave-

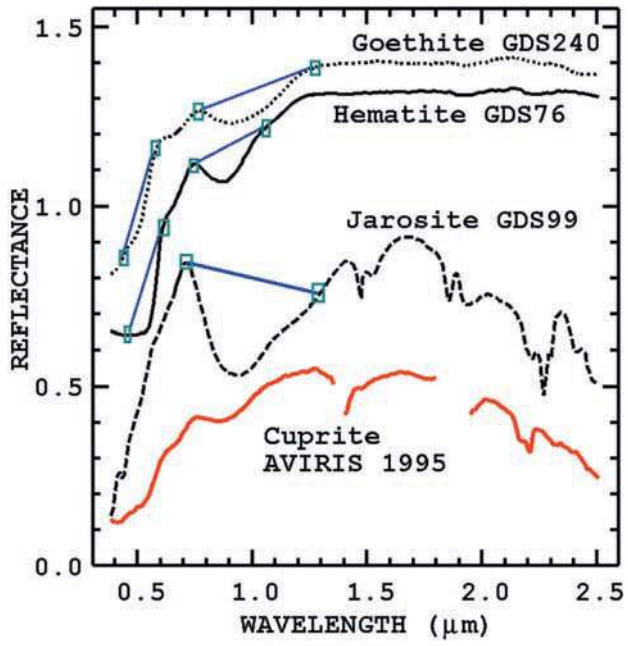

Figure 1a. Continuum removal process employed by the Tetracorder spectral feature shape matching algorithm. Three reference spectra are shown: goethite, jarosite, and hematite. Each spectral feature has its own continuum endpoints (illustrated by the boxes). The continuum is removed from both the observed and reference spectra. For example, the hematite 0.9-μm feature continuum is removed from the Cuprite unknown spectrum, then the goethite continuum is removed, and so on. This allows a specific comparison between each spectral library feature and the unknown. The spectra are offset for clarity.

lengths. A corollary of this innovation is that Tetracorder can, and routinely does, detect the presence of the influence of many materials in a spectrum. For example, the key spectral features of iron oxides are in the visible, while clay minerals exhibit diagnostic features between 2 and 2.5 microns. The presence of multiple materials may dilute the strength of their spectral features relative to those in a reference spectrum, but in many important and frequent cases the signatures do not confound each other.

[11] We learned early in our work that the degree of the similarity between reference and unknown (as quantified via a least squares shape-matching algorithm) was far from sufficient to allow robust detection. Above we cited the case where different materials have diagnostic spectral features that are well-separated in wavelength, but our large reference library contains many classes of materials that are chemically and spectrally similar and even spectrally similar but chemically different (e.g., carbonates, organic compounds, and some OH-bearing minerals have similar 2.3-μm absorptions). Though not identical, they are similar enough that noise and natural variations in field spectra make the assignment of the proper threshold at which to define identification or misidentification problematic. If we used the properties of only a single material in our identification, we found that for a very large number of materials there was no threshold setting to our least-squares fitting process which simultaneously provided a high probability of identification (low occurrence of missed identifications) with a simultaneously low probability of false alarm or misidentification owing to spectrally similar reference materials in the library. In other words, if we set the identification limit based on our goodness of fit criteria to ensure rejection of false identifications, we also failed to identify many locations where our material of interest was present. Further, the threshold levels seem to be different for different materials and what they are confused with. Conversely, if we set the limits to ensure identification, we admitted too many false alarms. In practice then, we find that in many important cases of comparison of a single material to a set of spectra, even when combined with proper attention to diagnostic features to reduce noise, there is no satisfactory way to map occurrence of materials in those cases with confidence.

[12] Our solution to this problem, and our second innovation, is to quantitatively compare the similarity of an unknown spectrum to all entries in the library with similar diagnostic features. Over the set of library entries that constitute candidate detections, various similarity parameters are compared, and identification is assigned to the reference material with the greatest similarity to the unknown. Thus Tetracorder not only compares the unknown's spectral properties to the spectral properties of each entry in the library, but the comparisons themselves are quantitatively compared, assessed, and judged to identify the components present.

[13] We discovered important but surprising false identifications remained even after the above processes were followed. In these cases very different materials share diagnostic spectral regions and coincidentally have very similar shapes over these regions. Our shape-matching

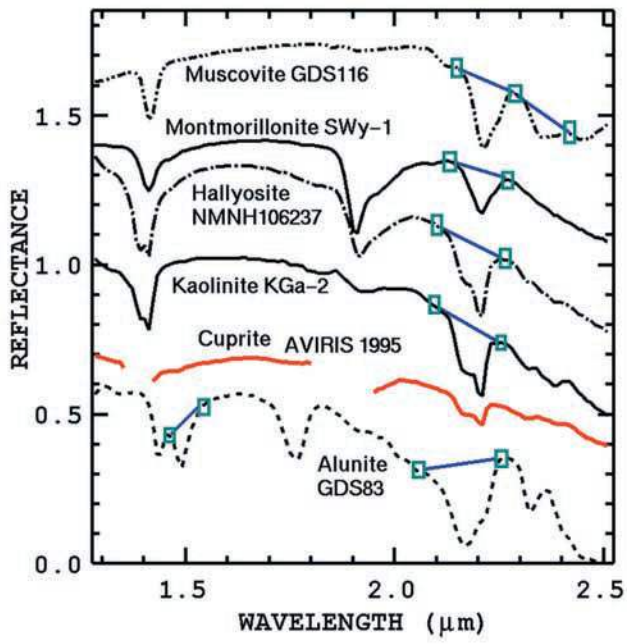

Figure 1b. Spectral features as in Figure 1a except for comparison with vibrational absorptions near 2.2 μm. Note that alunite also has a diagnostic absorption near 1.5 μm. The spectra are offset for clarity.

algorithm operates on data which has had the reflectance level and local slope removed and band depth normalized over a diagnostic spectral region and the coincidental similarities, which can result in identification ambiguities, almost always arise after this normalization. While the disparate materials in question may be similar in our primary diagnostic region as perceived by our normalization process, they never are similar at all other key wavelengths or in terms of the local spectral parameters which have been normalized (reflectance, local slope, and depth). Our third innovation is to mitigate these coincidental ambiguities using ancillary spectral information. We also use this same approach to resolve ambiguities involving related minerals that have similar diagnostic features but also differ in straightforward and consistent ways at other wavelengths. This approach complements and supersedes the comparisons of goodness of fit approach where possible.

[14] Our fourth innovation is to partition analyses across the spectrum. As different photon absorption processes tend to operate in different wavelength ranges, we split the spectral identification into several spectral regions we call groups. This allows multiple components to be identified without the need for mixture analysis. For example, Figure 1a shows diagnostic absorptions due to electronic processes near 1 μm, while Figure 1b shows vibrational absorptions in the 1.5 to 2.5-μm region. It is clear that the AVIRIS spectrum in Figures 1a and 1b displays absorptions due to both electronic and vibrational processes.

[15] Our fifth innovation is to allow Tetracorder to return a ''no answer,'' that is, a nondetection. It is a frequent occurrence that a remotely sensed spectrum does not pass even the liberal thresholds necessary to assign any candidate detections. In other cases the constraints applied to resolve ambiguities results in a rejection of an unknown in every case. Tetracorder explicitly flags a spectrum as a ''no answer'' that has no similarities to entries in the library as defined in the expert system.

[16] In summary, Tetracorder identifies materials by comparing them to a large spectral library. Our recognition that material spectral signatures are significant only in their diagnostic wavelengths allows detection of more than one material in a remotely sensed spectrum for common and important combinations of materials. Tetracorder mitigates false alarms caused by spectrally similar materials by quantitatively comparing the degree of similarity of an unknown to a set of spectrally similar reference spectra. Tetracorder mitigates coincidental false alarms permitted by our specific implementation of our shape-matching algorithm by including ancillary information. Finally, Tetracorder is not forced to provide a solution; it allows ''no answer'' as an answer.

[17] Implicit in our approach is that our library is comprehensive and unambiguous. In our experience we have found that for our applications it approaches comprehensive status because we have added materials as they have been found in field tests or for specific applications. However, Tetracorder cannot resolve ambiguities inherent to spectroscopy. Any cases where experts differ on the assignment of specific spectral features is as far as Tetracorder can go. For example, the controversy surrounding whether spectra of some portions of Europa's surface represent hydrated salts or radiolytic products cannot be resolved by our approach. However, Tetracorder does solve the problem of how to inspect large numbers of spectra in a way that mimics the method of a trained spectroscopist.

[18] In the following portions of this section we will describe our implementation of the above concept. We will begin with our shape-matching algorithm and its attendant normalizations. We will then illustrate our rejection of false alarms due to similar materials with specific examples. We will also show examples of coincidental false alarms. We will show specific examples of nondetections (''no answer''s). Closing this section we will describe the expert system framework in which we implement Tetracorder.

[19] First, we describe Tetracorder algorithms, which are the individual algorithms the Tetracorder system applies during analysis. It is our collective opinion that robust material identification with spectroscopy involves diagnostic spectral features, as these are the ''fingerprints'' of any material. Many analyses of spectra rely on unique spectral characteristics for identification [e.g., *Rencz*, 1999 and references therein] and the Tetracorder system is similar. The algorithms implemented in this version of Tetracorder isolate and analyze spectral features and their continua because the levels and slopes in a spectrum contain diagnostic information as do the absorption and emission features.

2.2. Feature Isolation: Continuum Removal Algorithm

[20] In order to identify a spectral feature by its wavelength position and shape, it must be isolated from other effects, such as level changes and slopes due to other absorbing (or emitting) materials. The first step in such isolation is continuum definition and removal [*Clark and Roush*, 1984]. Continuum removal examples are shown in Figures 1 and 2 and for several spectral features. A continuum is removed by division in reflectance, transmittance, and emittance spectra because of exponential absorption and scattering processes [*Clark and Roush*, 1984]. Conversely, a continuum should be removed by subtraction with absorbance or absorption coefficient spectra because multiple components are additive.

[21] To isolate and identify absorption features, the continuum removal algorithm first removes a continuum from a library reference spectrum and from the observed spectrum using a wavelength interval on each side of the absorption feature that is to be mapped (Figures 1a, 1b, 2a, and 2b). This can be described mathematically by:

$$L_c(\lambda) = L(\lambda)/C_l(\lambda) \tag{1a}$$

$$O_c(\lambda) = O(\lambda)/C_o(\lambda), \tag{1b}$$

where $L(\lambda)$ is the library spectrum as a function of wavelength, λ, O is the observed spectrum, C_l is the continuum for the library spectrum, C_o is the continuum for the observed spectrum, L_c is the continuum-removed library spectrum, and O_c is the continuum-removed observed spectrum.

[22] Most remotely sensed spectra are composed of mixtures, not pure materials, and as such will have spectral curves that combine to produce a continuum upon which diagnostic absorptions may be superimposed. The continuum removal

algorithm removes the effects of these other absorptions in the spectrum [*Clark and Roush*, 1984; *Clark*, 1999]. For instance, a sloping continuum modifies the appearance of an absorption feature by causing a shift of the local minimum in the curve [e.g., see *Clark*, 1999] and can also result in the absence of a local apparent minimum. If the minimum in the reflectance spectrum was used as a guide, the apparent minimum would shift with changes in contaminants and grain size. However, if the continuum is removed, the minima show a more stable position. Continuum removal normalizes the spectra, thus reducing the effects of lighting geometry on the level of the spectrum, as well as effects of contaminants and grain size variations [see *Clark*, 1999 and references therein].

[23] Including enough wavelength range in the spectral data is important to accurately define the continuum. Thus the definition of each continuum includes a wavelength interval on each side of the feature (Figures 1 and 2). We have implemented straight line continua in Tetracorder. The normalization results in a continuum-removed feature such as those in Figures 2a and 2b, which can then be compared to other spectra such as reference spectra of pure materials. In Figure 1a, which shows spectra from some materials in

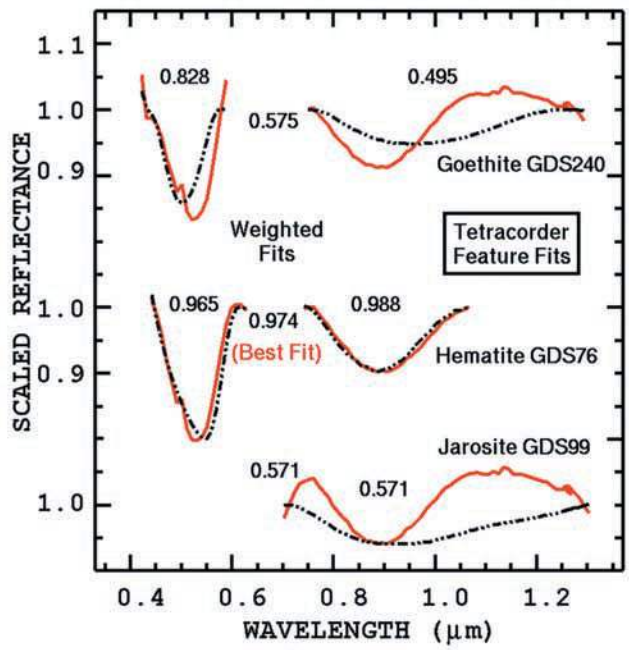

Figure 2a. The continuum removed spectra from Figure 1a are fit to each other using a modified least squares calculation. The library reference feature strength is increased or decreased to best match the observed feature. Tetracorder compares the least-squares fits to many features from many library reference spectra to determine which one matches best. The solid line in each case is the unknown and the dash double dotted line is the library reference feature. For each feature the least squares correlation coefficients (the fits) are given, and along a vertical central column, the weighted fits are shown. The best match to the Cuprite spectrum is hematite. Hematite has two features used in the identification: the 0.9 μm feature gives a fit of 0.988, and the 0.5 μm feature gives a fit of 0.965. The area-weighted fit is 0.974.

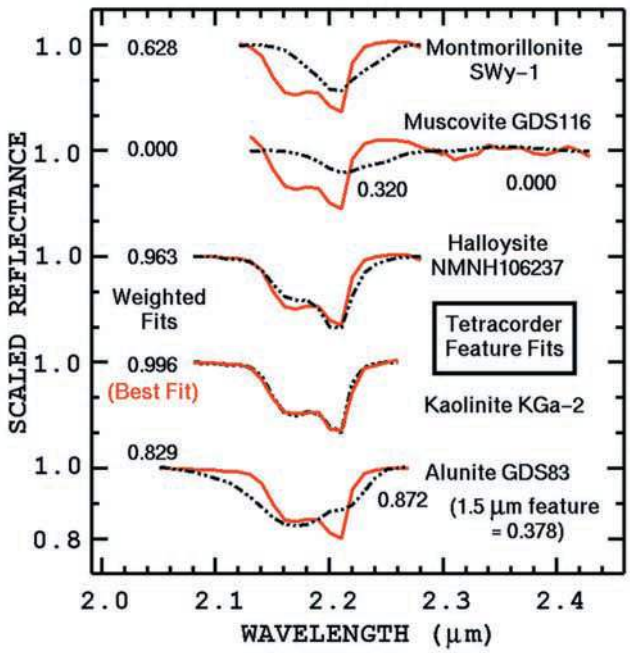

Figure 2b. The continuum removed spectra from Figure 1b are fit together using a modified least squares calculation. Kaolinite is the best match to the Cuprite spectrum. The muscovite spectrum has two features, one near 2.2 and the other near 2.3 μm. No 2.3-μm muscovite feature could be detected in the Cuprite spectrum, so the weighted fit is zero (left hand column). Note the very similar fits between kaolinite (0.996) and halloysite (0.963), yet the halloysite profile clearly does not match as well as the kaolinite profile. This illustrates that small differences in fit numbers are significant. Alunite has two diagnostic spectral features, but the 1.5-μm feature is not shown.

Appendix A (an electronic supplement to this paper), continuum endpoints for diagnostic iron absorptions in goethite, hematite, and jarosite are shown along with a remotely sensed spectrum from Cuprite NV.[1] Strong atmospheric water absorptions at 1.4 and 1.9 μm in the remotely sensed spectrum have the potential to interfere with spectral identifications, as do water absorptions in the surface materials; hence the continuum endpoints are selected to avoid these regions. This is most obvious in the selection of endpoints in the jarosite spectrum (Figure 1a), where the right side of the jarosite absorption band extends into the atmospheric water band. Similarly, in Figure 1b, which shows spectra from materials in Appendix A, the alunite continuum endpoints were selected to avoid the edge of the atmospheric water absorption. Such careful selection of continuum endpoints is crucial to the knowledge base of the expert system.

2.3. Shape-Matching Algorithm

[24] The apparent depth or strength of an absorption feature relative to the continuum is dependent on the intrinsic absorption strength, the grain size, and abundance of the material as well as the abundance, absorbing nature,

[1] Auxiliary material for this paper is available at ftp://ftp.agu.org/apend/je/2003JE001847.

Table 1. Example Tetracorder Commands[a]

group 2	\# spectral group
udata: reflectance	\# input spectrum must be in reflectance
convolve: no	\# no spectral convolution
preratio: none	\# no pre-ratio
preprocess: none	\# no pre-processing algorithms
algorithm: featfit1	\# analysis algorithm for this step
AVIRIS: [splib04] 27 d	\# input library reference spectrum
\# = TITLE = Alunite GDS83 Na63	\# library reference spectrum title
[DELETPTS]	\# channels to exclude (global variable)
Alunite GDS83 Na63	\# output title
2 0	\# 2 spectral features, 0 not features
Dw 2.048 2.078 2.247 2.277 ct.04	\# continuum wavelengths, threshold (ct)
Dw 1.466 1.476 1.535 1.555 ct.05	\# continuum wavelengths, threshold (ct)
FITALL>0.5	\# fit thresholds: if below 0.5, reject
output = fit depth fd	\# what to output: 3 images: fit, depth, fit*d
na63alun300c	\# Output base file name
8 DN 255 = 0.5	\# output 8-bits/pixel, scale 0.5 to DN 255
compress = none	\# do not compress output file
action: none	\# no subsequent action
endaction	\# done with actions
group 2	\# spectral group
udata through algorithm is same as above	
AVIRIS: [splib04] 296 d	\# input library reference spectrum
\# = TITLE = Montmorillonite Swy-1	\# library reference spectrum title
[DELETPTS]	\# channels to exclude (global variable)
Montmorillonite Swy-1	\# output title
1 1	\# 1 spectral feature, 1 not feature
Dw 2.118 2.137 2.267 2.287 ct.04	\# continuum wavelengths, threshold
NOT [NOTMUSCOVITE1] 2 0.12r1 0.3	\# NOT muscovite, relative depth.12, fit.3
\# NOT feature at wavelength 2.340 for:Muscovite GDS113 Ruby	
FITALL>0.5	\# fit thresholds: if below 0.5, reject
output = fit depth fd	\# what to output
montna	\# Output base file name
8 DN 255 = 0.5	\# output 8-bits/pixel, scale 0.5 to DN 255
compress = none	\# do not compress output file
action: none	\# no subsequent action
endaction	\# done with actions
group 3	\# spectral group
udata through algorithm is same as above	
AVIRIS: [splib04] 498 d	\# input library reference spectrum
\# = TITLE = Lawn_Grass GDS91 (Green)	\# library reference spectrum title
[DELETPTS]	\# channels to exclude (global variable)
vegetation2.grass	\# output title
3 0	\# 3 spectral features, and 0 not features
Dw 0.522 0.552 0.737 0.767 ct 0.05 rct/lct> 1.0	\# continuum wavelengths
Dw 0.870 0.900 1.063 1.093 ct 0.10	\# continuum wavelengths
Dw 1.063 1.093 1.265 1.305 ct 0.10	\# continuum wavelengths
FITALL>0.5	\# fit thresholds: if below 0.5, reject
output = fit depth fd	\# what to output
vegetation.map	\# Output base file name
8 DN 255 = 1.0	\# output 8-bits/pixel, scale 1.0 to DN 255
compress = none	\# do not compress output file
action: case 1 2 3 4 5	\# do additional analyses, case by case
endaction	\# done with actions

[a]For each spectral feature, the first two numbers represent the continuum interval on the left side, the second two numbers are the right side continuum interval (see Figure 1, 2). Alunite has two diagnostic features near 2.17 and 1.5 μm. ct = continuum threshold, for example if set to 0.05 the reflectance of the continuum must be greater than or equal to 0.05. rct/lct = continuum slope: right continuum/left continuum must be greater than the threshold. The montmorillonite entry shows a ''NOT'' feature: the 2.2-μm feature must be present, but not a 2.3-μm feature that resembles muscovite. See Figures 1b, 2b. The third example, detecting vegetation requires three diagnostic features: the chlorophyll at 0.69 μm, and two water features. If found, additional analyses in cases 1, 2, 3, 4, and 5 are executed. All analyses in a group are compared and the best answer for that group is chosen. For example, the alunite analysis and the montmorillonite analysis are in the same group. They both have spectral features near 2.2 μm so it is reasonable that the analyses compete. The answers from each independent analysis are compared and the best answer is chosen.

and grain sizes of the other materials mixed with the sample [e.g., *Clark and Roush*, 1984]. The spectral feature depth is generally proportional to the abundance of the material in the sample (holding grain size constant). The depth of a feature increases to a maximum with larger grain size, then decreases as absorption dominates over scattering [*Clark and Lucey*, 1984; *Lucey and Clark*, 1985; *Clark*, 1999]. The apparent depth of an absorption feature, D, relative to the surrounding continuum in a reflectance or emittance spectrum [*Clark and Roush*, 1984] is

$$D = 1 - R_b/R_c, \quad (2)$$

where R_b is the reflectance at the absorption-band center (the minimum in the continuum-removed feature), and R_c is

the reflectance value of the continuum at the wavelength of the band center (Figure 3).

[25] Owing to the presence of many materials, the diagnostic spectral features of materials measured remotely are almost always much weaker than those of pure reference materials. Finally, variations in lighting and local topographic slope affect the apparent reflectance level of materials. These factors do not allow direct comparison of spectra of reference materials to remotely sensed spectra except in highly specialized cases. Because geologic and biologic materials are almost always complex mixtures, comparisons must be made after normalizations that remove the complicating effects and isolate the diagnostic shape of the spectral features in question.

[26] The Tetracorder shape-matching algorithm is carried out in a two step process. First, the local spectral slope (the "continuum") is estimated and removed both from reference and observed (unknown) by fitting a straight line to predetermined wavelengths that straddle the diagnostic spectral region (or regions) of these spectra, then dividing these lines out of the observed and reference spectra (equations (1a) and (1b)). The continuum wavelength ranges for all materials and their diagnostic spectral features in our library are presented in an electronic supplement. Appendix A shows a couple of examples from the expert system and Table 1 shows how the continuum wavelengths are specified in the expert system.

[27] Because of the near universal weakness of remotely sensed features relative to those of pure materials, the intensity of the features must also be normalized prior to comparison. For example, the features in the AVIRIS spectrum from Cuprite, Nevada in Figures 1a and 1b are weaker than the features in any of the reference spectra. Tetracorder normalizes the intensity of the reference to that of the unknown by changing the spectral contrast of the continuum-removed reference over the diagnostic range to best match the continuum-removed unknown spectrum over the same range (Figures 2a and 2b). The continuum-removed depth (which we call "spectral contrast") in a reference library spectrum absorption feature can be modified by a simple additive constant, k, so that a shape match between the unknown and reference feature can be performed. We simultaneously perform the comparison between reference and unknown by determining the contrast that maximizes the correlation between reference and unknown. Equation (3) governs this process:

$$L'_c = (L_c + k)/(1.0 + k), \tag{3}$$

where L'_c is the modified, continuum-removed spectrum that best matches the observed spectrum. If k is less than zero, feature strength (spectral contrast) increases; if it is greater than zero, feature strength decreases. Equation (3) can be rewritten in the form:

$$L'_c = a + bL_c, \tag{4}$$

where

$$a = k/(1.0 + k), \text{ and}$$
$$b = 1.0/(1.0 + k). \tag{5}$$

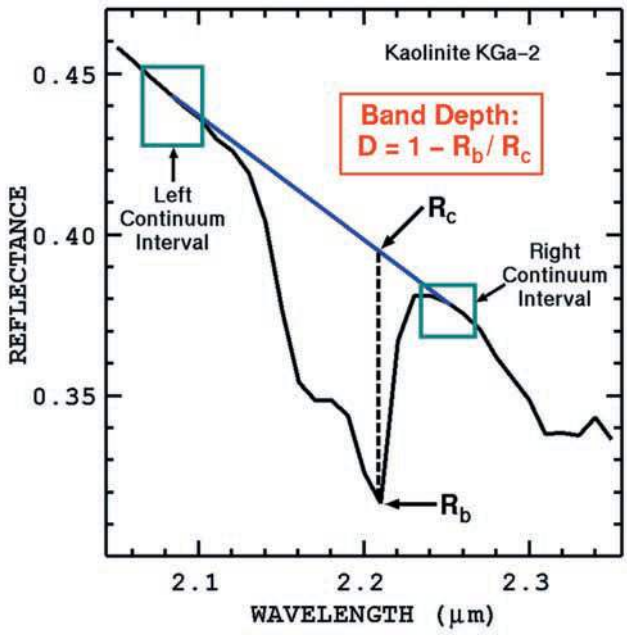

Figure 3. Characteristics of an absorption feature. A continuum interval is chosen on each side of the feature to reduce noise. The continuum intervals in this example are about 30 nm wide. A continuum is fit between the end points. The reflectance at the band center (R_b) and the corresponding continuum reflectance at the band center (R_c) are found to compute the band depth, D. The continuum is removed by division from both the library reference spectrum and from the unknown.

Equation (4) linearizes the spectral feature strength problem, so a direct solution can be found without iteration. In Equation (4) we want to find the a and b that gives a best fit to the observed spectrum O_c. The solution is found using standard linear least squares:

$$a = (\Sigma O_c - b\Sigma L_c)/n,$$
$$b = \frac{\Sigma O_c L_c - (\Sigma O_c \Sigma L_c)/n}{\Sigma L_c^2 - (\Sigma L_c)^2/n},$$

and

$$k = (1 - b)/b, \text{ also : } k = a/(1 - a) \tag{6}$$

where n is the number of spectral channels in the fit.

[28] Finally, the correlation coefficient, F, to the fit is derived for that feature:

$$b' = \frac{\Sigma O_c L_c - (\Sigma O_c \Sigma L_c)/n}{\Sigma O_c^2 - (\Sigma O_c)^2/n},$$
$$F = (b\, b')^{1/2}. \tag{7}$$

The fit, F, is a measure of how well the spectral features match. Tetracorder uses the highest fit value to decide which spectral feature is best matched by a given library reference feature, independently of the feature depth, and thus independent of the abundance of the material. Figures 2a and 2b illustrate graphically and numerically the matches between a remotely sensed spectrum and several Tetracorder library minerals.

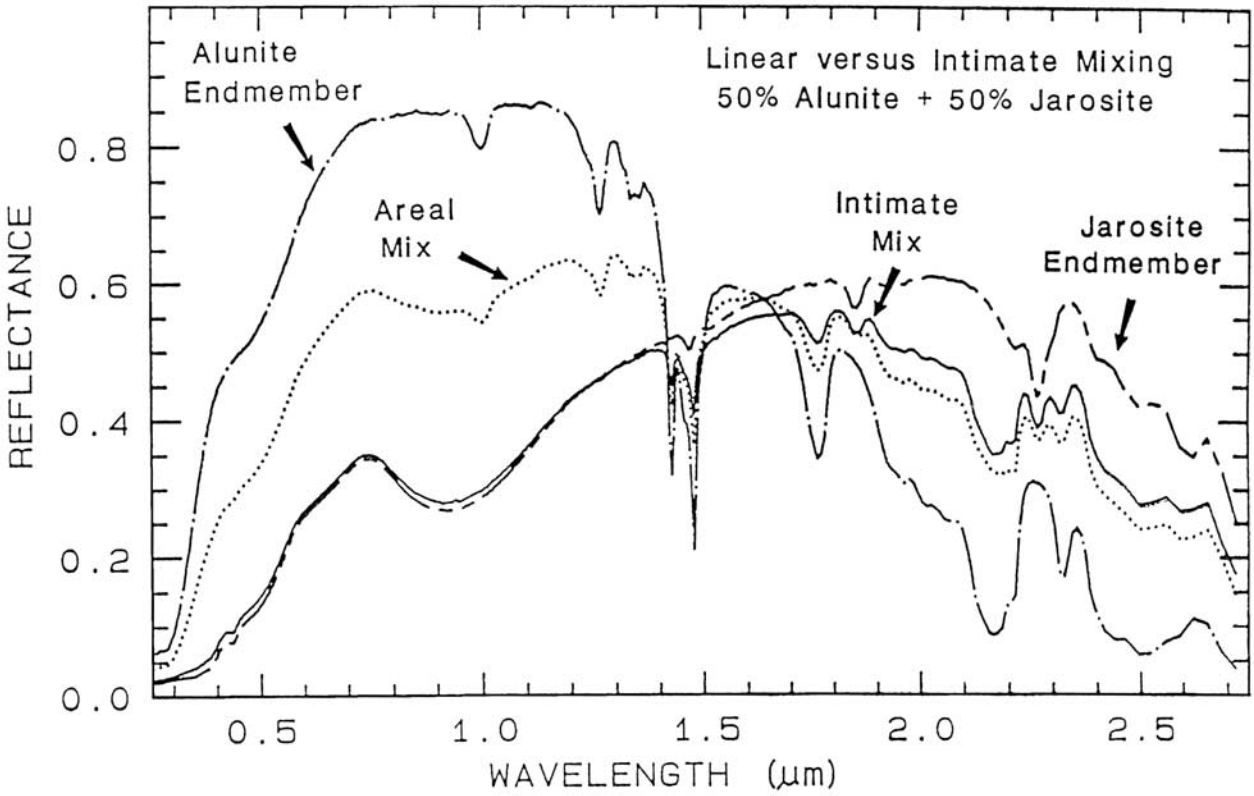

Figure 4a. Reflectance spectra of alunite, jarosite, and mixtures of the two. Two mixture types are shown: intimate and areal. In the intimate mixture the darker of the two spectral components tends to dominate at any given wavelength. In an areal mixture, the brighter component dominates. The areal mixture is strictly a linear combination and was computed from the end-members, whereas the intimate mixture is nonlinear and the spectrum of the physical mixture was measured in the laboratory. Jarosite dominates the 0.3 to 1.4-μm wavelength region in the intimate mixture because of the strong absorption in jarosite at those wavelengths and because the jarosite is finer grained than the alunite and tends to coat the larger alunite grains.

[29] The effect of different mixing types on shape-matching is shown in Figures 4a and 4b. Figure 4 shows the very distinct difference between spectra of linear (areal) and intimate mixtures of alunite and jarosite. Both shape-matching and linear unmixing algorithms that included all wavelengths would have difficulty with properly identifying cases involving the same components and abundances but different mixture types. However, the spectral shapes of the mixtures in diagnostic regions of the two minerals are similar (Figure 4b) and the components could be properly identified.

[30] Variations in grain size usually do not lead to strong variations in band shape so Tetracorder's task at these wavelengths is to remove the effects of the continuum, reflectance level, and band intensity in order to carry out shape comparisons with reference spectra. For example, continuum-removed and intensity-normalized spectra of the mineral hypersthene from the pyroxene mineral group, as a function of grain size, is shown in Figure 5. For a wide range of grain sizes the shape of the diagnostic feature is similar. Clay minerals which naturally have fine grain sizes show much less variation than do pyroxenes. However, some absorptions are so intense that the absorptions are saturated and their widths change with grain size. Hematite and goethite absorptions in the UV and near 0.9 μm often display these properties [e.g., see *Clark*, 1999]. In these cases the shape of the feature can indicate grain size independent of abundance. The pyroxene spectra in Figure 5 show this effect weakly. Very large pyroxene grains can be spectrally distinguished from very fine grains in this case. However, the pyroxene absorptions shift in wavelength as a function of composition, making grain size determinations difficult to separate from compositional variations if a sample is composed of more than one pyroxene composition.

2.4. Multiple Spectral Features: Weighted Results Algorithm

[31] For many materials (Appendix A, electronic supplement) we have defined only a single diagnostic spectral feature in the 0.4 to 2.5-μm spectral range for use in Tetracorder, despite the fact that for many of these materials other diagnostic features exist. In many of these cases one of the multiple diagnostic features present is considerably stronger than the others. We have found in practice that including diagnostic features that are too weak actually degrades performance because the ratio of spectral contrast to sensor noise is low and inclusion of these features adds noise to the weighted fit [*Swayze et al.*, 2003]. However, in

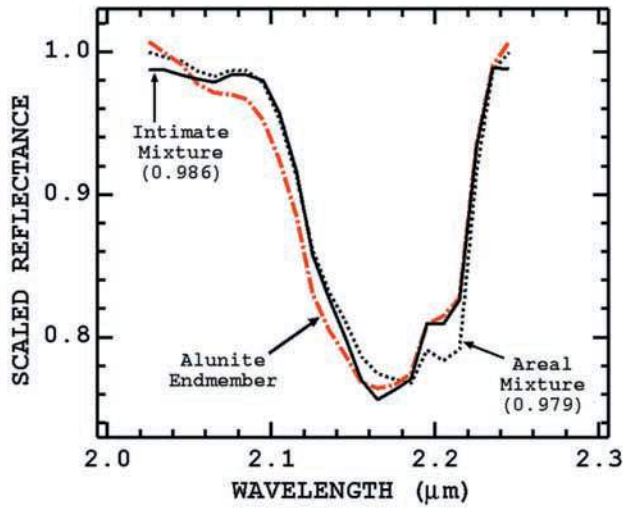

Figure 4b. Continuum removed spectral features of alunite and alunite plus jarosite mixture spectra from Figure 4a. The features for the pure alunite, intimate, and areal mixtures are very close to the same. The Tetracorder feature least squares fit of the pure alunite feature to the intimate mix feature has a correlation coefficient of 0.986 and for the areal mix 0.979. Variations in grain size and partial vegetation cover contributing to an imaging spectrometer pixel would cause variations in fits of similar magnitude.

a few cases multiple diagnostic features are strong and we have chosen to exploit them. Because the Tetracorder concept includes direct comparison of quality of fit metrics, the use of multiple features raises the issue of how to normalize our fitness metrics so fits to different materials can be compared.

[32] Tetracorder uses the relative sizes (including the widths) of reference continuum-removed-spectral features to compute a weighted fit which is used in the decision process. The continuum removal and feature fits to multiple features in a spectrum are illustrated in Figures 1a, 1b, 2a, and 2b. Three parameters for each spectrum are computed: weighted fit, F_w, weighted depth, D_w, and weighted fit times depth (fit $\times$ depth), FD_w. They are computed by weighting the relative areas of the absorption features of the reference library spectrum:

$$F_w = \Sigma\, c_i F_i,$$

$$D_w = \Sigma\, c_i D_i, \qquad \text{and} \tag{8}$$

$$FD_w = \Sigma\, c_i F_i D_i,$$

where "i" is the feature number, c_i is the relative fractional area of library reference features between each feature and its continuum:

$$\Sigma\, c_i = 1.0. \tag{9}$$

F_i, D_i are the fits (the correlation coefficients) and depths of the corresponding features. The feature depths and relative areas are calculated from the fitted library reference features. The relative area is found by integration of the continuum-removed feature (the area between the feature curve and 1.0) divided by the sum of the areas of all features analyzed for each reference material. Consider an observed spectrum with weak absorption features. The calculation of the areas of these features may be dominated by noise and could lead to bias in the decision process. Thus the areas are computed from the library reference spectra. This is also a computational advantage because they are computed only once and then used in tests against multiple unknown spectra.

[33] The areas of features help choose the correct solution. Consider the two muscovite features in Figure 1b (top) near 2.2 and 2.35 μm. We will call them feature A and B, respectively. Feature A has a weight of 0.7 and feature B has a weight of 0.3. If an observed spectrum had two features with areas A = 0.2 and B = 0.8, it would not be a pure muscovite. The fit to feature A would be given more weight, but being weaker, it would be more dominated by noise. The weighted fit would likely be lower and another mineral or mineral mixture would likely show a better fit,

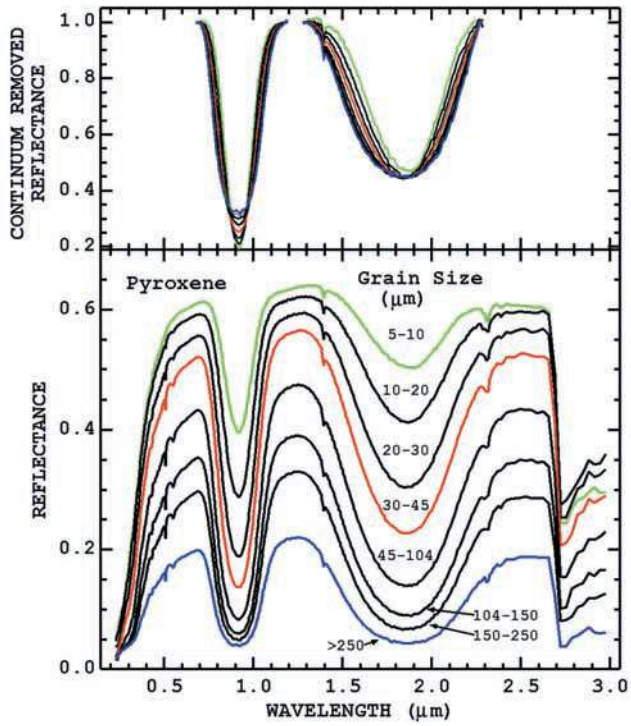

Figure 5. Reflectance spectra of a pyroxene as a function of grain size. As the grain size becomes larger, more light is absorbed, the reflectance decreases, and the absorption feature bottoms flatten (from *Clark et al.* [1993b]). Note the trace tremolite contamination causing the narrow absorption features near 1.4 and 2.3 μm. The broader pyroxene absorptions are the continuum background to the narrow tremolite features. This example shows how the components in a mixture can be readily identified even though no unmixing analysis is done. The component features are "spectrally separated" in wavelength. Continuum-removed feature fits (top) show the similarity in shape of features at different grain sizes. The small change in shape can be used to coarsely determine grain size from the spectra, independent of abundance.

thus reducing the probability that pure muscovite is the correct answer.

[34] In the above discussion we described how we derive our key metrics used for candidate identifications, but sometimes these are not final decisions. In the next section we describe how we use these metrics and other constraints to finalize our decisions.

2.5. Spectral Constraint Algorithms

[35] In the shape-matching exercise performed on each library entry for an unknown we extract all the constraints we require to perform and refine detection. The identification of materials from their spectra is constrained by (1) the goodness of fit of a spectral feature to a reference, (2) reflectance level, (3) continuum slope, and (4) presence or absence of key ancillary spectral features.

[36] If a spectral match is too poor, we assume either that the material is not present or that signal-to-noise ratios were too low to allow detection. If the fit metric is below a set threshold, the material is rejected as not detected. It is possible and frequently happens that no library entry passes this constraint which leads to Tetracorder declaring a ''no answer,'' rather than forcing a solution dominated by noise. Tetracorder evaluates constraints imposed on each spectral analysis (example constraints are shown in the command set in Appendix A and Table 1).

[37] Because some materials or combinations of materials can mimic one another in terms of shape, we add additional constraints. The first is that the reflectance level of the continuum of the observed spectrum must be consistent with the presence of a particular candidate material. If not, that particular identification will be rejected. Figure 6 shows an example of a continuum difference between two dissimilar materals (water and olivine). If only a continuum-removed spectral feature were analyzed, they would appear similar. Indeed, we have encountered conditions where shallow water mapped as iron-bearing minerals such as olivine. In these cases we know water has a low reflectance and has different continuum slope than many minerals (continuum slope is discussed below).

[38] In setting reflectance thresholds, consideration must be given to lighting conditions, contaminants that might be present, and in special cases, like water, what other effects might influence levels and spectral features. For example, shadows are dark, and on the Earth are illuminated by the blue sky, so spectra of shadows can be similar to that of lakes and by setting continuum level constraints, dark shadows can be rejected from being identified as certain materials. The constraint can be set to a minimum and maximum for each spectral feature. If a continuum level does not fit within the minimum and maximum specified, the candidate material's detection is rejected. We also use this constraint frequently to reject very dark materials because detection is signal-to-noise ratio dependent. The darker a spectrum, the more spectral features are suppressed when in an intimate mixture and the higher the signal-to-noise ratio required to detect that feature. Thus for many materials the threshold is set at 4% reflectance to eliminate false alarms owing to noise. In principal the fit constraint should catch low signal-to-noise ratio cases, but noise can cause features to occasionally pass this constraint. The continuum reflectance constraint catches additional cases.

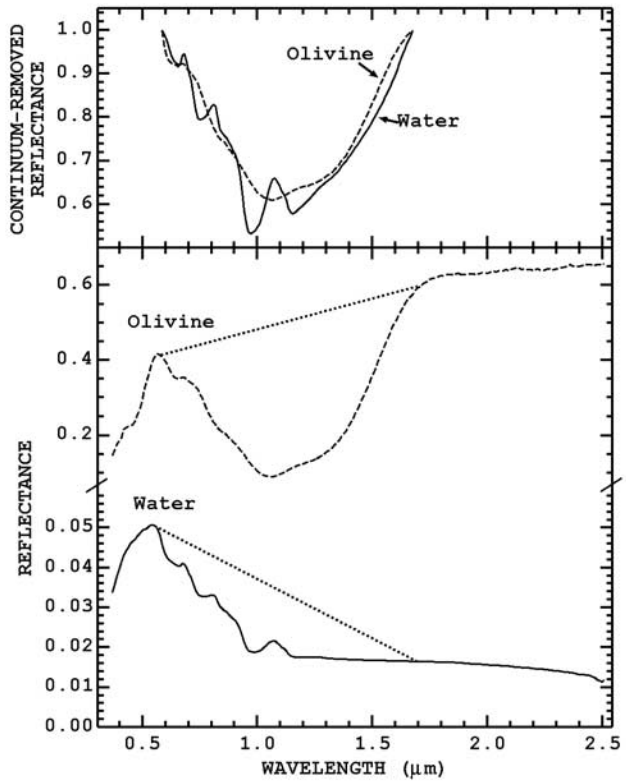

Figure 6. Continuum-removed spectral features sometimes have similar overall shapes for different materials. Here, an example for olivine and water is shown. The scattering peak at green wavelengths is similar in position to the green peak in olivine. When the continuum is removed from both spectra (top), the broad olivine feature roughly tracks the water response. Tetracorder would normally only compare the correlation coefficients of the fitted features to check for olivine. Constraining reflectance levels and the slope of the continuum can help distinguish between the two cases. Water has a lower reflectance and a negative continuum slope but olivine has a higher reflectance and positive slope.

In practice we employ the right, center, and/or left continuum level limits**.** We should note that continuum level constraints are not a match to the reference material continuum because mixtures can change both the average reflectance and local spectral slopes.

[39] Example continuum constraints are shown in Table 1. Examine the entries for ''Lawn_Grass GDS91.'' The continuum constraints require a minimum reflectance of 0.05 for the 0.69-μm chlorophyll feature and 0.10 for the 0.95 and 1.15-μm water absorptions. This requires an increasing reflectance from visible to near-IR wavelengths as is commonly observed in spectra of vegetation. The levels are set lower than typical grass reflectance levels because the vegetation may by illuminated by low Sun angle (e.g., north slope of a mountain in the Northern Hemisphere).

[40] Just as the continuum reflectance level must be consistent with experience, so to does the local spectral

slope across the continuum. The slope constraint we apply is

$$\begin{aligned} \text{slope} &= O_{left}/O_{right} > X, \text{or} \\ \text{slope} &= O_{right}/O_{left} > X, \end{aligned} \quad (10)$$

where O_{left} and O_{right} are the observed continuum levels on the left and right sides of the feature center, respectively, and X is a threshold. If the slope in the spectrum falls below the level set by equation 10, the fit for that feature (equation (7)) is set to zero. For example, this constraint is needed in the mapping of iron-bearing soils. The curvature of the water spectrum in the near IR is sometimes very similar to the hematite absorption feature after continuum normalization, so occasionally the goodness-of-fit metric can pass remotely sensed water as an Fe-bearing mineral. However, the strong positive visible slope is an additional required characteristic of some minerals such as hematite, in addition to its absorption feature shape. Water is distinguished from Fe-bearing minerals based on slope: an approximately flat or positive sloping spectrum is indicative of Fe-bearing soils, while a negative sloping spectrum is indicative of water spectra. An example of slope differences of water versus that of an Fe-bearing mineral is shown in Figure 6.

2.6. Not-Feature Algorithm

[41] Despite our best efforts including the constraints above, some materials or mixtures of materials have virtually identical spectral features at some diagnostic wavelengths which are too difficult to distinguish. However, invariably they differ markedly at other wavelengths. For example, Figure 1b shows spectra of the minerals montmorillonite $[(Na,Ca)_{0.33}(Al,Mg)_2Si_4O_{10}(OH)_2 \times nH_2O]$ and muscovite $[KAl_2(Si_3Al)O_{10}(OH,F)_2]$. These minerals share a very similar and strong diagnostic absorption near 2.21 μm. Clearly, in this case the term "diagnostic" is used loosely. More strictly, the 2.21 micron feature is compelling evidence for the presence of montmorillonite, illite, or muscovite. However, montmorillonite has no absorption feature near 2.35 μm but both illite and muscovite have a feature there. Therefore in testing for montmorillonite, we attempt to detect a 2.35 micron feature. If such a feature is detected, montmorillonite is rejected. In this particular case we borrow the detection parameters from the Tetracorder test for the 2.35 micron feature of muscovite. If the depth and fitness parameters for this feature exceed our defined thresholds we consider the feature detected, and therefore montmorillonite must be rejected. An analogous example is illustrated in Figure 2b. In this case the feature fits show there is no 2.35-μm feature present in the Cuprite AVIRIS spectrum shown, therefore muscovite cannot be present so muscovite is rejected (while Figures 1b and 2b show what appears to be one continuum from about 2.15 to 2.43 μm, really two features are defined with a common continuum interval near 2.3 μm).

[42] The detection of a feature in the wavelength position of a NOT feature rule can be accomplished by measuring more than one metric. The metrics currently implemented are band depth threshold (equation (2)) and threshold relative to the strength of another feature. For example, in Appendix A and Table 1, the NOT condition to detect montmorillonite is a 2.35-μm muscovite feature that is 12% the strength of the montmorillonite 2.2-μm feature. If the 2.35-μm feature strength was determined to be greater than 12%, montmorillonite would be rejected. In practice, identifying montmorillonite-muscovite (or illite) mixtures is possible. The 2.35-μm feature normally is about 30% the strength of the 2.2-μm feature in muscovites and illites, so constructing several tests with different levels of the NOT feature could, in principle, be used to derive several levels of montmorillonite + muscovite/illite mixtures.

2.7. Diagnostic/Optional Features

[43] Some materials have spectra with less intense and/or subordinate absorption features in addition to stronger diagnostic absorptions. The diagnostic absorptions may be detectable if the abundance of the material is high enough. However, weaker absorptions might be concealed by absorptions from other materials or might be too weak to be detected at low abundances of the material. In Tetracorder, every feature is assigned as either diagnostic or optional. If a feature is defined as diagnostic or optional, and it is detected in the spectrum, its weighted fit will be included in the analysis and decision process. If an optional feature is not detected, its fit and depth are set to zero and the material might still be identified by the presence of other absorption features (either diagnostic or optional). Of course if a feature is defined as diagnostic, the feature must be detected in the spectrum to identify that material. If any diagnostic feature is not detected, even though other features (diagnostic or optional) for that material are detected, that material is not indicated by the spectrum and is declared to be undetected (fit, depth, and fit × depth are all set to zero).

[44] Care was used in developing the expert system command set because a material's diagnostic feature could potentially be masked by absorptions in other materials. If that is a possibility, the feature would be flagged as optional and not diagnostic. For example, hematite and goethite spectra (Figures 1a and 2a) have features near 0.5 and 0.9 μm. The shorter wavelength features in both minerals are more intense, and when hematite or goethite is present in low abundance, the 0.9-μm feature can be absent. Thus the 0.9-μm feature for both minerals is optional and the 0.5-μm feature is diagnostic in the Tetracorder expert command set.

2.8. Nothing Found is an Answer

[45] Tetracorder's spectral feature identification algorithm and supporting constraints are not forced to return a detection. Diagnostic spectral features must be present in the spectrum to find that material in the spectrum. Indeed, it is possible that all Tetracorder output is "nothing found." Not finding a material can be important. For example, in doing an environmental assessment, not finding a toxic material can be an indicator of environmental health.

2.9. Grouping Decisions

[46] The final aspect of the materials detection process in Tetracorder is explicitly dealing with broad classes of detections. Above we discussed how mixtures of materials might have well-separated diagnostic features, in which case all such materials can be detected in a spectrum given

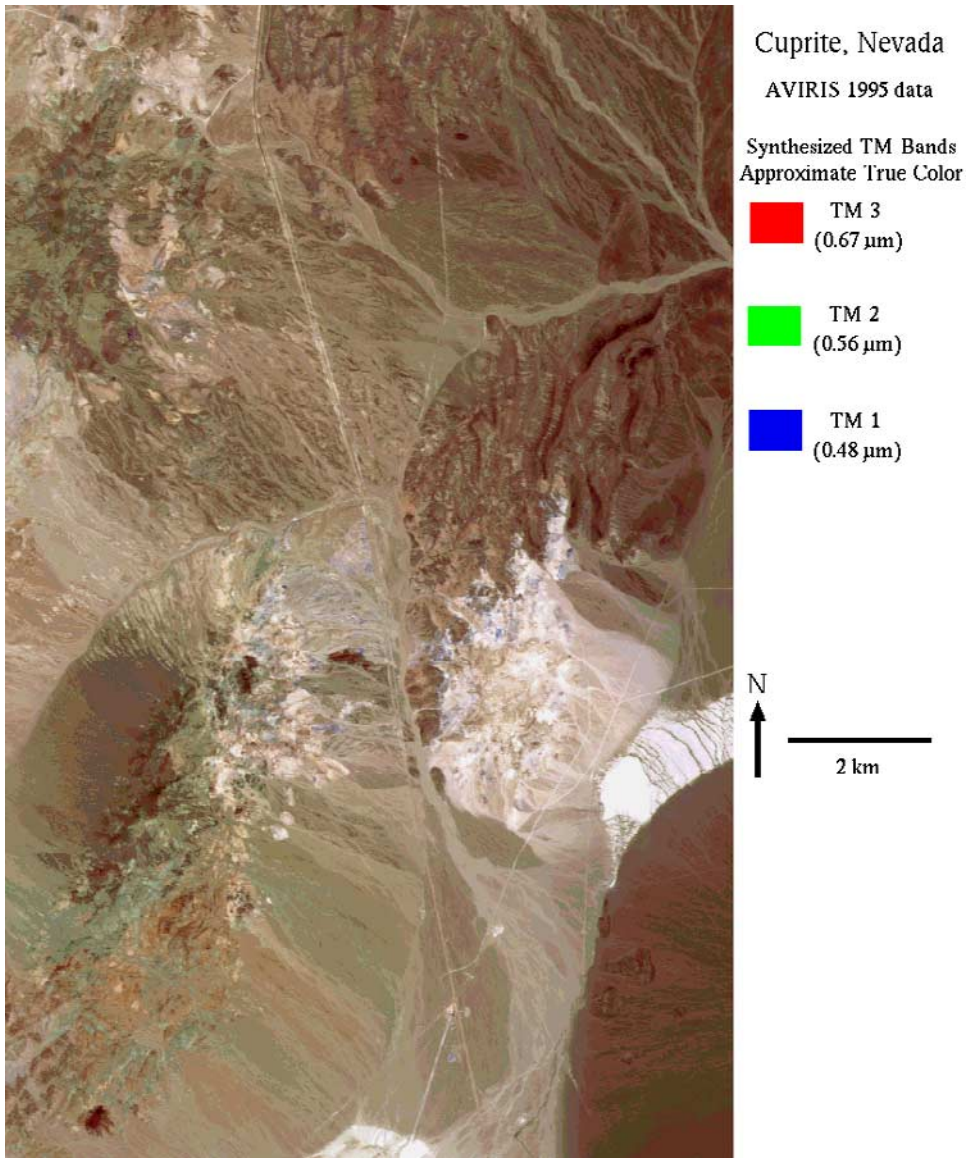

Figure 7a. Pseudo-true color composite AVIRIS image of Cuprite, Nevada. The image has a width of 10.5 km (614 pixels) and a length of 18 kilometers (972 pixels). The spacing between pixels is 15 meters, and the size of each pixel is about 18 meters.

sufficient signal-to-noise ratio. We also discussed how we deal with materials that have similar or overlapping diagnostic features by comparing the fitness parameters and exploiting ancillary spectral information. In order to achieve the various detections, Tetracorder analyzes portions of the spectrum by partitioning or isolating portions of the spectrum for various tasks needed to identify different materials. We call this partitioning groups and cases.

[47] Tetracorder makes decisions by explicitly grouping reference materials by the wavelength ranges of their diagnostic features. For example, vegetation and iron-bearing minerals with Fe^{2+} and Fe^{3+} absorptions occupy one group with their diagnostic features in the visible and very near infrared. Clays and other sheet silicates are grouped because their diagnostic features dominate the 2 to 2.5-μm region. Within a group, spectral features can confound one another so Tetracorder selects a single library entry as present. Thus to identify mixtures within a group, reference spectra for those mixtures must be included. On the other hand, Tetracorder can in principle (and usually in practice) report a detection from each group and therefore finds multiple components without specific reference mixture spectra. Mixtures will be discussed in more detail in sections 3.2 and 3.3. Section 4.2 defines the groups, cases, and their wavelength ranges.

[48] Partitioned analyses could be done in parallel or serially, and Tetracorder does both. Groups are partitioned decision making analyses that are done independently but in parallel before doing any case analyses. A case is an independent analysis partition completed only after all the group analyses are completed and a specific decision is made to perform a case analysis. Case analyses can be both parallel and sequential and invoke additional case analyses. A group or case analysis can operate in one of two modes:

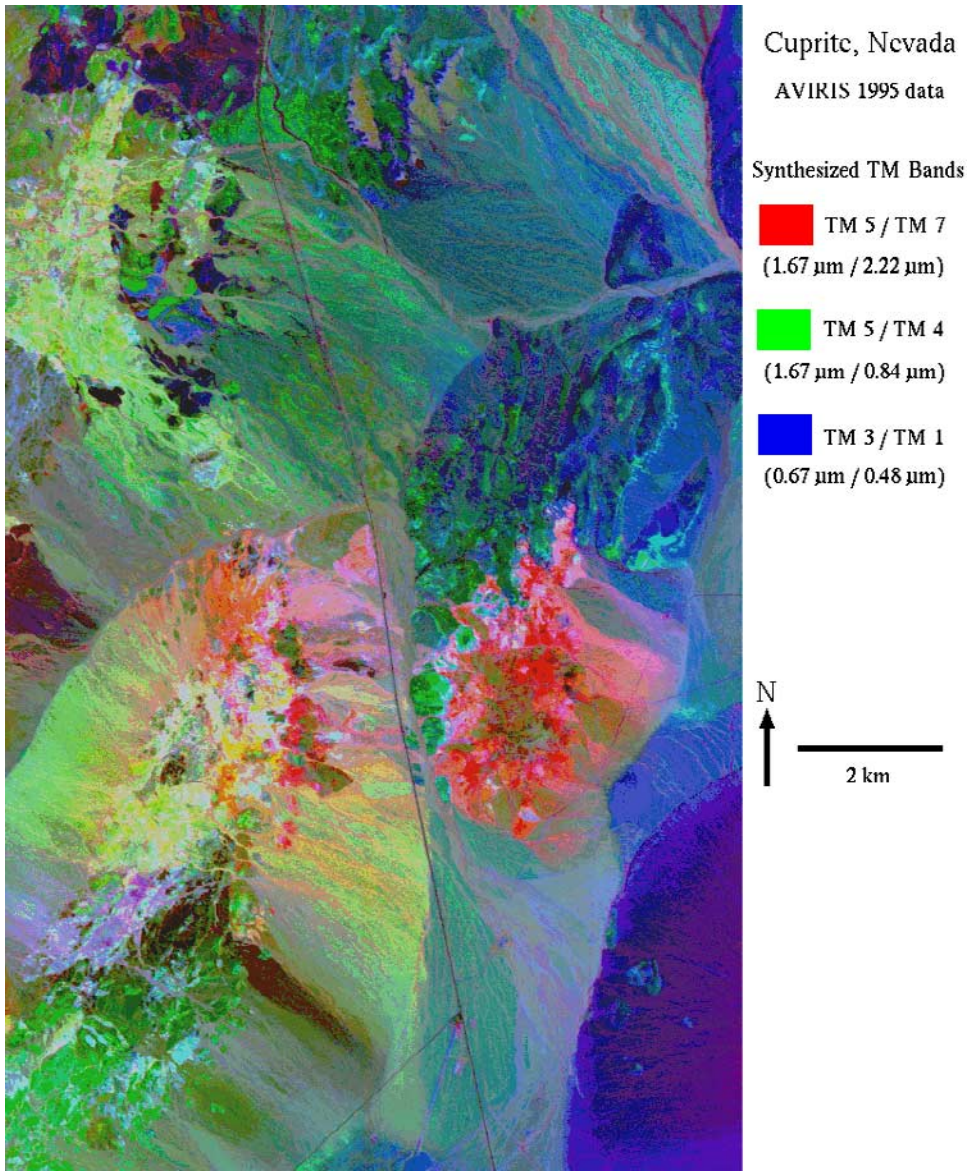

Figure 7b. The same AVIRIS data shown in Figure 7a were used to synthesize Landsat TM response for each of the six TM bands in the AVIRIS spectral range. The synthesized data have the same spatial resolution as AVIRIS (18 m not 30 m of actual TM data) so only the effects of spectral bandpass and sampling are compared. The TM band ratios shown here are commonly used by researchers to discriminate surface materials, and the many colors seen here show the power of this method. The color composite shows the hydrothermal alteration system appearing different from surrounding unaltered areas, but specific mineral identifications are not possible.

(1) do one analysis and output an answer for that analysis or (2) do multiple analyses, examining the results from all the analyses in that group or case, and decide which analysis gives the best answer and output that result.

[49] Figures 1 and 2 show an example of partitioned analyses for two groups. In Figures 1a and 2a, multiple spectral features are compared and a decision is made to identify hematite as the best answer (Figure 2a). In Figures 1b and 2b, multiple analyses lead to the decision that kaolinite is the best answer (Figure 2b). Again, in each group, only one answer is chosen as the correct answer but multiple groups lead to multiple answers. In this example, the Cuprite spectrum is identified as a mixture of hematite and kaolinite, even though only pure mineral spectra were used to identify these materials.

3. Tetracorder Applied to Imaging Spectroscopy

[50] Tetracorder was developed largely in response to the potential of imaging spectroscopy data sets provided by NASA via the Earth Observing System HIRIS, the Galileo NIMS, the Cassini VIMS, and potential Mars imaging spectrometers. However, excellent data sets became available for testing using the JPL Airborne Visible/Infrared Imaging Spectrometer (AVIRIS) sensor, for which testing and verification at test sites were accessible by our team.

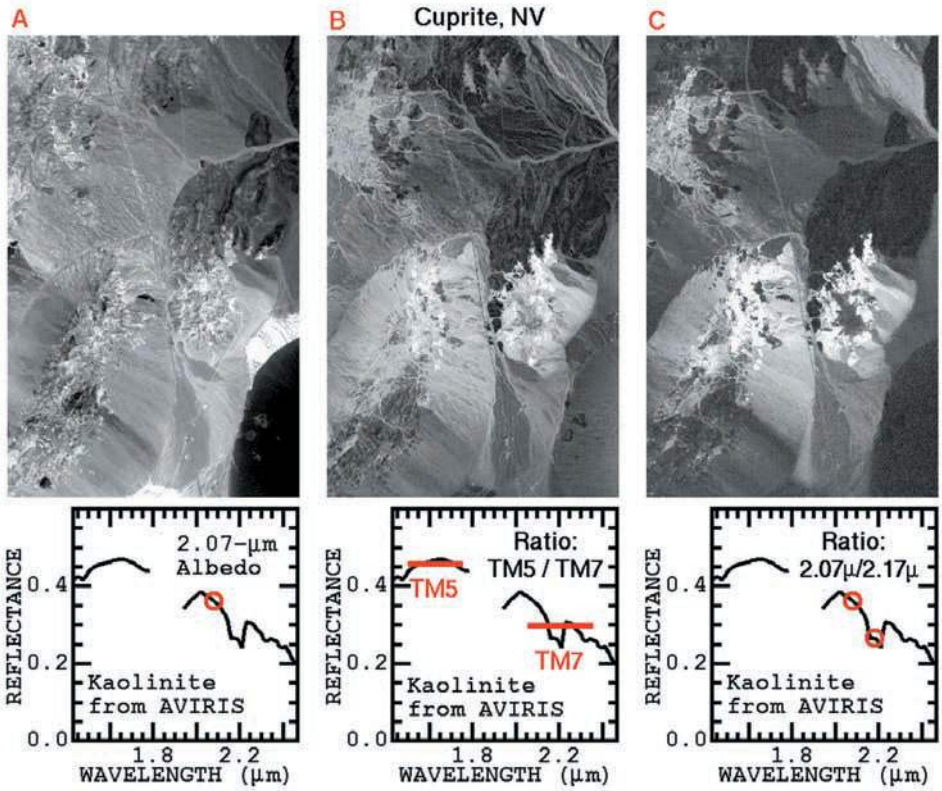

Figures 8a–8c. Cuprite analysis examples. (a) 2.07 μm albedo image. (b) The AVIRIS-synthesized TM band ratio image is shown for TM band 5 divided by band 7, which indicates a decreasing spectral reflectance from 1.5 to 2.2 μm. Such slopes are common in spectra of clay minerals but are also common in spectra of carbonates, sulfates, and generally moist or wet soils, rocks, or other materials. (c) Image of the AVIRIS 2.07-μm reflectance divided by the 2.17-μm reflectance shows possible kaolinite absorption or strong spectral slope between these two wavelengths. This ratio should discriminate absorptions near 2.2 μm, but surprisingly, there is little difference compared to the TM ratio image in Figure 8b.

AVIRIS is arguably the highest performing and most widely used visible and near-IR imaging spectrometer operational today for terrestrial remote sensing. With a spectral sampling and bandpass of ~10 nm and signal-to-noise ratios exceeding 500 at most wavelengths, AVIRIS data are extremely useful for spectral analysis at the individual spectrum level. Corrections of AVIRIS data for atmospheric transmission are well developed, effective, and routinely applied so our applications of Tetracorder detection can ignore atmospheric effects, except in portions of the spectrum where transmittance is so low that essentially no reflected signal is present in the data. In this section we will use AVIRIS data collected in 1995 over the Cuprite Mining District (Figure 7) in Nevada to illustrate the processes described above.

3.1. Comparison of Analysis Methods

[51] Let us first examine some common analysis methods and compare results to a spectroscopic analysis. This range of examples shows that material identification results do not improve much in ability to discriminate materials until the analysis becomes quite sophisticated. This may explain how some in the scientific community have not seen the advantage of imaging spectroscopy. Simple spectral analyses produce results that are hardly any better than that achievable with data from broader-band multispectral systems. To illustrate these effects, we synthesized broader-band systems from the AVIRIS data so that there is no change in spatial resolution. The signal-to-noise ratio of the synthesized channels is very high, much higher than actual systems such as TM, and has better atmospheric correction. Thus the examples and observed limitations in the more simple methods are not limited by signal-to-noise ratio.

[52] Multispectral systems contain only a few broad spectral channels. Spectral analysis is not possible with such systems, so more simplistic approaches have been developed to produce "indicator" maps. The ratio of the signals through two different filters (or bands) is called a band ratio and is probably the simplest computation beyond a color image. A color image derived from band ratios is called a color-ratio composite.

[53] A pseudo-true color representation made from three broad bands simulating the color response of the human eye (Figure 7a) shows lighter areas that may be indicative of hydrothermal alteration. Band-ratios can be computed from measurements of any two spectral channels, whether from broad-bands or narrow spectral bands. The broad bands of Landsat Thematic Mapper (TM) were computed from the AVIRIS data and ratios between the five broad bands were calculated. A color image of TM band ratios, called a color-

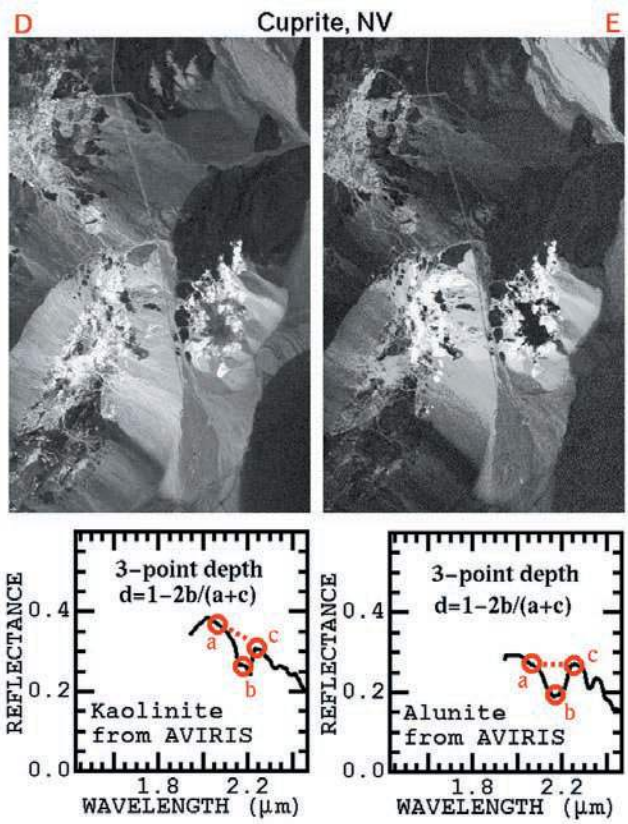

Figures 8d–8e. (d) A ''three-point band depth'' using AVIRIS data for Cuprite, Nevada shows locations where an absorption feature, centered near 2.2 μm, like that in kaolinite, is expressed in spectra of surface materials. In all these images, brighter levels indicate a greater spectral abundance of that material. (e) A corresponding ''three-point band depth'' for alunite shows locations where an absorption feature, centered near 2.17 μm, is expressed in spectra of surface materials. There is little difference between the alunite and kaolinite 3-point band depth images, showing that more sophistication is needed to spectrally discriminate between these two minerals.

ratio composite (Figure 7b), shows that many surface materials are distinguished, but specific mineralogic identifications cannot be made. Further, sometimes (but not always) the same color is caused by completely different mineralogy (see verified mineralogy given by *Swayze* [1997]). Images such as these are guides for field investigations and are not mineral maps.

[54] In the next example, let us assume we were interested in finding locations of the clay mineral kaolinite [$Al_2Si_2O_5(OH)_4$]. Well-crystallized kaolinite is the primary mineral used in the production of ceramics. Kaolinite is also commonly found in hydrothermal alteration systems which may contain deposits of economically valuable minerals, such as gold. Weathering of pyrite-rich hydrothermally-altered rocks can produce acidic waters which can pollute drinking water sources [e.g., *Swayze et al.*, 2000 and references therein]. Hydrothermal systems may also have provided an environment where life evolved on the Earth and possibly on Mars as well [*Shock*, 1996; *Farmer*, 1996 and references therein]. So, for this discussion, let us assume we are interested in locating well-crystallized kaolinite and not other minerals in the kaolinite group nor other clay minerals.

[55] The sequence of images in Figures 8a to 8g shows the results of increasingly sophisticated analyses. A kaolinite spectrum is shown below each image to illustrate the analysis method. Our reference spectral library [*Clark et al.*, 1993a] entry for kaolinite shows it has a high reflectance (>0.7) at visible wavelengths and a reflectance >0.7 at 2.1 μm, higher than the reflectance typically found for soils (reflectance ~0.2). Could reflectance alone show kaolinite occurrence? The infrared albedo image (Figure 8a) shows many levels of intensity (apparent surface reflectance) and does not discriminate kaolinite from other minerals.

[56] A commonly used ''clay'' mineral discriminator is a TM band ratio: TM channel 5 divided by 7. A high 5/7 ratio indicates a decreasing slope to the spectrum from 1.6 to 2.2 μm, a trait commonly found in clay minerals. The ratio image of TM bands 5/7 (Figure 8b) shows areas of decreasing IR slope as lighter portions of the image. The TM ratio image shows the two alteration centers in the middle of the image as lighter, indicating possible clay content, but does not distinguish kaolinite versus other clay

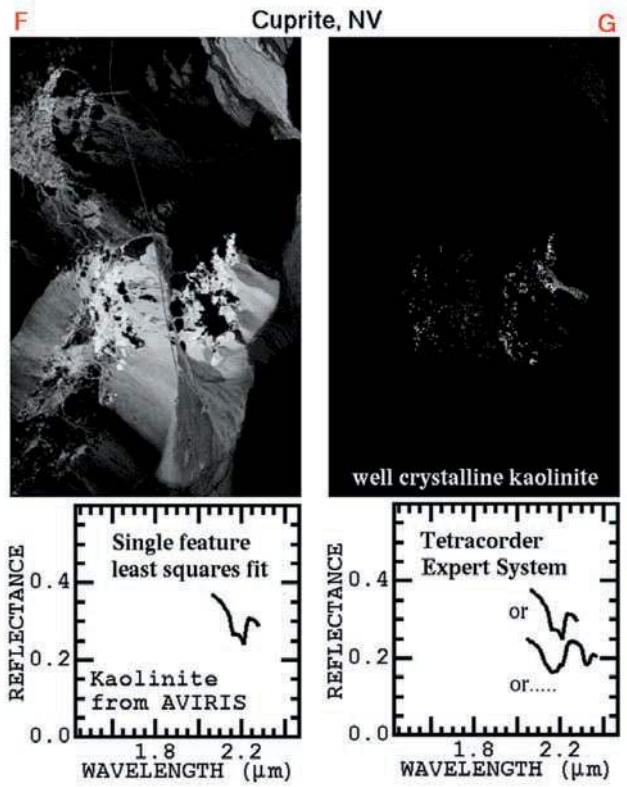

Figures 8f–8g. (f) A spectral feature shape match was applied to the imaging spectrometer data with a kaolinite 2.2-μm feature shape. The resulting image distinguished kaolinite better but spectral features from other minerals also contribute to the bright areas in the image. (g) The Tetracorder decision results in an image of kaolinite locations shows much less than seen in the other images. The Tetracorder expert system has determined locations of kaolinite versus other minerals based on comparison to a library of spectral features from many materials.

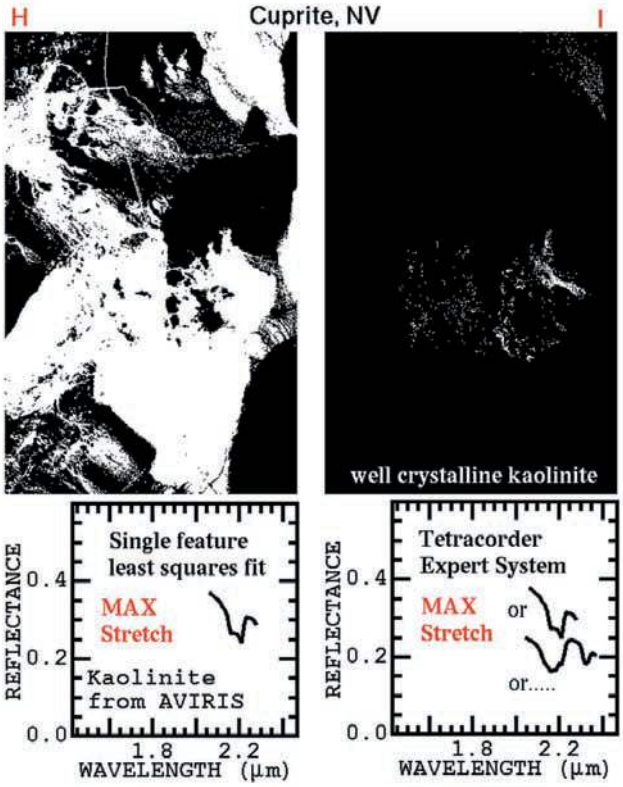

Figures 8h–8i. These two images are the same as in Figures 8f and 8g, except that all of the DNs greater than zero in the image are stretched to appear white. The feature fit image (h) shows kaolinite-like response over large areas of the image, where we know kaolinite is not present. The result from such a simplistic analysis is subjective and depends on how much the analyst stretches the resulting image. The Tetracorder result (i), however, shows little change from Figure 8g. The main difference is that low abundance areas of kaolinite now appear white in the image. The result agrees with field work [*Swayze*, 1997].

mineralogy. Similar slopes are also found in spectra of any mineral or soil containing OH or water and in spectra of carbonates [e.g., *Clark et al.*, 1993a] so the spectral slope is not a unique indicator of kaolinite.

[57] The higher spectral resolution of AVIRIS allows refinement of the band ratio concept (Figure 8c). A "narrow-band-ratio" image computed from the reflectance at wavelength 2.07 μm divided by the reflectance at 2.17 μm shows the spectral slope over a short wavelength range (lighter in the image means greater slope) and has a better probability of indicating the presence of a narrow absorption feature than does a broad-band ratio. In this case a few more areas became darker in the image in Figure 8c compared with Figure 8b. It may be somewhat surprising that there is so little difference between Figures 8b and 8c. That is because there are several minerals in the imaged area that have strong absorption near 2.2 μm, including alunite [$KAl_3(SO_4)_2(OH)_6$], muscovite [$KAl_2Si_3O_{10}(OH)_2$], and the clay montmorillonite [$(Na,Ca)_{0.33}(Al,Mg)_2Si_4O_{10}(OH)_2 \times nH_2O$].

[58] Because AVIRIS spectra resolve absorption bands, a simple "three-point band depth" image can be computed (Figure 8d). Such a depth computation further restricts the analysis to detect a relative minimum between the two "continuum" end points. The image is coded to show increasing absorption strength as increasing brightness level (whiter). The results in Figures 8b, 8c, and 8d show a lot of similarity, which could lead the analyst to conclude there is extensive kaolinite in the region. However, as noted above, other minerals also have absorptions near 2.2 μm that overlap the kaolinite absorption. A three-point band depth computation for alunite (Figure 8e) shows nearly the same image as that for the kaolinite three-point band depth. Field checking shows that neither the alunite nor kaolinite is as extensive as indicated by these images [*Swayze et al.*, 1992; *Clark et al.*, 1993b; *Swayze*, 1997]. More sophistication is required to derive the correct locations of kaolinite deposits.

[59] A simple three-point band-depth analysis does not examine the unique shape of the kaolinite doublet feature nor distinguish it from similar absorptions in spectra of other minerals. Our shape-matching algorithm (equations (2)–(9)) was applied to the Cuprite data with a kaolinite spectral library reference spectrum (Figure 8f). Note that more of the imaged area is now dark compared with the images in Figures 8b–8e. The shape matching gives results closer to the actual locations of kaolinite, but it is still not completely correct. Other minerals with absorptions near 2.2 μm also show a match to the least squares fit but usually at reduced intensity (note the alluvial fans are darker than the source regions for the fans). Alunite, in particular, gives a response very similar to kaolinite in this analysis as it did in the three-point band depth analysis (Figures 8d and 8e).

[60] It should be clear from these examples that there is no simple algorithm that can be applied to imaging spectroscopy data to map a single mineral (or material) without inadvertent inclusion of other materials. There are too many other common materials and minerals with absorption features similar to each other for simple analyses, like shape-matching algorithms, to map materials robustly. Successful materials mapping must be able to distinguish between materials with similar spectral properties.

[61] The Tetracorder map of kaolinite is shown in Figure 8g. The distinguishing step is the Tetracorder decision process: evaluating multiple tests of the spectral feature to determine the best match. The difference between the image in Figure 8f and that in Figure 8g is that for most of the pixels in Figure 8g, Tetracorder determined which pixels contained minerals other than well-crystallized kaolinite. This is the quantum leap of the Tetracorder analysis methods over the previous generations of analyses: the comparison of results competition and decision process allows materials to be uniquely distinguished, identified, and mapped.

[62] A simple pattern-matching algorithm like that in Figure 8f produces image maps that are dependent on how much the image is contrast stretched. Compare Figure 8f to Figure 8h. Any curvature to the spectrum will give a response in the shape-matching analysis. If the resulting image is stretched hard so that the smallest absorption depths show as white, one might conclude that kaolinite is present throughout many parts of the image (Figure 8h). This has led to the analyst needing to adjust images based on their knowledge of the area to indicate what is there. In other words, the results are subjective.

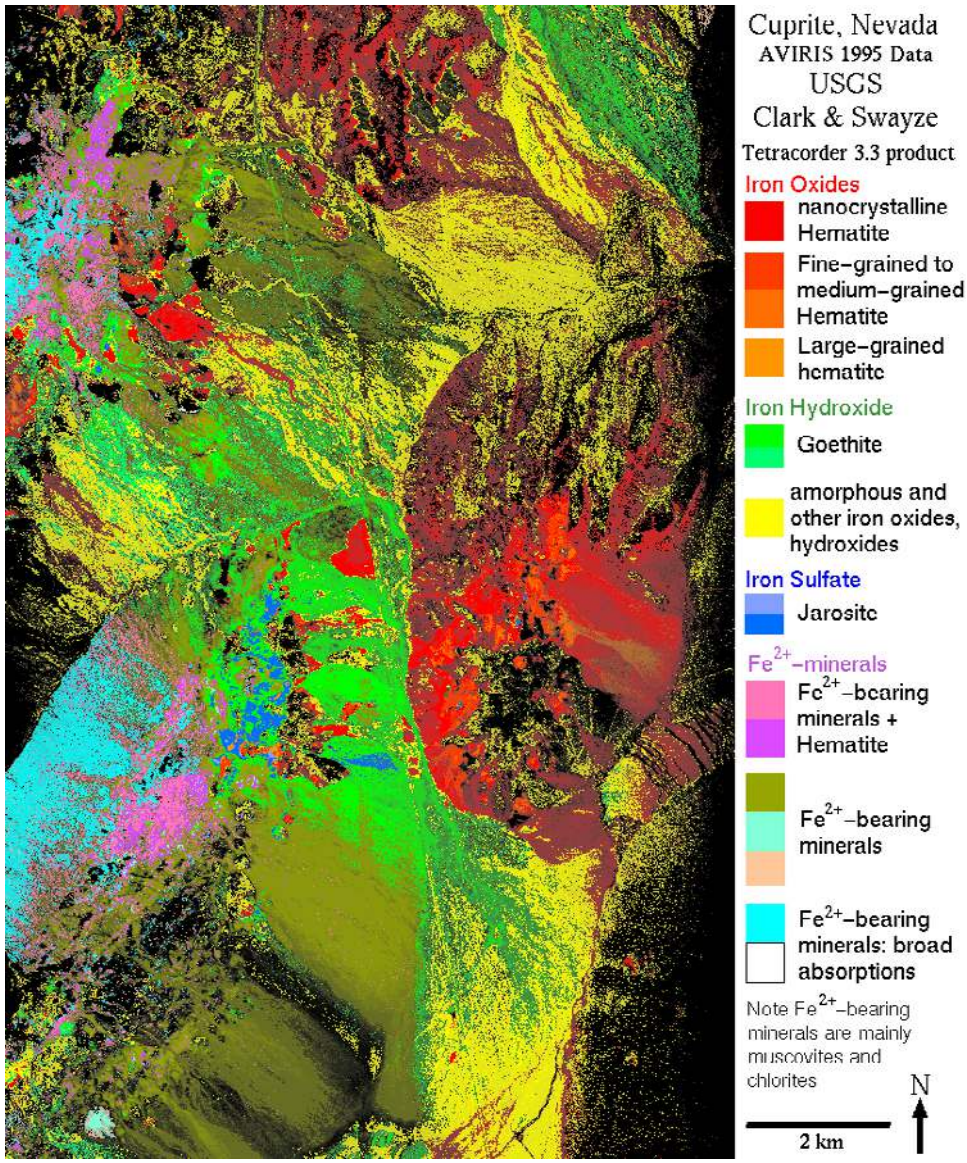

Figure 9a. Tetracorder mapping results from AVIRIS imaging spectrometer data over Cuprite, Nevada. The Tetracorder results distinguish iron-bearing minerals, including hematite grain sizes. Fe^{3+}-bearing minerals can usually be uniquely identified. However, Fe^{2+} absorptions are not always diagnostic for uniquely distinguishing specific mineralogy; thus we usually label our images as simply Fe^{2+}-bearing. The different colors of Fe^{2+}-bearing minerals usually indicate distinct mineralogy or lithologic units.

[63] The decision-making process of Tetracorder, however, is more objective. Tetracorder has made the decisions as to which spectra indicate the presence of kaolinite and which ones indicate other minerals through its spectral identification process. In our Cuprite example, Figure 8i shows the maximum stretch for the Tetracorder analysis, and it appears similar to the less stretched image in Figure 8g. Compare that result with the maximum stretch in the least squares single feature analysis (Figure 8h), which shows large portions of the image as kaolinite compared to the less stretched Figure 8f image. The Tetracorder results are less subjective because the decision process has robustly identified spectral features. The hard stretch of the Tetracorder result (Figure 8i) shows where the well-crystallized kaolinite occurs with high confidence even at low feature strengths (which correlates with low abundance). The kaolinite that mapped in Figures 8g and Figure 8i agrees with field observations and verifications [*Swayze*, 1997 and references therein].

[64] Because Tetracorder spectrally identifies materials, a color-coded map of materials can be constructed that presents more information than a single material image (as in Figure 8f) and is more specific than a color-ratio composite (as in Figure 7b). If the image in Figure 8g is colored (in this example, yellow) such that a stronger absorption feature strength indicates a brighter intensity of that color, and other mineral images are coded as different colors, the color-coded images can be combined into mineral maps (Figures 9a and 9b). Mineral maps such as these have been extensively field checked to confirm the

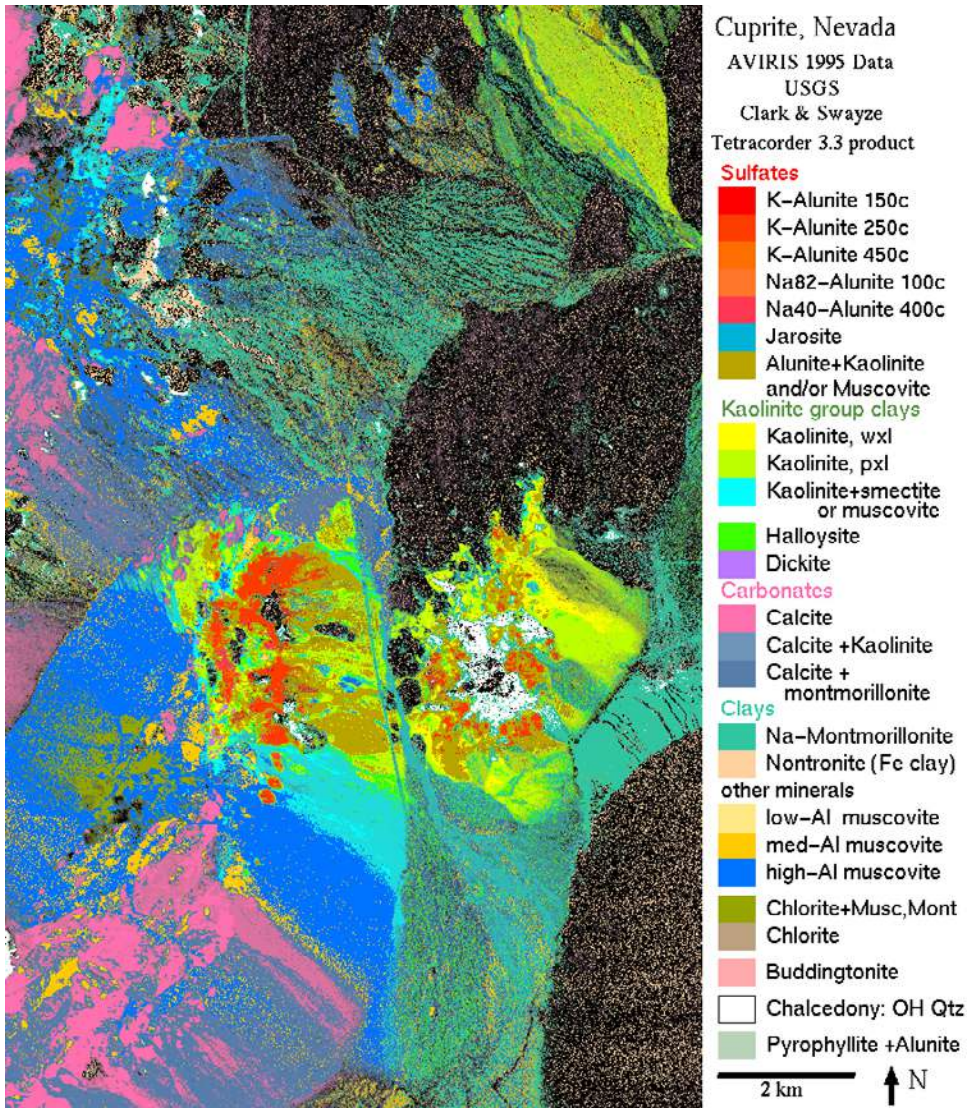

Figure 9b. Tetracorder mapping results from AVIRIS imaging spectrometer data over Cuprite, Nevada. The Tetracorder results distinguish kaolinite minerals as well as many others, show a much more limited extent of kaolinite than was seen in Figures 8a–8f and 8g, separate kaolinite from alunite areas, and also indicate where both occur as mixtures.

accuracy of the algorithm [e.g., *Swayze*, 1997]. Comparison of the images in Figure 7 and 8 to those in Figure 9 show how much more information can be derived from imaging spectroscopy compared to that from broad-band remote sensing. The minerals in Figure 9a correspond to the Tetracorder group analysis for the electronic absorptions in the visible and near-IR, while those in Figure 9b correspond to the group analysis for vibrational absorptions occurring primarily in the 2–2.5 μm wavelength region.

3.2. Decisions in Real-World Situations

[65] The decision processes we have discussed so far are straightforward but give no measure of the difficulty in making correct decisions in real-world situations. To begin, we will use data over "alunite hill" in the Cuprite scene where well-exposed outcrops of muscovite, alunite, kaolinite, and other minerals are present. Figure 10 shows index images of Cuprite from Figures 9b (mineral map) and Figure 7a (pseudo-true color) and higher spatial resolution, low-altitude AVIRIS data from 1998. Figure 10 also shows a traverse across a portion of alunite hill that has been field sampled and the fits derived from Tetracorder analyzes of low-altitude AVIRIS data for six minerals/mineral mixtures along the traverse. Of note are small differences between some of the decisions: fit value differences of <0.01 when the fit is greater than 0.95 are significant!

[66] We show in Figure 11a the mapped depths, fits, and fit × depths for six minerals plus mixtures from the analysis of the AVIRIS data that are shown in Figure 10. The band depth maps (Figure 11a, left column), where bright represents the deepest band and dark represents the shallowest, are all very similar except for the muscovite. This raises the issue of how to use these band depth maps to distinguish the minerals. The band depth maps for kaolinites, alunites, and mixtures are highly correlated, suggesting that applying a simple threshold to the images will give rise to many false

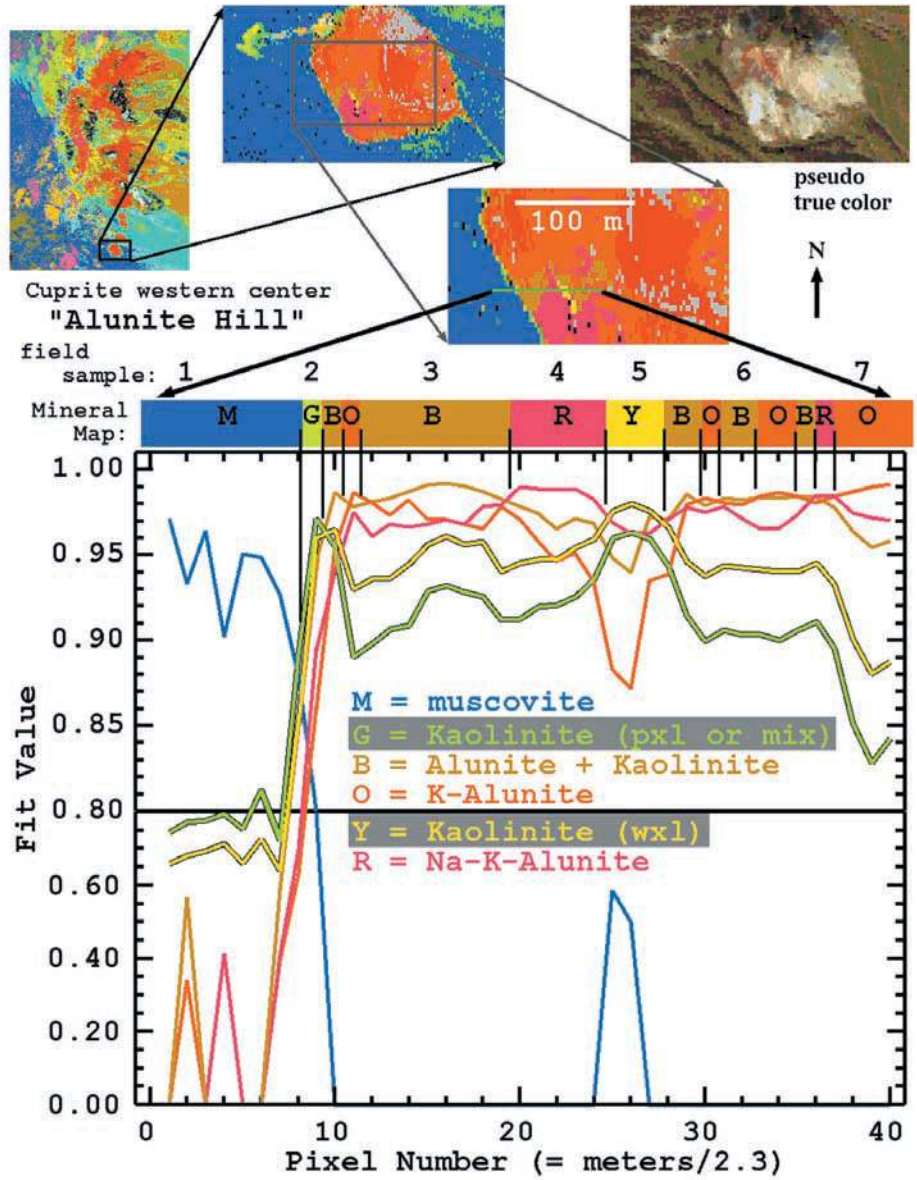

Figure 10. Tetracorder mapping over ''alunite hill.'' The upper left index image is a portion of Figure 9b for context. The other index images zooming in are low-altitude AVIRIS data from a 1998 flight having approximately 2.3 m/pixel. A traverse across a portion of alunite hill shows varying mineralogy along the traverse. The samples along the traverse line were collected and analyzed in our laboratory, including XRD analysis. The Tetracorder fit values for the six dominant minerals/mixtures are shown in the plot. Note the scale change. The colors of the curves match the colors in the map and those along the traverse line. Tetracorder chooses the highest fit in the identification process. There are subtle differences in fit values for which decisions are made: sometimes differences less than 0.01 are significant. The kaolinite outcrop labeled Y at pixel position 26 was nearly impossible to identify in the field as all rocks were similarly bleached and fine grained, but field sampling (locations numbered) at station 5 verified the Tetracorder identifications. Note the relatively small difference in fit values between kaolinite and alunite and even smaller differences between mixtures.

alarms or in other words ambiguous detections. The same is true for the fit and fit $\times$ depth data (Figure 11a, center and right, respectively).

[67] We could define a detection of a mineral where the band depth of one exceeds that of another, perhaps scaled to their relative strengths in the library of reference spectra. Such an ''identification'' based on band depth is shown in Figure 11b, left column. By choosing the maximum depth, we see that different areas show different mapped minerals. However, this method would include all the factors besides relative abundance which control band depth. Further, this method would not distinguish a pure exposure from a mixture dominated by one component or the other. Indeed, from our field data, we know the mineral maps based on

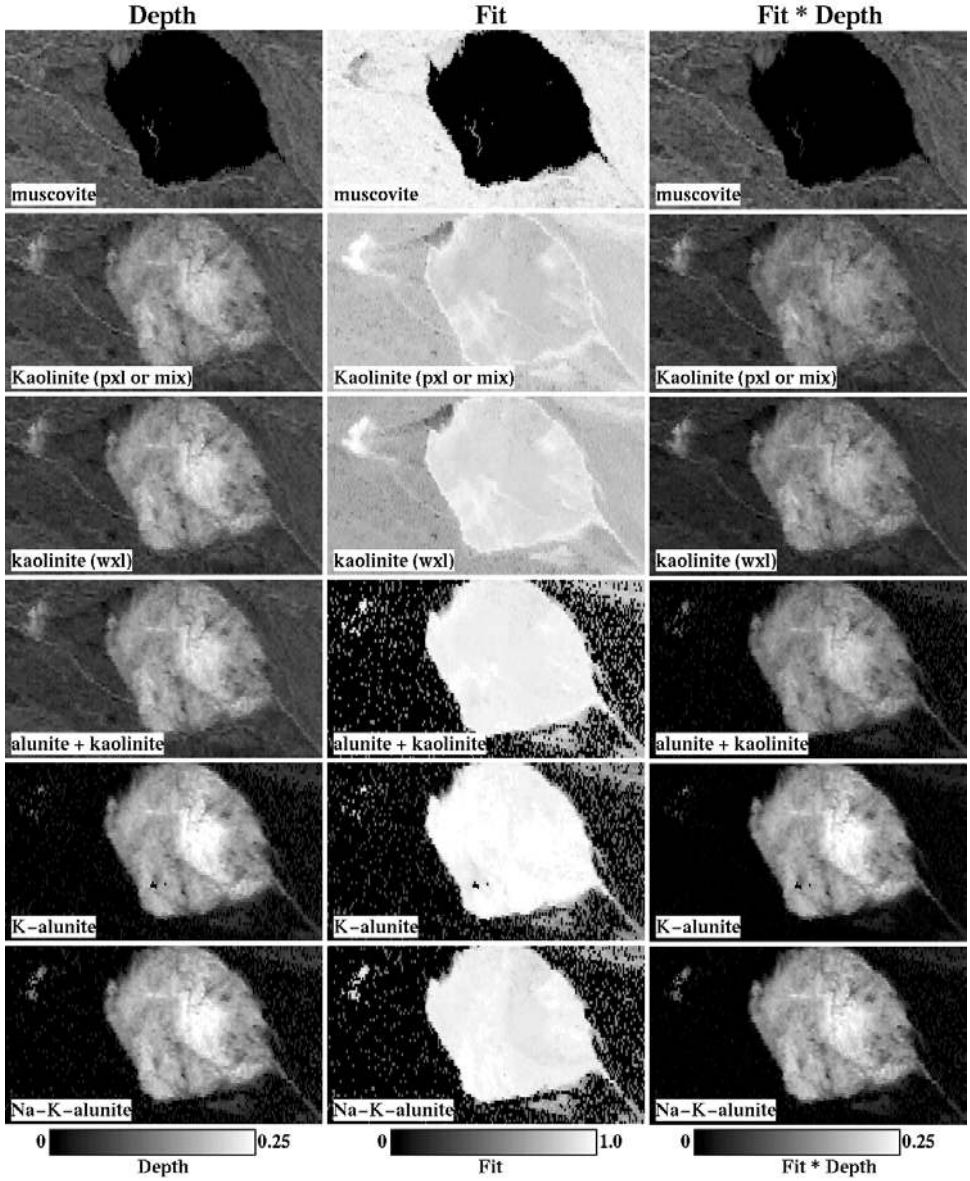

Figure 11a. The six dominant minerals/mixtures from the alunite hill traverse in Figure 10 were mapped using Tetracorder with the identification step turned off to illustrate the derived depths, fits and fit × depth images. Note the similarity of the images; the muscovite image shows the greatest difference. Most pixels show a response (illustrated as increasing brightness) to the least squares fitting of the features for each mineral. This is due to the similarity in the spectral features which all occur near 2.2 μm, not because all these materials are present in these locations. Compare with Figure 11b.

maximum depth are not correct. Neither are the maximum fit × depth maps (Figure 11b, right column).

[68] Contrast the maximum band depth maps (Figure 11b, left column) with maps of maximum goodness of fit in (Figure 11b, center column). Clearly, the patterns mapped by maximum fit are different than either maximum depth or fit * depth, but which is correct? Some have suggested that plotting the value of one parameter (like depth) on one mineral against the same parameter of another mineral would show the separation between the two (this is called a two-dimensional histogram). The degree of separation, however, is not necessarily indicative of a correct answer. Proof of the correct answer requires ground sampling to show the mapped minerals are correctly identified.

[69] We conducted a traverse across part of alunite hill, doing field sampling and subsequent X-Ray Diffraction (XRD) analysis of the collected field samples. Figure 12 shows the results for sample locations shown on Figure 10. The field sample numbers (1–7) indicate the XRD sampling locations (Figures 10 and 12). In Figure 12 the spectra of the field samples, AVIRIS spectra, and reference spectral features used to make the identifications in Tetracorder are shown. Note the subtle absorption feature shifts in the Na-K alunite compared to other alunites (the arrows on the diagram are all at the same wavelength). It is small spectral changes like these shifts that mean the difference in correct spectral identifications and why the fits between such similar spectra are so small. The XRD analysis results are shown in Table 2,

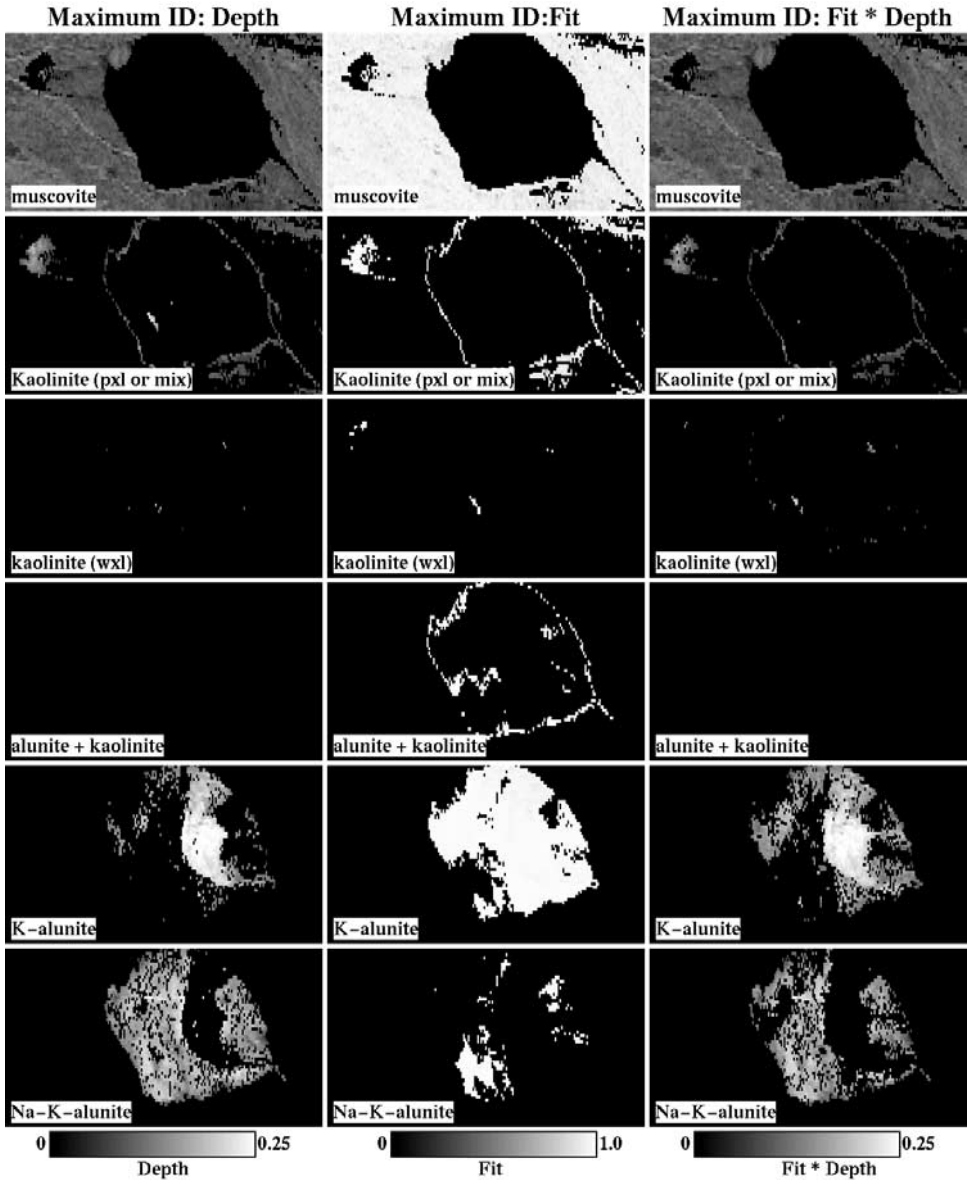

Figure 11b. Illustration of choosing the maximum value to identify materials. The depth column (left) makes an ''identification'' assuming the maximum depth, the fit column (middle) assumes the maximum fit, and the right column assumes the maximum fit × depth. For materials that are not maximum at a given pixel, the value of the pixel is set to zero. Can depth be used for identification? The alunite + kaolinite row illustrates why identification based on depth is incorrect: the depth and fit × depth columns show no alunite + kaolinite, inconsistent with field verification results. Only the identification based on fit agrees with verification data. Identification is based on spectral feature position and shape and not on feature strength.

first seven entries. The Tetracorder and XRD results for this traverse confirms that the maximum fit correctly identifies the observed mineralogy. Note the small vein of kaolinite at field sample location 5 is correctly mapped by the Tetracorder fit value (see Figure 11b, middle column). Note also that the maximum depth and fit × depth (Figure 11b) miss the alunite + kaolinite mixture, but the maximum fit correctly shows it, agreeing with the traverse results.

3.3. Tetracorder and Mixtures

[70] When different materials have widely separated spectral features and occur in different Tetracorder groups, Tetracorder deals with mixtures by explicitly detecting the separate components. By definition, a detection of more than one material constitutes a detection of a mixture. When a mixture occurs within a group the solution is more complicated. In this case, mixtures are particularly insidious because the shape of a spectrum of a mixture is a poor fit to both of the components of the mixture.

[71] A simple mixture series that illustrates Tetracorder identification of mixtures is shown in Figures 13a and 13b. Using a simple linear combination we constructed areal mixture spectra for a montmorillonite-kaolinite mixture series. In Figure 13a (top) we show the pure kaolinite

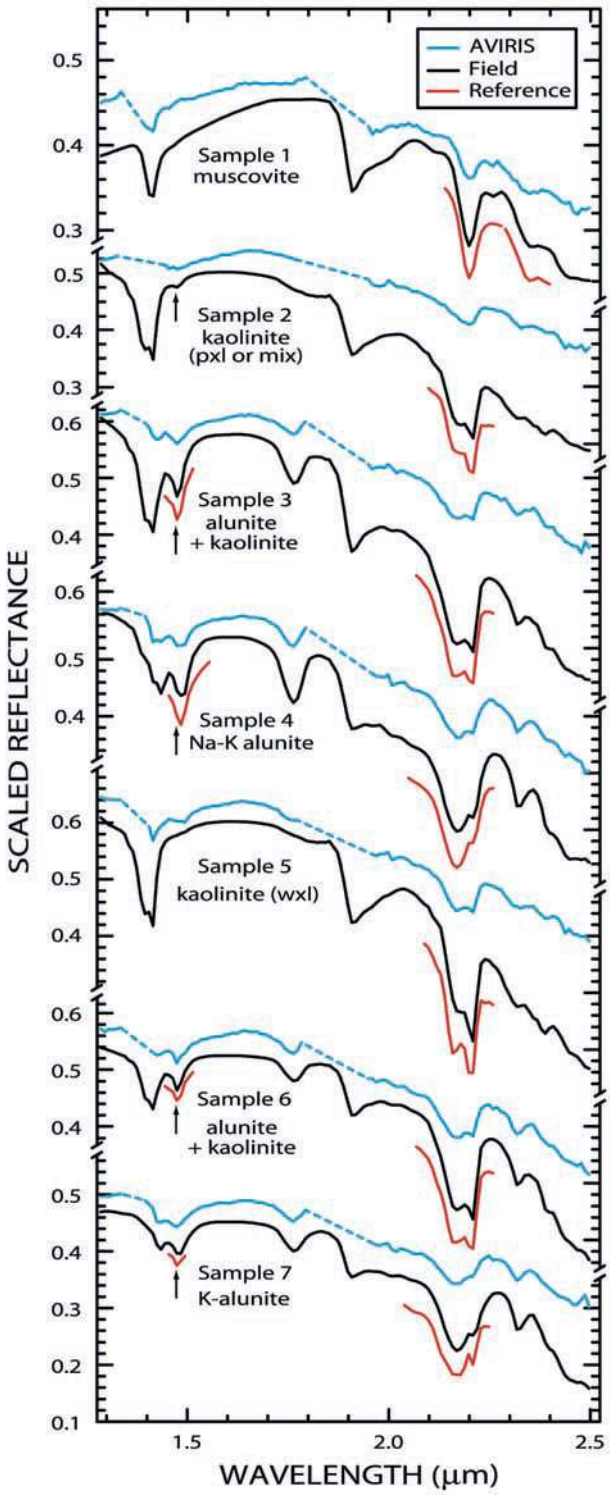

Figure 12. Spectra from the alunite hill traverse from Figure 10. The spectra from the AVIRIS pixel where a sample was collected is shown in blue, the laboratory spectrum of the field sample is shown in black, and the reference spectral feature(s) used by Tetracorder for identification are shown in red. The mineral listed is what Tetracorder found and agrees with the XRD analysis of the sample (Table 2).

(red) and montmorillonite (green) spectra and a 50-50 mix (blue). In Figure 13a (bottom) is a mixture series between the two end members. If we only used the kaolinite and montmorillonite end members and fit each of the mixtures to these end members with Tetracorder, we would derive the fit curves in Figure 13b (top). Where the kaolinite fit is higher than that for montmorillonite, kaolinite would be chosen as the answer (red on Figure 13b, top). Similarly for montmorillonite (green on Figure 13b, top). Clearly the fit value "droops" as the mixture approaches about 60:40 (the asymmetry is due to the area of the reference spectral features; see section 2.4). Mixture reference spectra need to be included if we want to identify mixtures.

[72] If we include a 50-50 mixture spectrum in the Tetracorder reference library (blue in Figure 13a), then Tetracorder can find one of three answers: pure kaolinite, pure montmorillonite, and kaolinite-montmorillonite mixture. Applying the mixture series using the three reference spectra, Tetracorder would derive the fits shown in Figure 13b, bottom. Here we see that the mixture is identified between about 27% to 82% montmorillonite, otherwise the pure end members are identified. More reference mixture spectra could be added to do finer binning of the mixture series, but note how small the differences in fit would be to distinguish between bins. Finer discrimination of kaolinite versus 50% kaolinite + 50% montmorillonite would require fit differences on the order of <0.01 with fits >0.99. The two small points plotted at the pure end members, labeled "v" in Figure 13b indicate the degradation of the fit due to an areal mixture of 50% dry, nonphotosynthetic vegetation in the spectra. The fact here is that other components will degrade the fits, so one wonders how accurately such mixtures could be separated. Add the issues of grain-size effects, coatings, intimate versus areal mixtures, and accurate fine abundance binning of the mixture series becomes problematic. We have included coarse mixture bins such as that shown here in the Tetracorder reference library to the extent we believe such mixtures can be differentiated. This solution to mixture problems is simple and surprisingly effective: we include a small number of mixtures as library entries and do not try to rigorously refine the mixture amounts.

4. Tetracorder Expert System

[73] The development of Tetracorder has been evolutionary, and early in the development process it became evident that using an expert system structure facilitated development of spectral identification methods. We regularly add new constraints, minerals, and new types of analyses to our system. Using an expert system gives us ease of modification and a logical layout for implementing our constraints as a set of parallel and hierarchical rules. However, there is no reason why our concept cannot be implemented in other ways.

[74] Specifically, an analysis of a spectrum proceeds as follows:

[75] First, before analysis of spectra, prepare the spectral library: remove the continuum from each feature, compute relative areas, and find absorption/emission minima/maxima. These computations need only be performed once, thereby speeding up the imaging spectroscopy analysis.

[76] Second, choose algorithm(s) to be applied. For the spectral feature analysis algorithm the following describes

Table 2. Example Tetracorder Verification Results[a]

Sample ID	Sample Location	Tetracorder Result	Verification
		Cuprite, Nevada	
CU02-1A CU02-1D (pixel is a linear mix of two rock types)	Alunite Hill *Wctn* traverse station 1	**goethite**, **med.high Al-muscovite**	*XRD*: CU02-1A = **muscovite** (M), quartz (m), clinochlore[b] (m); CU02-1D = albite (M), quartz (M), **muscovite** (tr), montmorillonite (tr), dickite? (tr), kaolinite (tr) *LS*: CU02-1A = **high Al-muscovite**, chlorite; CU02-1D = **trace goethite**, **med. Al-muscovite**
CU02-2A	Alunite Hill *Wctn* traverse station 2	**Fe-mineral(s)**, pxl **kaolinite** or **wxl kaolinite** + other	*XRD*: quartz (M), **wxl kaolinite** (m), dickite? (tr), K-alunite (tr) *LS*: tr. **Fe-mineral(s)**, **kaolinite**, alunite (tr)
CU02-3A	Alunite Hill *Wctn* traverse station 3	**Fe-mineral(s)**, **alunite + kaolinite**	*XRD*: quartz (M), K-**alunite** (m), **kaolinite** (m), hematite (tr) *LS*: **tr. Fe-mineral(s)**, K-**alunite + kaolinite**
CU02-4A	Alunite Hill *Wctn* traverse station 4	Fe-mineral(s), **Na-K alunite**	*XRD*: quartz (m), **K-alunite** (m), **Na-alunite** (m), calcite (tr), kaolinite (tr) *LS*: two component **alunite** (X_{Na} =.05 and X_{Na} =.74)
CU02-5B	Alunite Hill *Wctn* traverse station 5	**Fe-mineral(s)**, **wxlkaolinite**	*XRD*: quartz (M), **kaolinite** (m), calcite (tr), hematite (tr) *LS*: tr. **Fe-mineral(s)**, **wxlkaolinite**, tr. alunite
CU02-6A	Alunite Hill *Wctn* traverse station 6	**Nanohematite**, **alunite + kaolinite**	*XRD*: quartz (M), K-**alunite** (m), **kaolinite** (m), **hematite** (tr), calcite (tr), dolomite (tr) *LS*: **nanohematite**, **alunite**, **koalinite**
CU02-7A	Alunite Hill *Wctn* traverse station 7	**Fe-mineral(s)**, **K-alunite**	*XRD*: quartz (M), **K-alunite** (m) *LS*: tr. **Fe-mineral(s),** Na-K **alunite**[c]
CU91-20A	N part *Ectn*	**Jarosite**, alunite + kaolinite CUMC-1A	*XRD* of coating: K-**jarosite** *LS*: **jarosite**
CU91-228A	Central part *Wctn* along E margin	**Jarosite**, **alunite** + kaolinite CUMC-2B	*XRD* of coating: K-**jarosite** *LS*: **jarosite**, **alunite**
CU91-236A	Central part *Wctn* along W margin CUMC-3C	**Goethite**, halloysite[d] or wxl **kaolinite** + muscovite[e]	*XRD*[e]: **goethite**, **kaolinite**, quartz *LS*: **goethite**
CU91-223A	NW part of *Ectn* CUMC-4D	**Hematite**, **kaolinite**	*XRD*: pxl **hematite**, **kaolinite**, quartz, calcite, and tridymite (tr)? *LS*: **hematite and kaolinite**
CU91-238A	SW part of *Wctn* CUMC-5E	**Chlorite** + **muscovite**/illite	*XRD*: Fe-**chlorite**, **muscovite**, quartz, and kaolinite *LS*: **chlorite** and **muscovite**/illite
CU91-200A	Koalinite Hill, S part of *Ectn* CUMC-6F	**Wxl kaolinite**	*XRD*: **wxl kaolinite**, quartz, feldspar, and alunite *LS*: **wxl kaolinite**
CU00-19A	SW part of *Ectn*	**Hematite**, pxl kaolinite or **wxl kaolinite** + muscovite/**illite**/ **smectite**	*XRD*: clay separate contains **wxl kaolinite**, **smectite** (tr), and **illite** (tr) *LS*: **hematite**, pxl kaolinite or **wxl kaolinite** + muscovite/**illite/smectite**
CU00-20A	SW part of *Ectn*	**Hematite**, halloysite or **wxl kaolinite** + muscovite/**illite**/ **smectite**	*XRD*: clay separate contains wxl smectite, **wxl kaolinite**, **illite**? (tr) *LS*: **hematite**, halloysite or **wxl kaolinite** + muscovite/**illite/smectite**
CU91-242D	SW part of *Wctn* CUMC-9I	Jarosite[f] + goethite, **halloysite** or wxl kaolinite + muscovite/illite/ smectite	*XRD*[f]: **halloysite**, quartz, mica, alunite, possibly dickite *LS*: **halloysite** or wxl kaolinite + muscovite/illite/smectite
CU91-219B	Dickite Ridge, SW part of *Wctn* CUMC-10J	Jarosite[f] + goethite, **dickite**	*XRD*[f]: **dickite** plus some solid-solution with kaolinite, quartz, calcite *LS*: **dickite**
CU91-217H	Alunite Hill, SW part of *Wctn* CUMC-7G	**Na - K alunite**	*XRD*: Na-**alunite** and quartz *XRF*: alunite X_{Na} = 0.64 *LS*: **Na - K alunite** (X_{Na} = 0.65)
CU91-217G	Alunite Hill, SW part of *Wctn* CUMC-8H	Trace Fe-mineral, **K-alunite**	*XRD*: **K-alunite** and quartz *XRF*: alunite (X_{Na} = 0.05) *LS*: **K-alunite** (X_{Na} = 0.0)
CU91-6A	SE part of *Ectn* CUMC-11K	Trace Fe-mineral **hydrated quartz**	*XRD*: quartz *SEM*: **chalcedony** *LS*: **hydrated quartz**
CU93-260B	Buddingtonite Bump, W central portion of *Ectn* CUMC-12	Jarosite[f], **buddingtonite** ± Na-**montmorillonite**	*XRD*[f]: **buddingtonite** in solid-solution with K-feldspar, also quartz *LS*: **buddingtonite** and Na-**montmorillonite**
CU00-5B	S part of *Wctn*	**High Al**-muscovite/**illite**[g]	XRD: quartz (M), **illite** (both 1M and 2M2 polytypes) *EM*: **high Al-illite***LS*: **high Al**-muscovite/**illite**
CU91-252D	SW part of *Wctn* CUMC-13M	Fe-mineral(s), **med. high Al-muscovite**/illite	*XRD*: quartz (M), **muscovite** (mostly 2M1 with trace 1M polytypes), clinochlore (tr) *EM*: **med. high Al-muscovite** *LS*: **med. high Al-muscovite**

Table 2. (continued)

Sample ID	Sample Location	Tetracorder Result	Verification
CU91-250A	SW part of *Wctn* CUMC-27	Fe-mineral(s), **med. low Al-muscovite**/illite	*XRD*: quartz (M), **muscovite** (both 2M1 and 1M polytypes) *EM*: **med.low Al-muscovite** *LS*: **med. low Al-muscovite**
CU98-8H	N part of *Wctn* CUMC-26	Fe-mineral(s), **low Al-muscovite**/illite	*XRD*: quartz (M), **muscovite** (both 1M and 2M1 polytypes) *EM*: **low Al-muscovite** *LS*: **low Al-muscovite**
CU00-13A	4 km NW of *Wctn* CUMC-15	Fe-mineral(s), **nontronite**[h]	*XRD*: clay separate contains **smectite**[h,i] (M), kaolinite (tr), mica (tr) *LS*: **nontronite**
CU00-2C	Near Buddingtonite Bump, W central portion of *Ectn*	Fe-mineral(s), **NH_4-smectite**	XRD: quartz (M), sanidine (M), orthoclase (M), cristobalite (M), **montmorillonite** (tr)[j,k] *LS*: **NH_4-smectite**.
		Leadville, Colorado	
LV96-1GH	Venir Pile 30 m station	**Goethite**[l], **muscovite**/illite	*XRD*[l]: bulk: quartz (M), **muscovite** (m), microcline (tr), Albite (tr), K-jarosite (tr), clinochlore (tr), kaolinite (tr), ankerite (trace?) *LS*: **goethite** and **muscovite**/illite
LV96-1KL	Venir Pile 50 m station	**Jarosite** + **goethite**, muscovite/**illite**	*XRD*[l]: surface: quartz (M), amorphous component (M), K-**jarosite** (tr), **illite** (tr) orthoclase (tr), kaolinite (tr) *LS*: **jarosite** + **goethite**, muscovite/**illite**
LV96-1QR	Venir Pile 80 m station	**Jarosite** + **goethite** muscovite/**illite**	*XRD*: *surface*: quartz (M), amorphous component (M), K-**jarosite** (M), **illite** (tr), goethite (tr), kaolinite (tr) *LS*: **jarosite** + **goethite**, muscovite/**illite**
LV96-1UV	Venir Pile 100 m station	**Jarosite**, **muscovite/illite**	*XRD*: surface: **muscovite** (M), **illite** (M), amorphous component (M), quartz (m), K, H3O-**jarosite** (m), Na-**jarosite** (tr), plagioclase (tr), K-feldspar (tr) *LS*: **jarosite**, **muscovite/illite**
LV96-1A2B	Venir Pile 130 m station	**Jarosite, muscovite**/illite	*XRD*: bulk: quartz (M), **muscovite** (m), pyrite (m), K, H3O-**jarosite** (tr), microcline (tr), kaolinite (tr), amorphous component (tr). *LS*: **jarosite**, **muscovite**/illite.
LV96-1E2F	Venir Pile 150 m station	**Jarosite**, **muscovite**/illite	*XRD*: surface: quartz (M), **muscovite** (m), coquimbite (m), pyrite (m), amorphous component (m), orthoclase (tr), kaolinite (tr). Bulk: quartz (M), coquimbite (m), K,H3O-**jarosite** (tr), pyrite (tr), montmorillonite (tr), **muscovite** (tr), kaolinite (tr), lanarkite (trace?). *LS*: **jarosite, muscovite**/illite
LV96-1M2N	Venir Pile 190 m station	**Goethite, muscovite**/illite	*XRD*: surface: quartz (M), **geothite** (m), **muscovite** (m), K-jarosite[m] (m), amorphous component (tr) *LS*: **geothite, muscovite**/illite
LV96-1O2	Venir Pile 200 m station	**Goethite**, muscovite/**illite**	*XRD*: surface: quartz (M), amorphous component (M), K-jarosite (m), **geothite**[j] (tr), **illite** (tr) *LS*: **geothite**, muscovite/**illite**
LV95-25	Apache Tailings	**Copiapite**	*XRD*: bulk: quartz, sulfur, H_3O-jarosite, Na-jarosite, **ferricopiapite**, gypsum, fibroferrite, **copiapite**. XRD sample from approximately the same site as AVIRIS pixels
Tailings	Oregon Gulch Tailings	**Pyrite**	*FM*: **pyrite** as identified by its crystal morphology and brassy color
Water	Lakes, streams	**Water**	*FM*: **water** agrees with published maps and field observations
Vegetation	General-all over scene	**Vegetation**	*FM*: **vegetation** agrees with published maps and field observations
		Arches National Park, Utah	
Morisson Formation	Morisson Formation, Arches N. P.	**Fe^{2+}mineral(s)**, muscovite/**illite**	*FM*: **Fe-illite**, agreement with published geologic map [*Doelling*, 1985]
Mancos Shale	Mancos Shale, Arches N. P.	**Goethite, montmorillonite**	*FM*: **goethite, smectite**, agreement with published geologic map [*Doelling*, 1985]
Water	Colorado River and small lakes, Arches N. P. region	**Water**	*FV*: **water**, agreement with published maps and field observations (e.g., the Colorado River)
Dry grass	Dry grass, Arches N. P. region	**Dry** long **grass**	*FV*: **dry grass**, various types
Green grass	Farm field s of Colorado rover	Lawn **grass**	*FV*: green **grass** farm field, lawns in the town of Moab
ANP90-14	Desert varnish, Arches N. P.	**Desert varnish**	*FV*: **desert varnish**, float from outcrops near Wolf Ranch.
ANP91-15G	Upper Chinle Formation	**Hematite**, muscovite/**illite**	*FM*: **hematite, illite**, agreement with published geologic map [*Doelling*, 1985]

Table 2. (continued)

Sample ID	Sample Location	Tetracorder Result	Verification
ANP93-10A	Upper Ferron Sandstone Mb.	**Fe^{2+}**-bearing mineral + hematite[f] (**Fe^{3+}**) **kaolinite-muscovite**/illite intimate mix	*XRD*[f]: **muscovite**, quartz, calcite, microcline, orthoclase *FM*: **goethite, kaolinite group**, agreement with published geologic map [*Doelling*, 1985] *LS*: hematite or goethite **(Fe^{3+})** with **Fe^{2+}**-bearing mineral, **kaolinite** group mixed with weak **muscovite**/illite
ANP93-10B	Upper Ferron Sandstone Mb.	**Fe^{2+}**-bearing mineral[5], **calcite**	*XRD*[f]: **calcite**, quartz. *FM*: agreement with published geologic map [*Doelling*, 1985] *LS*: weak **Fe^{2+}**-bearing mineral, kaolinite group, **calcite**
ANP93-8	Middle Ferron Sandstone Mb.	**Goethite**[f] (coarse grained), **kaolinite** + **muscovite**/illite intimate mix	*XRD*[f]: **calcite**, **kaolinite**, quartz, albite, orthoclase *FM*: agreement with published geologic map [*Doelling*, 1985] *LS*: **goethite**, **kaolinite** group, **muscovite**/illite.
ANP93-12	Lower Ferron Sandstone Mb.	**Goethite**, **muscovite**/illite	*FM*: agreement with published geologic map [*Doelling*, 1985] *LS*: **geothite**, trace kaolinite group, **muscovite**/illite
ANP93-14	Entrada sandstone, Delicate Arch Trail	Nano**hematite**[f], **kaolinite** + **muscovite**/illite intimate mix	*FM*: agreement with published geologic map [*Doelling*, 1985]. *XRD*: calcite, **kaolinite**, quartz, orthoclase *LS*: **hematite** (poorly crystallized), **kaolinite** group, **muscovite**/illite, trace calcite
ANP91-22	Cedar Mountain Formation	**Fe^{2+}**-bearing mineral[f], **kaolinite** + muscovite/**illite** intimate mix	*XRD*[f]: **calcite**, **illite**, quartz, orthoclase, poorly crystalline illite or clays *FM*: agreement with published geologic map [*Doelling*, 1985]. Blue-green color consistent with Fe^{2+}**illite** *LS*: **Fe^{2+}**-bearing minerals, **calcite**, **kaolinite** + muscovite/**illite**
		Canyonlands National Park, Utah	
CNP91-18	Wingate Sandstone	**Hematite**[f], halloysite/**kaolinite** mix	*XRD*[f]: trace **kaolinite***FM*: **hematite**, agreement with published geologic map [*Huntoon et al.*, 1982] *LS*: **hematite, kaolinite group** minerals.
CNP91-15	Keyanta Formation	**Hematite**[f], **dolomite**	*XRD*[f]: **dolomite, kaolinite**, calcite, quartz, orthoclase *FM*: agreement with published geologic map [*Huntoon et al.*, 1982] *LS*: **hematite, dolomite**, trace clay at 2.2-μm
CL00-3A	Upheaval Dome Area	Amorphous Fe-hydroxide (weak **Fe^{3+}**), **calcite** + **dolomite**.	*LS*: weak **Fe^{3+}** and weaker Fe^{2+} absorptions, **calcite** + **dolomite**
Water	Lakes, streams	**Water**	*FM*: agrees with published maps and field observations of **water**
Vegetation	General-all over scene	**Vegetation**	*FM*: agrees with published maps and field observations **vegetation**
		Oquirrh Mountains region, Utah	
MKR99-81	Mercur Canyon outwash, Utah 40°17′38.73″N 112°16′31.06″W	**Goethite**[f], pxl **kaolinite** or **kaolinite** + **muscovite**	*XRD*[f]: quartz (M), **kaolinite** (m), calcite (m), dickite (m), gypsum (m), **muscovite** (tr), plumbogummite (tr) *LS*: **goethite, kaolinite**
MKR99-88	Mercur Canyon outwash, Utah 40°13′59.09″N 112°17′28.50″W	**Goethite**[f], halloysite[d] or **kaolinite** + **muscovite**	*XRD*[f]: quartz (M), calcite (m), **kaolinite** (m), dickite (m), **muscovite** (m), albite (tr), plumbogummite (tr) *LS*: **goethite, kaolinite**
MKR00-89	Mercur Canyon outwash, Utah 40°14′03.45″N 112°17′21.00″	**Goethite**[f], halloysite[d] or **kaolinite** + **muscovite**	*XRD*[f]: quartz (M), calcite (m), **kaolinite** (m), dickite (m), **muscovite** (tr), albite (tr), plumbogummite (tr) *LS*: **goethite, kaolinite**
MKR99-90	Mercur Canyon outwash, Utah 40°14′11.05″N, 112°17′23.51″W,	**Goethite**[f], halloysite[d] or **kaolinite** + **muscovite**	*XRD*[f]: quartz (M), calcite (M), **kaolinite** (m), dickite (m), **muscovite** (m), albite (tr), dolomite (tr) *LS*: **goethite, kaolinite**
MKR99-94	Mercur Canyon outwash, Utah 40°17′45.61″N 112°16′29.83″W	**Goethite**[f], halloysite[d] or **kaolinite** + **muscovite**	*XRD*[f]: quartz (M), **kaolinite** (m), calcite (m), **muscovite** (m), albite (tr), orthoclase (tr), dolomite (tr) *LS*: **goethite, kaolinite**
MKR99-95	Mercur Canyon outwash, Utah 40°17′47.20 N 112°16′31.68″W	**Goethite**[f], halloysite[d] or **kaolinite** + **muscovite**	*XRD*[f]: quartz (M), calcite (M), **kaolinite** (tr), albite (tr), orthoclase (tr), dolomite (tr), **muscovite** (tr) *LS*: **goethite, kaolinite**
MKR99-96	Mercur Canyon outwash, Utah 40°17′49.41″N 112°16′33.70″W	Other **Fe^{3+}bearing** minerals	*XRD*: quartz (M), calcite (M), kaolinite (m), muscovite (m), albite (tr), orthoclase (tr), dolomite (tr) *LS*: **Fe^{3+}mineral**
MKR99-97	Mercur Canyon outwash, Utah 40°17′44.70″N 112°16′28.31″W	**Calcite** + **muscovite**	*XRD*: quartz (M), kaolinite (m), dickite (m), **calcite** (m), **muscovite** (tr), orthoclase (tr), plumbogummite (tr) *LS*: **goethite, kaolinite, calcite** (acid fizz)

Table 2. (continued)

Sample ID	Sample Location	Tetracorder Result	Verification
MKR99-98	Mercur Canyon outwash, Utah 40°17′39.40″N 112°16′25.31″W	**Goethite**[f], halloysite[d] or **kaolinite** + **muscovite**	*XRD*[f]: quartz (M), calcite (M), **kaolinite** (tr), dickite (tr), gypsum (tr), **muscovite** (tr), orthoclase (tr) *LS*: **goethite, kaolinite**
MKR99-100	Mercur Canyon outwash, Utah 40°17′34.02″N 112°16′22.33″W	**Fe^{3+}-bearing mineral, calcite, muscovite**	*XRD*[f]: **calcite** (M), quartz (M), **muscovite** (tr), albite (tr), orthoclase (tr), dolomite (tr), kaolinite (tr) *LS*: **Fe^{3+}mineral, muscovite, calcite**
MKR99-101	Mercur Canyon outwash, Utah 40°17′31.54″N 112°16′20.19″W	**Nanohematite**	*XRD*[f]: quartz (M), calcite (M), dolomite (tr), albite (tr), magnesiohornblende (tr), muscovite (tr), orthoclase (tr) *LS*: weak Fe^{3+} consistent with **very fine grained hematite** (e.g., nanohematite)
Water	Lakes, streams	**Water**	*FM*: **water** agrees with published maps and field observations
Vegetation	General-all over scene	**Vegetation**	*FM*: **vegetation** agrees with published maps and field observations
		Summitville, Colorado	
SM93-101	Quartz Latite Porphery, Mine area	**Alunite**	*FV*: hand specimen identified as **alunite** *LS*: Na-**alunite**.
SM93-14A	Mine area, edge of pond	"Green slime" copper bearing soil, jarosite	*XRD*[f]: quartz (m) other phases amorphous and uncertain. *FM*: sample collected from this location is the reference spectrum for copper-bearing soils. Tetracorder maps observed locations as "green slime." *LS*: peak at 0.55 μm characteristic of a copper-bearing solid
BZ93-1	Deposits on banks and rocks downstream from alteration zones	**Schwertmannite** (poorly crystallized **Fe^{3+}-bearing mineral**)	*XRD*: **Schwertmanite** possible near detection limit, otherwise only quartz (tr) *LS*: poorly crystallized **Fe^{3+}-bearing mineral**
SU93-103	Summitville Mine	**Alunite**	*XRD*: quartz (M), **alunite** (M), pyrite (tr), kaolinite (tr), *LS*: **alunite**
SU93-106	Summitville Mine	Amorphous Fe-hydroxide (**Fe^{3+}** absorption), muscovite + jarosite	*XRD*[f]: quartz (M), phlogopite (m), albite (m), microcline (m) *LS*: **Fe^{3+}**-bearing coating
Water	Lakes, streams	**Water**	*FM*: **water** agrees with published maps and field observations
Vegetation	General-all over scene	**Vegetation**	*FM*: **vegetation** agrees with published maps and field observations
		Mountain Pass, California	
Calcite	Calcite, Mtn Pass	**Calcite**	*GM*: **calcite** (acid fizz)
Dolomite	Dolomite, Mtn Pass	**Dolomite**	*GM*: **dolomite**
Epidote	Epidote, Mtn Pass	**Epidote**	*GM*: **epidote**
MP395r3A	Mohawk Hill	**Calcite**	*XRD*: **calcite** (M), vermiculite-2M (M), clinochrysotile-1Mc1 (m), orthochrysotile-6Oc1 (m), dolomite (tr), quartz (tr), *LS*: **calcite** (acid fizz)
MPBWA	Mtn Pass	**Goethite**[f], **muscovite**	*XRD*[f]: **muscovite**-3T (m). quartz (m) albite (M), clinochrysotile-2Mc1 (tr) *LS*: **goethite, muscovite**/illite
MPCMA2a	Coliseum mine area	**Goethite, muscovite**	*XRD*: **muscovite**-3T (m). illite-2M1 (m). quartz (m) microcline, (m) albite (m), **goethite** (tr) *LS*: **goethite, muscovite**/illite
MPCMA2b	Coliseum mine area	**Goethite, muscovite**	*XRD*[f]: **muscovite**-2M1 (m), quartz (m), microcline (m) albite (m), calcite (tr) *LS*: **goethite, muscovite**/illite.
MPCMA2f	Coliseum mine area	**Goethite** (coarse grained), **muscovite**	*XRD*: **goethite** (m), quartz (m), orthoclase (tr),, **muscovite**-2M1 (tr) *LS*: coarse grained **goethite, muscovite**/illite
MPCM1.a-a	Coliseum mine area	**Siderite**, **Fe^{2+}**	*XRD*: **siderite** (M), pyrite (M), muscovite-2M1 (tr), quartz (tr) *FV*: pyrite, **siderite** *LS*: **siderite**, strong **Fe^{2+}**, trace 2.2-μm absorption
MH395B.1	Mohawk Hill	**Calcite** + **dolomite**	*XRD*: **calcite** (M), **dolomite** (m), vermiculite-2M (m), clinochrysotile-2Mc1 (tr) and/or lizardite-1T (tr), quartz (tr), albite (tr) *LS*: **calcite** (acid fizz) + OH bearing phase
MH395Br3a,B	Mohawk Hill	**Calcite + dolomite**	*XRD*: orthochrysotile-6Oc1 (M), clinochrysotile-2Mc1 (M),: lizardite-1T (m), **calcite** (m), quartz (tr), kaolinite-1Md (tr), **dolomite** (tr), muscovite-2M1 (tr) *LS*: lizardite or chrysotile
MPCMA	Coliseum mine area	**Jarosite**[f], **muscovite**	*XRD*[f]: quartz (M), **muscovite**-2M1 (m), calcite (tr), pyrite (tr), vermiculite-2M (tr), lizardite-1T (tr) and/or clinochrysotile-2Mc1 (tr) *LS*: **jarosite, muscovite**/illite

Table 2. (continued)

Sample ID	Sample Location	Tetracorder Result	Verification
		Barstow, California	
BR93-5A	Galway Dry Lake Area	**Fe^{2+}**	*XRD*: actinolite (M), tremolite (M), phlogopite (m), **chlorite**-clinochlore (tr) *LS*: **Fe^{2+}**
BR93-5B	Galway Dry Lake Area	**Fe^{2+}, hematite**	*XRD*: phlogopite (M), magnetite (m), magnesioferrite (m), albite (tr) *LS*: **hematite** and mineral with broad **Fe^{2+}** band.
BR93-20	Red Hill Area	**Fe^{2+}**	*XRD*: phlogopite (M), albite (m), microcline (m), chlorite-clinochlore (m), actinolite (tr?), magnesiohornblende (tr?) *LS*: very broad **Fe^{2+}** band. Weak 2.3-μm features consistent with amphiboles.
BR93-22B	Bessemer Mine	**chlorite**	*XRD*: lizardite (M), orthochrysotile (tr), antigorite (tr), **chlorite**-clinochlore (tr) *LS*: **chlorite**
BR93-22C	Bessemer Mine	**Fe^{2+}**	*XRD*: albite (M), actinolite (M), tremolite (M), microcline (tr) *LS*: **Fe^{2+}** (amphibole?), tremolite
BR93-25A	Red Hill	**Hematite**	*XRD*: quartz (M), albite (m), microcline (m), **hematite** (tr), muscovite (tr) *FV*: desert varnish on quartzite *LS*: **hematite**, kaolinite, muscovite (tr)
BR93-25B	Red Hill	**Hematite**	*XRD*: quartz (M), albite (m), microcline (m), muscovite (m), **hematite** (tr) *FV*: desert varnish on quartzite *LS*: **hematite**, kaolinite, muscovite (tr)
BR93-25C	Red Hill	**Hematite**	*XRD*: **hematite** (m), quartz (m), jarosite (m), albite (m), muscovite (m), kaolinite (m), goethite (tr) *FV*: desert varnish on quartzite *LS*: **hematite**, kaolinite, muscovite (tr)
BR93-33	Rodman Mtns	**Epidote**	*XRD*: **epidote** (M), albite (M), quartz (M) *FV*: **epidote** veins within biotite quartz monzonite *LS*: **epidote**
BR93-34A	Rodman Mtns	**Jarosite**	XRD: **jarosite** (good standard), goethite (tr) *FV*: **jarosite** on quartzite, muscovite *LS*: **jarosite**
BR93-34A2	Rodman Mtns	**Jarosite**, **muscovite**	*XRD*: quartz (M), **jarosite** (m), muscovite (tr) *FV*: **jarosite** on quartzite, **muscovite** *LS*: **jarosite**, **muscovite**
BR93-34B2	Rodman Mtns	**Hematite, kaolinite + muscovite**	*XRD*[f]: quartz (M), **muscovite** (m), orthoclase (m), albite (m) *FV*: **hematite** on quartzite, **muscovite** *LS*: nanocrytalline **hematite, kaolinite + muscovite**
BR93-34C	Rodman Mtns	**Hematite**	*XRD*: quartz (M), **hematite** (m), pinnoite (tr) *FV*: **hematite** on quartzite, muscovite *LS*: **hematite**
BR93-34D2	Rodman Mtns	**Hematite** (nanohematite)	*XRD*: quartz (M), **hematite** (m), muscovite (tr) *FV*: hematite on quartzite, muscovite *LS*: hematite spectral structure consistent with **nanohematite** with some fine-grained hematite
BR93-36A	Rodman Mtns	**Fe^{2+}**	*XRD*: quartz (m), albite (m), microcline (m), biotite (tr), pyrite (tr) *LS*: **Fe^{2+}**
BR93-43	Newberry Mtns	**Fe^{2+}, hematite**	*XRD*: Calcite (M), anorthite (m), augite (m)(source of **Fe^{2+}**), **hematite** (m), montmorillonite (tr) *FV*: purple iron-oxide coated tuff *LS*: **Fe^{2+}**, **hematite**, 2.3-μm feature (tr)
BR03-46B	Newberry Mtns	**Fe^{2+}**	*XRD*: anorthite (M), tridymite (m), cristobalite (m), augite (m) (**Fe^{2+}** source), quartz (m) *FV*: desert varnish on basalt *LS*: **Fe^{2+}**
BR93-60B	Galway Dry Lake Area	**Fe^{2+}**	*XRD*: calcite (M), antigorite (m), clinochlore (m), lizardite (m) orthochrysotile (m), dolomite (tr) *FV*: desert varnish on limestone *LS*: **Fe^{2+}**
		Joshua Tree National Park, California	
JT96-120Aa	Epidote Ridge	**Epidote**	*XRD*: **epidote** (M), quartz (tr), orthoclase (tr) *FV*: green hand specimens characteristic of **epidote** *LS*: **epidote**

Table 2. (continued)

Sample ID	Sample Location	Tetracorder Result	Verification
JT96-120Ab	Epidote Ridge Region	**Calcite** + Ca-**montmorillonite**, goethite (**Fe^{3+}** thin film)	*FV*: **calcite** (acid fizz). Calcite forms a caliche coating. *LS*: **calcite, montmorillonite**, trace **Fe^{3+}**-absorption
JT96-120Ac	Epidote Ridge Region	**Weak Fe^{2+}, calcite** + **montmorillonite**	*FV*: **calcite** (acid fizz) *LS*: **weakFe^{2+}** absorption, **calcite** + **montmorillonite**/muscovite/illite
JT96-120B	Epidote Ridge Region	**Dolomite, trace Fe^{2+}**	*XRD*: **dolomite** (M), calcite (m), quartz (tr), clinochlore (**trace Fe^{2+}**) *FV*: characteristic dolomite appearance and weathering pattern *LS*: **dolomite**, trace **Fe^{2+}**
JT96-112A	E Joshua Tree	**Calcite** + montmorillonite, **very broad Fe^{2+}**	*XRD*: **calcite** (tr), clinochlore (tr), phlogopite (m), microcline (tr), albite (tr), quartz (M) *FV*: **calcite** (acid fizz) Calcite in caliche soil *LS*: **calcite**, 2.2-μm phyllosilicate (weak), **very broad Fe^{2+}** from clinochlore+phlogopite
JT96-118	Epidote Ridge	**Fe^{2+}**, chlorite	*XRD*: quartz (M), albite (M), magnesiohornblende (m), goethite (tr) *LS*: **Fe^{2+}** bearing minerals, 2.3-um band is from an amphibole
JT96-116-209A	E Joshua Tree	**Muscovite**	*XRD*: quartz (M), jarosite (tr), **muscovite** (m) *LS*: **muscovite**
JT96-116-209B	E Joshua Tree	**Muscovite**	*XRD*: quartz (M), clinochlore (tr), **muscovite** (tr), albite (tr) *LS*: **muscovite**

[a]Entries in bold indicate agreement between Tetracorder and verification results. *XRD* = X-ray diffraction analysis; *LS* = laboratory spectroscopy; *XRF* = X-ray fluorescence; *SEM* = scanning electron microscopy; *EM* = electron microscopy; *FM* = field mapping; *FV* = field verification (methods commonly practiced by a field geologist); X_{Na} = mole fraction Na (*XRF* assumes a single alunite phase); wxl = well crystallized; pxl = poorly crystallized. CUMC = Cuprite Map Code from *Swayze* [1997]. Approximate XRD abundance indicators: (M) = major component 20wt% or more; (m) = minor 5–20 wt%; (tr) = trace <5 wt%. N = north; E = east; W = west; S = south; *Ectn* = eastern center; *Wctn* = western center. Bulk = ground up sample; surface = optical surface. Mercur Canyon field sample positions accurate to ±4m (positions based on NAD83 datum).

[b]Clinochlore is a type of chlorite.

[c]Sample may have been collected just south of the traverse where two component alunite dominates.

[d]Halloysite, in the kaolinite group, is spectrally similar to kaolinite mixtures with muscovite, illite, or montmorillonite and is sometimes confused, especially at low abundances.

[e]*XRD* may not detect low abundances of muscovite.

[f]Trace hematite, goethite, jarosite, and other Fe^{3+}-bearing minerals can be difficult for XRD to detect, even when red and yellow Fe^{3+} colors are present in the sample.

[g]Spectroscopy cannot differentiate muscovite from illite at AVIRIS spectral resolution.

[h]Nontronite is a type of smectite.

[i]*XRD* unable to identify specific mineralogy of smectite.

[j]The *XRD* database does not have an example of a NH_4-smectite.

[k]Montmorillonite is a type of smectite.

[l]XRD analysis may not detect poorly crystalline goethite [*Swayze et al.*, 2000].

[m]Jarosite may be converted to goethite on rock surfaces by exposure to precipitation [*Swayze et al.*, 2000].

the analysis sequence. Other algorithms could have a different sequence. The sequence is repeated for all entries in all groups.

[77] 1. Apply initial algorithms, if necessary (e.g., data conversions; ratio to a specific curve or spectrum).

[78] 2. Remove the continuum for each spectral feature in the unknown using the same continuum wavelengths as those defined in the reference library spectrum (equation (1b)).

[79] 3. Perform a feature-fitting shape analysis deriving a "fit" parameter for each spectral feature of each material (equation (7)).

[80] 4. Apply constraints regarding the presence of diagnostic and optional features, continuum level, and slope constraints (equation (10)) to each feature.

[81] 5. Derive the weighted fit (equation (8)) for each material which passes the constraints of step 4.

[82] Third, apply constraints regarding the goodness of fit values (threshold values).

[83] Fourth, find the highest fit for each material in each group: this is the best answer in each group.

[84] Fifth, implement further analysis (e.g., determine vegetation red edge or apply other algorithms not directly involved in detection but contingent on a particular detection). These are cases. A case can call another case, so an answer from the fourth step can lead to multiple additional answers.

[85] Finally, write results of all analyses. We record three results: the weighted fit, weighted depth and weighted fit × depth for each library entry. For those materials not chosen in the fourth and fifth steps, the results are set to zero. For a Tetracorder imaging spectroscopy analysis using 300 reference materials, 900 output images are created. Note, that for AVIRIS data with 224 spectral channels, the Tetracorder output can be greater than the input (more output fit images than input wavelengths).

4.1. Expert System Lessons Learned

[86] Reflectance and emittance spectra of mixtures typically found in nature are complex not only because of the numerous mixture possibilities but also because of the

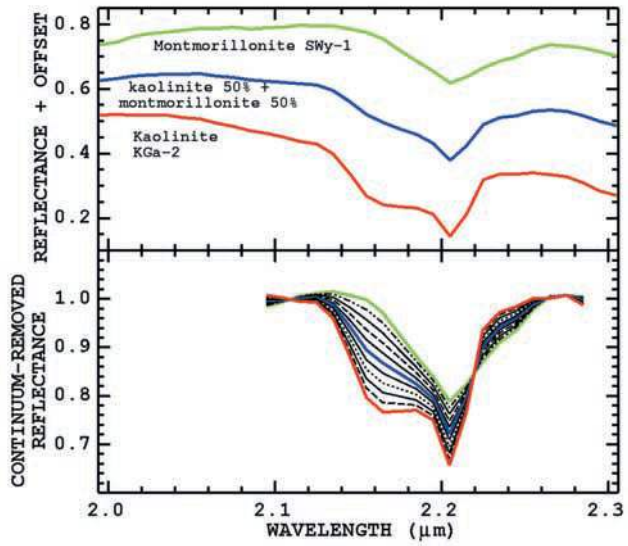

Figure 13a. Montmorillonite-kaolinite areal mixture series. End members montmorillonite (green) and kaolinite (red) spectra and a 50-50% mixture in blue are shown (top). A mixture series at 10% intervals for a continuum removed spectral feature is shown (bottom).

multiple scattering typically encountered by photons interacting with a particulate surface [*Clark*, 1999 and references therein]. Thus spectroscopic analysis must handle such conditions, including changes in grain size (Figure 5), abundance in a mixture (Figure 4), overlapping absorption bands from multiple materials in a mixture (Figure 4), level shifts due to incident lighting, the finite spectral bandpass of each spectral channel, and the spectral sampling. In developing, testing, and verifying Tetracorder accuracy, we learned many lessons. Here are some of the important ones.

[87] Continuum-removed kaolinite and montmorillonite spectra are shown in Figure 13a. How is it best to distinguish between these two minerals as well as other possible materials? The end points to the continuum-removed spectra, by definition, average 1.0 after normalization, and because all spectra are analyzed similarly, it may seem that using the continuum end points would not help in a least squares analysis. However, by comparing identification success as a function of signal-to-noise ratio we found that including continuum end points significantly improves identification success [*Swayze et al.*, 2003].

[88] Using fit thresholding, Tetracorder finds nothing in the spectrum as the spectral features become too weak to identify, rather than identify the wrong material. The fit threshold appears in the expert rules tables (electronic supplement) as parameters with "FIT" in their labels.

[89] Some minerals have a main diagnostic absorption plus a few subordinate absorptions, which if detected further indicate the presence of that material. Can the weaker features help in identification? Comparing identification accuracy with and without the weaker features, we found that weak features do not help [*Swayze et al.*, 2003].

[90] Sometimes an absorption occurs at a similar wavelength position as an absorption in some other material. Such is the case with some Fe^{3+}-bearing minerals (Figure 1a), plants with chlorophyll absorption, and some photosynthetic bacteria and algae. For example, goethite has a UV absorption near 0.5 μm, an absorption near 0.65 μm, and an absorption near 1-μm (Figure 1a), but chlorophyll in plants has an intense 0.6 to 0.7-μm absorption centered at nearly the same location as the middle goethite feature. Trace vegetation contributing to a spectrum can appear to intensify the 0.65-μm Fe^{3+} absorption and can change its shape. Thus we do not use the 0.65-μm feature when trying to identify Fe^{3+}-bearing minerals. Confusion with other spectral features that

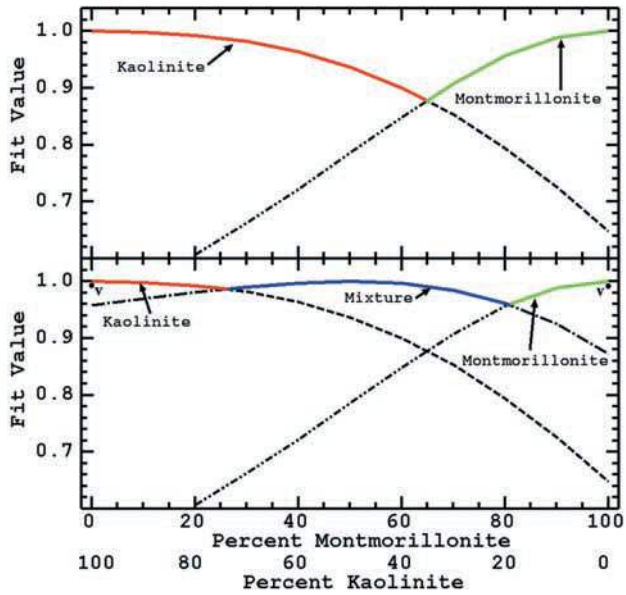

Figure 13b. The Tetracorder feature fits for the mixture series in Figure 13a are shown. If the end member kaolinite feature is fit to each mixture spectrum, the correlation coefficient (the fit) is shown as the red or dashed line. For the montmorillonite feature fit to the mixture spectra, the fit values are shown in green or dash-dot-dot. If only the end member reference spectra are used by Tetracorder (top), Tetracroder would derive a kaolinite or montmorillonite answer where the curve is colored red or green, respectively. The crossover point occurs at about 65% montmorillonite. So any kaolinite-montmorillonite mixture with more than 35% kaolinite would be identified as kaolinite. However, if Tetracorder included one 50%-50% kaolinite-montmorillonite mixture reference spectrum (bottom), kaolinite abundances from about 73% to 18% kaolinite (27% to 82% montmorillonite) would be identified as a kaolinite-montmorillonite mixture. More mixtures could be added to the reference library, but the differences between mixtures and therefore the fit differences needed to identify different mixture abundances becomes correspondingly less. Other factors, including grain-size effects, coatings, and other components such as vegetation contributing to the spectral signature confuse accurate mixture abundance determinations. For example, 50% dry-vegetation cover reduces the fit of the pure end members slightly (designated by the points labeled "v" on the bottom plot).

are not handled correctly in the expert system are described in the deficiencies section 5.

4.2. Tetracorder Groups and Cases

[91] We have chosen to program the Tetracorder expert system by separating analysis into groups and special cases. This section gives an overview of the strategy.

4.2.1. Group 0: The Global View

[92] The group 0 entries in the electronic supplement provide an overview of the spectrum and what spectral features dominate. For example, if the spectral signature of water dominates, it may be difficult to detect mineral absorption features. If there are snow or vegetation features that dominate the spectrum, then it will be difficult to detect other mineral features. All group 0 entries are included in each group (1, 2, 3, 4, etc.) analysis. Separating these entries into a group reduces repetition in coding and in computation time. In the Tetracorder analysis, these entries are computed once and the results are added to the results for the other groups before the identification decisions are made.

4.2.2. Group 1: 1-μm Broad Region

[93] The group 1 entries in Table 1 in Appendix A in the electronic supplement describe electronic and other absorption features seen in materials in the visible and near-infrared.

4.2.3. Group 2: 2-μm Vibrational Absorption Region

[94] The group 2 entries in Table 2 in Appendix A in the electronic supplement describe vibrational overtone and combination bands in the 2 to 2.5-μm spectral region with supporting information at shorter wavelengths when appropriate.

4.2.4. Group 3: Vegetation Chlorophyll Detection

[95] The chlorophyll detection method presented in Table 3 in Appendix A in the electronic supplement gives a result proportional to green leaf area index. Note the entries include several combinations, from a green lawn grass spectrum (100% cover) to 20% grass cover on a hematitic soil background (material 228 in Table 3^{10} in the electronic supplement). These entries provide detection of trace vegetation in environments ranging from deserts to full canopy forests.

4.2.5. Group 4: Rare Earth Materials

[96] The rare earth absorptions are quite narrow (see spectra given by *Clark et al.* [1993a] and *Clark* [1999]) and thus have different requirements for detection (Table 4 in Appendix A in the electronic supplement). They can be detected in the presence of other broad absorptions such as those due to Fe^{2+} and Fe^{3+}. However, vegetation spectra seem to include a weak spectral structure that can be confused with trace neodymium oxide, thus a ''not feature'' NOTGREENVEG variable is necessary. This implies that it is difficult to detect neodymium oxide in the presence of vegetation, so if significant vegetation is indicated in the spectrum, there can be no detection of lower abundances of neodymium.

4.2.6. Case 1: Vegetation Red Edge

[97] The position of the chlorophyll red edge absorption feature can be found, as shown in Table 5 in Appendix A in the electronic supplement, by ratioing to a fixed reference spectrum [*Clark et al.*, 1995a; *Clark*, 1999]. Detection of shifts a fraction of the channel-to-channel spacing is possible with a ratio method. The reference spectra are unshifted divided by shifted spectra and the spectral structure in the ratio is used for the red-edge position detection. This special case is only done if vegetation is detected by an analysis in group 3.

[98] Similar methods could be employed to track shifts in spectral features in other materials. For example, this method could be used to track temperature when an absorption shifts wavelength position with temperature, like the conduction band edge in sulfur.

4.2.7. Case 2: Vegetation Spectral Type

[99] Vegetation spectra change with species. Table 6 in Appendix A in the electronic supplement spans a range of shapes found in the chlorophyll absorption from desert plants to lush lawns. The spectra are not unique identifiers of these species, but indicate a spectral type. In different environments, it is our experience that these spectral types often delineate vegetation communities. This special case is only done if vegetation is detected by an analysis in group 3.

4.2.8. Case 3, 4, 5: Vegetation Leaf Water Content

[100] The absorption strength of each leaf water absorption (Table 7 in Appendix A in the electronic supplement) is determined by case 3: 0.95 μm, case 4: 1.15 μm, and case 5: 1.4 μm absorptions. The strength of these features correlates with the amount of water in the plants and the fractional cover by plants in the pixel. These special cases are only done if vegetation is detected by an analysis in group 3.

5. Verification

[101] Through our experience in analyzing millions of spectra from imaging spectroscopy data, field checking the results [*Clark et al.*, 1990b, 1991; *Clark and Swayze*, 1995; *Clark et al.*, 1992a, 1992b, 1993a, 1993b; *King et al.*, 1995a, 1995b, 2000; *Swayze*, 1997; *Swayze et al.*, 1992, 1996, 2000 and references therein], analyzing over 40 million synthetic spectra [*Swayze and Clark*, 1995; *Swayze et al.*, 2003], and selected tests with laboratory spectra, the Tetracorder material identification system has worked well for our team and our sponsors at several agencies. However, strict statistical verification of Tetracorder results as applied to remote sensing data is extremely difficult because ground truthing of pixels 3 to 20 m in size in itself is extremely challenging at best. In the absence of highly accurate subpixel ground-truth, we assume a different stance regarding verification.

[102] In principal we would like verification to be expressed in terms of four metrics: true positives, true negatives, false positives, and false negatives. The relative values of these metrics gives us formal detection performance. In practice, deriving these metrics has widely varying difficulty. True positives are straightforward: determine the number of cases where Tetracorder predicted the presence of a mineral and the mineral is present. True negatives are much more difficult because it requires establishing the predicted absence of a material to some level of confidence. For some materials this is straightforward (water, vegetation), but for minerals, fully sampling a 20-m pixel is a challenge. False positives are similarly difficult: can we be sure that our field verification methodology is as effective as Tetracorder? Finally, false negatives are similarly difficult because we must find materials incorrectly predicted to be absent.

[103] To our knowledge, no remote sensing study has ever statistically sampled a scene to determine if the mineralogy mapped correctly, especially on the scale of imaging spectroscopy identifications such as presented here. We investigate Tetracorder results by several methods, checking for true positives, true negatives, false positives, and false negatives by characterizing multiple sites to the ability of our time and resources. Within the context of this claim, Tetracorder is extremely successful as shown below. We verify this claim in two ways. There are two types of verification of remote sensing imagery information: virtual [*King and Clark*, 2000] and in situ. Virtual verification can be done by examining the remote sensing data directly if there is sufficient spatial and/or spectral information to positively identify objects in the image by inspection. In situ verification requires direct sampling of the environment to verify the remotely sensed information.

[104] Note that there is a distinction between ''identification'' and ''classification'' of results from the analysis of remote sensing imagery. While some objects can be identified directly from the imagery, others can only be inferred to some level of confidence (classification) that requires in situ field checking. Information gained from the analysis of remotely sensed data increases with better spatial resolution and/or spectral resolution and, in general, is maximized when both high spectral and high spatial resolution are used together, although in some instances only high spatial or spectral resolution is needed. For example, identifying cars requires high spatial resolution but only low spectral resolution. Black and white imagery would suffice to identify cars; a simple color photo could be used to determine its color.

[105] Using imaging spectroscopy data, with suitable spectral resolution, it is possible to identify specific minerals in soils, such as kaolinite, based on the wavelength position and shape of characteristic absorption features. The detection of unique kaolinite spectral absorption features allows the positive identification of the mineral and the capability to map its distribution, based on the limits of the spatial resolution of the instrument. In this case, there is no need for in situ field checking because the spectra are of sufficient resolution to be certain of their identification. The derived kaolinite maps can be verified by examining spectra from the imaging spectrometer data at a computer monitor in a laboratory. This is virtual verification.

[106] From the above discussion it follows that certain things can be verified directly from the imaging spectroscopy data, both by spectral and spatial contexts. For example, bodies of water, including lakes and streams, are self evident in the images. Verification by spatial context can be further proved by examining spectra. Thus Tetracorder maps of bodies of water are readily verifiable by examining the resulting images and further verified by comparing to published maps. Fields of vegetation are also easily verified by spatial context and examination of the unique spectral properties of vegetation (both green chlorophyll absorptions and drier vegetation showing lignin, cellulose, and protein absorption features). Ice and snow, at least in terrestrial environments, can also be verified by spatial context using apparent albedo and with essentially 100% confidence by examining the spectra. By spatial context and spectral features, we have verified that Tetracorder analysis for water, snow, and vegetation has a high true positive and true negative rate and low false positive and false negative rate. There are exceptions, and these are noted in the deficiencies section below.

[107] Certain minerals have unique absorption features so that they can be verified by extraction of spectra at a computer without visiting the site. However, such virtual verification can only have a high certainty if the spectral feature is strong enough relative to the noise in the spectrum and if there are no other minerals present with similar features that can confuse the identification. Examples of such cases we have encountered for minerals will be discussed in the ''deficiencies'' section below. It is usually evident from our experience that such mineral mixtures are obvious by examination of the spectra, meaning that a spectroscopist can tell the spectrum is ambiguous and that the Tetracorder result is uncertain. Such areas are commonly targeted for field investigation to determine what is really there and how Tetracorder performed and what modifications, if any, are required to do a better job. It is these field investigations at hundreds of locations in many different geologic environments that have led to the current sophistication of the expert system.

[108] Tetracorder results are based on the following experiences. First, we have made numerous spectral measurements in the laboratory of minerals and other materials where sample purity, grain size, and measurement viewing geometry were either closely controlled or measured. Second, we have analyzed millions of real-world spectra obtained with the NASA AVIRIS and subsequently verified the resulting mineral maps in the field (e.g., *Swayze et al.* [2000, 2003], *Clark et al.* [2001], and references in these papers and in the applications section below). We have discovered situations not envisioned in the laboratory, made spectral measurements of relevant samples encountered in the field, and devised strategies to detect them. Third, we have encountered, investigated, and simulated many noisy mineral spectra and identified them under variable signal-to-noise ratio, bandpass and sampling conditions [*Swayze et al.*, 2003], showing which ones were confused with each other and which diagnostic spectral features could be used to better discriminate among them. Fourth, we have measured spectra of minerals, rocks, soils, and other materials in the field where the spectroscopist could visually assess conditions, again not necessarily envisioned in previous laboratory studies, and rapidly obtain and evaluate the spectra under those conditions. (We use two portable field spectrometers which provide spectra in the 0.4–2.5-μm wavelength region on time scales of a few seconds per measurement.) Fifth, in field studies we collect hand samples to verify the Tetracorder results. We have brought these samples back to our laboratories and have done additional analyses on them, including laboratory spectroscopy (range 0.2 to 150 μm), X-Ray Diffraction (XRD), electron microprobe, X-Ray Fluorescence (XRF), Mossbauer spectroscopy, petrographic and binocular microscope examinations, and other analyses as appropriate. Example results of field verification studies are shown in Table 2. Sixth, we have analyzed spectra, collected by telescopes and interplanetary spacecraft, of materials under nonlaboratory conditions, some of which have yet to be duplicated and

measured in the lab. From this we have gained a better understanding of these materials from modeling done by us and from published research.

[109] Table 2 presents a portion of our results of verifying Tetracorder analyses at numerous sites studied in the western United States. In verifying a Tetracorder result in the field, the field team identifies an area in the image that needs verification and goes to that location. This is not always easy, as sometimes visual field geologic methods cannot identify minerals (e.g., a few percent clay in a soil). Portable field spectrometers are used to survey the area. Such surveys are often sufficient to verify the presence of materials in question. Hand samples are collected that appear representative of the surface materials that contribute to a pixel. Even with field spectroscopic verification, traditional geologic field techniques, like hand lens examination and acid fizz tests are done. We also collect hand samples and return them to the lab for more detailed analyses.

[110] Table 2 shows verification analyses for over 100 examples of Tetracorder identifications from Cuprite, Nevada; Leadville, Colorado; Arches National Park, Utah; Canyonlands National Park, Utah; the Oquirrh Mountains region, Utah; Summitville, Colorado; Mountain Pass, California; Barstow, California; and Joshua Tree National Park, California. In nearly every case the materials predicted were identified in hand samples returned from the field pixel location by at least one analysis method. Tetracorder did not report the presence of all materials detected by XRD, nor did XRD identify all the minerals evident spectroscopically, but this reflects the differing sensitivities of the two techniques. This exercise shows that detections reported by Tetracorder are extremely reliable indicators of the presence of the predicted minerals and that Tetracorder exhibits a high rate of true positives.

[111] In examining the verification results in Table 2, note that different methods are sensitive to different abundances of materials. For example, the visible to near-IR (Vis-NIR) spectrum (0.4 to 2.5 μm) is very sensitive to Fe^{3+}-bearing minerals and to clay minerals, more so than XRD [e.g., see *Farmer*, 1974]. However, the minerals quartz and low-iron feldspars have no diagnostic absorptions in this spectral range, Vis-NIR spectroscopy cannot detect them, but XRD is very sensitive to them. For example, a red sandstone with an obvious hematite and kaolinite spectrum may only show quartz by XRD. Laboratory reflectance spectroscopy, however, can be a definitive test of the presence of hematite and kaolinite, if the absorptions appear strong. We have found XRD to be of the greatest help in verifying mixtures. Mixtures of minerals with overlapping absorption bands can be difficult to interpret with spectroscopy, unless suitable examples are known. XRD has provided that critical link.

5.1. Known Deficiencies in the Presented Tetracorder and Expert System

[112] The algorithms and set of expert system rules presented here, while doing an excellent job of spectral identification and mapping, are not perfect. The known deficiencies are presented below so others who may use our system will be able to appropriately interpret the results. In all cases cited below, additional research is required to address the deficiency.

[113] Deficiency 1 is calcite-epidote-chlorite mixtures. These three minerals have similar absorptions near 2.3 μm and in a mixture can be difficult to distinguish. The chlorite absorption shifts with composition, which adds to the complexity. The pure end members are well mapped with the current expert rules, but as increasing abundances of the other two are added, results can be inaccurate. For example, initial mapping in the Animas watershed region of Colorado showed abundant calcite that could not be located in the field. Calcite is important for buffering acidic rock drainage in the area. It was found that much of what mapped as calcite was actually chlorite-epidote-calcite mixtures, including minor amounts of calcite.

[114] Deficiency 2 is shallow water/sediment suspended in water. Certain shallow water depths have a spectral signature that is a combination of water transmission and bottom reflectance that results in unusual combined absorption features. These often map as unusual minerals that have broad absorptions in the 0.6- to 1.3-μm region, for example olivine. These errors are readily identifiable by spatial image context. The solution is to include more water spectra in the spectral library simulating such conditions and placing continuum constraints on reference minerals to restrict water-like continuum slopes.

[115] Deficiency 3 is halloysite versus kaolinite plus montmorillonite/muscovite/illite. Kaolinite absorption plus another clay absorption near 2.2 μm can produce a spectral feature similar to that of halloysite. The long wavelength side of the halloysite feature rises faster than the mixtures, so additional mixture reference spectra will solve the problem. The expert rules already contain such mixtures, so some mixtures are correctly identified, but additional reference spectra are needed to increase the accuracy of the identifications.

[116] Deficiency 4 is talc-hectorite-saponite. These minerals have similar absorptions near 2.3 μm and are difficult to distinguish at AVIRIS sampling (∼0.01 μm) and bandpasses (∼0.01 μm). The absorption features change shape with different grain sizes. A grain size series is needed for each library mineral. Higher spectral resolution than that of AVIRIS would also help distinguish between these minerals.

[117] Deficiency 5 is that wet vegetation and/or some desert vegetation maps as melting snow plus vegetation. As ice melts, the absorptions shift to shorter wavelengths. The absorption due to water in plants can be broader than in liquid or solid water, thus can be similar to a combination of ice and vegetation. Succulent desert plants (e.g., cactus family) often show broader absorptions than grasses and trees. The current set of vegetation reference spectra in the expert system is limited, so some vegetation is sometimes misidentified as snow plus vegetation (this error is usually obvious when mapping desert regions with data acquired in the heat of summer). The solution is additional vegetation species added to the expert system.

[118] Deficiency 6 is clouds. Most of our data sets have been acquired under excellent clear sky conditions, so we

have limited experience with the effects of clouds on mapping results. A small cloud can reflect light from adjacent surfaces and change the shape of broad spectral features (like Fe^{2+} or Fe^{3+} absorptions) causing unusual minerals to be mapped where the cloud or cloud shadow is located. Cloud and cloud shadow detection algorithms must be designed and implemented.

[119] Deficiency 7 is calibration. While not directly a deficiency, we must note that calibration errors can translate into spectral features or modification of spectral features. This can cause Tetracorder to misidentify materials. Such errors seem to occur mostly between mixtures where the spectral characteristics are only slightly different. Thus the accuracy of the resulting maps is directly proportional to the accuracy of the calibration to reflectance. Wavelength calibration is also important to the Tetracorder identification accuracy: shifts in wavelength calibration can result in errors in identification.

[120] Deficiency 8 is the question "How diagnostic is the Fe^{2+} absorption?". The expert system includes many minerals with Fe^{2+} absorptions. However, many such absorptions are similar in position and shape, [e.g., see *Hunt*, 1977; *Clark*, 1999 and references therein]. Minerals like jadeite, cummingtonite, and others often map large areas where those minerals do not exist. We typically label our maps "Fe^{2+}-bearing mineral" and not the specific mineral identification. Fe^{2+}-absorptions must be analyzed in greater detail to see how diagnostic such absorptions are. Studies to date that have indicated diagnostic abilities have included only a limited number of samples. When all minerals are considered, along with likely mixtures found in terrestrial environments, it is not clear how diagnostic the absorption is, except perhaps in a few cases, like that of olivine.

[121] Deficiency 9 is that alunite paleothermometry may give false high temperature results for some low temperature supergene alunites. The direct measurement of formation temperatures from the width of the 2.17-μm absorption may be restricted to those areas dominated by Al-deficient alunites. Apparently, the width of this absorption is sensitive to Al deficiencies in the octahedral layer, and when there are none as in some supergene alunites, the shape of the 2.17-μm band assumes that of the high temperature configuration. More study is needed to confirm this restriction [*Swayze*, 1997].

[122] Deficiency 10 is that the reference entry for staurolite maps vegetation plus water because overall its continuum resembles vegetation plus water, and staurolite only has one broad band and no smaller diagnostic spectral features. Thus maps of staurolite are a spectral shape indicator only, and usually only indicate a spectral vegetation type or certain vegetation density on a background soil. The solution is to include NOT features that exclude snow and vegetation features.

[123] Deficiency 11 is that pyrophyllite incorrectly maps too much in areas of hydrothermal alteration. Low levels of pyrophyllite map because of spectral structure near 2.16 μm, the position of the strong pyrophyllite absorption feature, due to incomplete removal of atmospheric absorption features and/or spectral structure in vegetation that may cover part of a pixel. Pyrophyllite is a high temperature indicator mineral so its detection is important for determining characteristics of hydrothermal systems.

6. Applications

[124] Planetary surfaces are complex. The Earth's surface is probably the most complex in our solar system, showing varied geology, oceans, ice caps, abundant life, and anthropogenic influences. Other planets have different geology and different surface compositions. In order to understand our own planet as well as others, we produce maps of materials and other measurable quantities. Maps of the Earth's surface can depict many themes, including geology, ecosystems, environmental, hazards, land management, and global change. Geologic mapping can include the depiction of geologic formations (thus providing information on ages and placements of units through geologic time), soils, mineral occurrence, faults, mineralized zones, and aggregate for building materials. Ecosystems maps might include habitat, vegetation species/communities, vegetation health and canopy chemistry, and riparian zone distributions. Environmental applications can include acid rock drainage, oil or toxic waste spills, forest fire potential (including fuel load), water quality, and other distributions. Geologic hazards maps can include volcanic eruption potential, swelling clays, and landslide hazards. Land management maps can include ecosystems impact by human activity, grazing impacts by cattle, and others. Global change maps might include surface albedo as a function of time, vegetation type and global distribution, ice and snow distribution. The need for accurate and more detailed maps has never been greater. Here are a few examples of how imaging spectroscopy can provide useful data in some of these areas.

6.1. Geologic Applications: Mapping Minerals and Amorphous Materials

[125] Spectra of minerals as well as amorphous materials show many diagnostic absorption features. Minerals are the components of rocks, soils, and geologic formations, so maps of mineralogy contain geologic information.

[126] Continuing with our Cuprite, Nevada example, we mapped the area for minerals and amorphous and other iron oxides. The Cuprite AVIRIS data were calibrated to apparent surface reflectance to remove atmospheric absorptions and scattering and to remove the solar response [*Clark et al.*, 1993b; *Swayze*, 1997]. Next, the reflectance data were analyzed by the Tetracorder algorithm and over 254 spectral categories were sought, producing 762 output images (254 × 3: fit, depth, and fit × depth). About 70 categories had significant fits as determined by spatial groupings of pixels with fit values above the thresholds. Some of those categories are vegetative; others are mineralogical and the best 45 (approximately) of those are shown in Figure 9. Some mixture series were combined into one color for display in Figure 9. The material maps, shown in Figures 9a and 9b show the diversity of minerals and depict their complex distribution. Also significant but not shown were vegetation occurrence, vegetation species (spectral type), and vegetation leaf water abundance. Some minerals mapped in only a few pixels and are not shown, but subsequent higher resolution imaging has confirmed these small outcrops. All mineralogic entries in the map keys have been confirmed by field work

except pyrophyllite. Pyrophyllite plus alunite has been searched for without success in the field. Subsequent work indicates trace vegetation plus alunite sometimes mimics this mixture spectrally confirming deficiency 11, above.

[127] The Cuprite area consists of dual relic hydrothermal systems whose origins appear to be chronologically independent [*Swayze*, 1997]. The western hydrothermal center is zoned from muscovite (sericite) at the exterior, to kaolinite, Na-alunite, through K-alunite (Figure 9, spectra in Figures 1 and 12). The eastern center is similarly zoned from kaolinite to intermediate temperature K-alunite to high temperature K-alunite, with a central cap of siliceous rocks. The western center is eroded so that the highest portions of the hydrothermal system, where the siliceous cap would be, is no longer present, and we are now seeing exposed a once deeper level of the system. Some of the minerals exposed in the eastern center formed higher up in the hydrothermal system, further from the source of heat, and thus had lower temperatures involved in their formation compared to the minerals exposed in the western center [*Swayze*, 1997]. The presence of certain minerals and their positions in their solid solution series (e.g., high versus low aluminum muscovite, Na- versus K-alunite, dickite, and others) in the different centers places constraints on the formation conditions [*Swayze*, 1997] that would be difficult to determine in the field without considerable sampling and extensive laboratory analysis. The Cuprite mineral maps also provide new insight into structures: there are boundaries in the mineral maps that indicate faults not shown on existing geologic maps [*Swayze*, 1997]. Even with detailed field sampling, it is unlikely that maps of this detail showing the complex relationships could be produced by any other method than imaging spectroscopy.

[128] Additional geologic studies at Yellowstone National Park using Tetracorder analysis [*Livo et al.*, 1999, 2000] relates altered mineral occurrences to geologic processes and hydrothermal water chemistry. Kaolinite, alunite, and hematite form from rising acidic waters where the water flow is restricted in volume. These mineral deposits form topographic highs resistant to erosion. Higher-volume neutral pH waters form altered ground within basins that are capped with siliceous sinter and montmorillonite and usually lack iron-oxides.

[129] Geologists usually map geologic formations. Mineral occurrence maps, such as those for Cuprite, do not necessarily depict geologic formations. However, geologic formations are composed of minerals, so mineral maps can usually be used to map the extent of geologic formations. Mineral maps can also be used to subdivide geologic member units, if there is a compositional change between members. Mineral maps provide a significant new tool for the field geologist, enabling him or her to focus on the interesting areas, helping to produce a better product, refine interpretations, and permitting coverage of larger areas in less time.

6.2. Environmental Applications

[130] There are many environmental applications where imaging spectroscopy can contribute by mapping chemistry. We have studied acid rock drainage, which is a particularly pervasive environmental problem in the western United States. While metals and minerals are essential to an industrialized society, mining activities can impact the environment. Mines and entire mining districts have been abandoned in the United States when mining operations were no longer economic and, until recently, little consideration has been given to environmental impacts. The Leadville mining district in central Colorado shows examples of environmental damage from abandoned mines.

[131] The Leadville mining district, located at an elevation of 3000 m in the central Colorado Rockies, has been mined for gold, silver, lead, and zinc for over 100 years. This activity has resulted in waste rock and tailings, rich in pyrite and other sulfides, sulfates, and secondary minerals being dispersed over a 30 km^2 area including the city of Leadville. Oxidation of these sulfides releases lead, arsenic, cadmium, silver, and zinc into snow melt and thunderstorm runoff, which drains into the Arkansas River, a main source of water for urban centers and agricultural communities. The U.S. Environmental Protection Agency (EPA), U.S. Bureau of Reclamation (USBR), contractors, and responsible parties have remediated the mined areas to curtail further releases of heavy metals into various tributaries of the Arkansas River.

[132] The size of the Leadville mining district and presence of spectrally detectable secondary minerals from the pyrite oxidation-weathering process (Table 3) made imaging spectroscopy analysis an effective tool for locating those minerals related to the acid rock drainage sources. AVIRIS data were collected over Leadville on 27 July 1995, calibrated to apparent surface reflectance and mapped with Tetracorder [*Swayze et al.*, 1996, 2000]. The AVIRIS-derived minerals map (Figure 14) was field checked [*Swayze et al.*, 1996, 2000] and confirmed by USBR studies [*Pearson*, 1997]. The mineral map shows the sources of alteration that contribute to acid rock drainage, thus focusing cleanup efforts to those sites. Pyrite weathers to jarosite, creating acidic waters which leach heavy metals from the rocks and soils. Thus maps of pyrite and jarosite show the source regions of acidic water. Other tailings piles showed no acidic rock drainage-related minerals, showing investigators the areas where no cleanup was necessary (or would contribute little to improving the local environment). As a result of this study, the USEPA estimated that the imaging spectroscopy mineral mapping saved over $2 million in remediation costs and accelerated cleanup efforts by 2.5 years [*U.S. Environmental Protection Agency*, 1998]. The extensive field verifications at Leadville and the cost and time savings for the cleanup effort are testaments to the accuracy of imaging spectroscopy and the Tetracorder method.

[133] Rapid response materials maps of the World Trade Center disaster [*Clark et al.*, 2001] were produced by calibrating AVIRIS data to apparent surface reflectance, performing Tetracorder analysis, writing a report of the results which was formally reviewed, and then distributing the results to emergency response teams within 10 days of AVIRIS data receipt. The Tetracorder maps showed no highly concentrated widespread distribution of asbestiform minerals or other toxic materials in the dust/debris from the collapse of buildings, in agreement with ground sample analyses. The Tetracorder maps also showed asymmetric debris distribution indicating a nonsymmetric collapse of the buildings. Thermal hot spots were also detected, and those maps were used by fire fighters on scene to direct fire fighting efforts. Thus

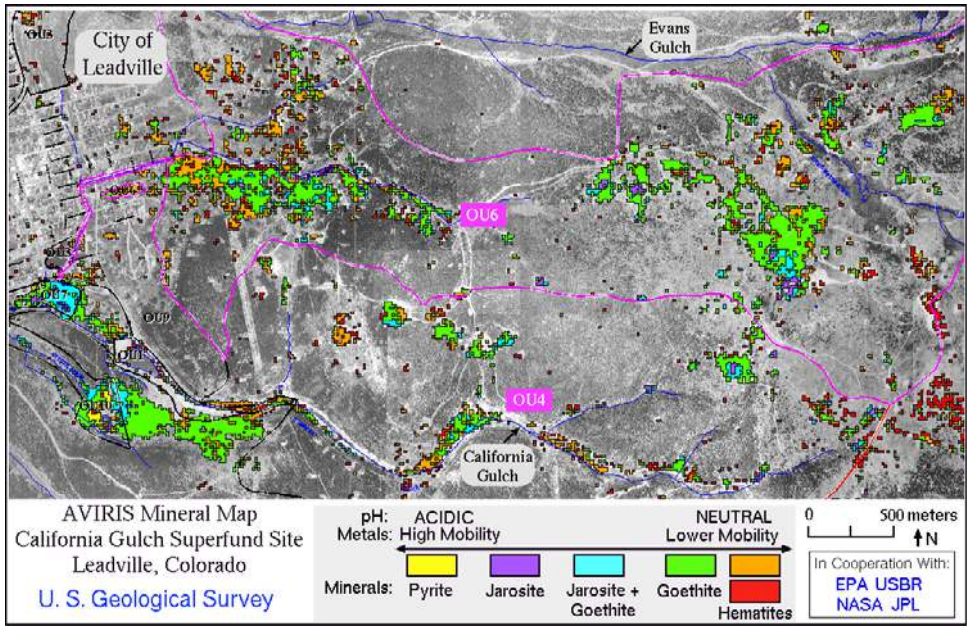

Figure 14. The Leadville Tetracorder mineral map overlaid on an orthophotographic base. The mineral patterns pinpointed sources of acid mine drainage and resulted in a savings of over $2 million and accelerated cleanup efforts by 2.5 years at this U. S. EPA Superfund site.

imaging spectroscopy and Tetracorder played a role in the recovery effort. The mapping results were verified with laboratory analysis of field samples. The rapid response was possible because the Tetracorder algorithm produces consistent and robust results in diverse environments.

6.3. Vegetation Species/Communities, Health/Senescence Indicators, and Green Leaf Water Abundance

[134] Spectra of vegetation come in two general forms: green and wet (photosynthetic) and dry (nonphotosynthetic), but there is a seemingly continuous range between these two end members. The spectra of these two forms are compared with a soil spectrum in Figure 15. Because all plants are made of the same basic chemical components, their spectra generally appear similar. However, the chlorophyll absorption at 0.69 μm shows subtle shape variations that can be distinguished with shape matching algorithms such as employed in Tetracorder. The near-infrared spectra of green vegetation are dominated by liquid water vibrational absorptions. The water bands in vegetation are shifted slightly in wavelength compared with those in liquid water,

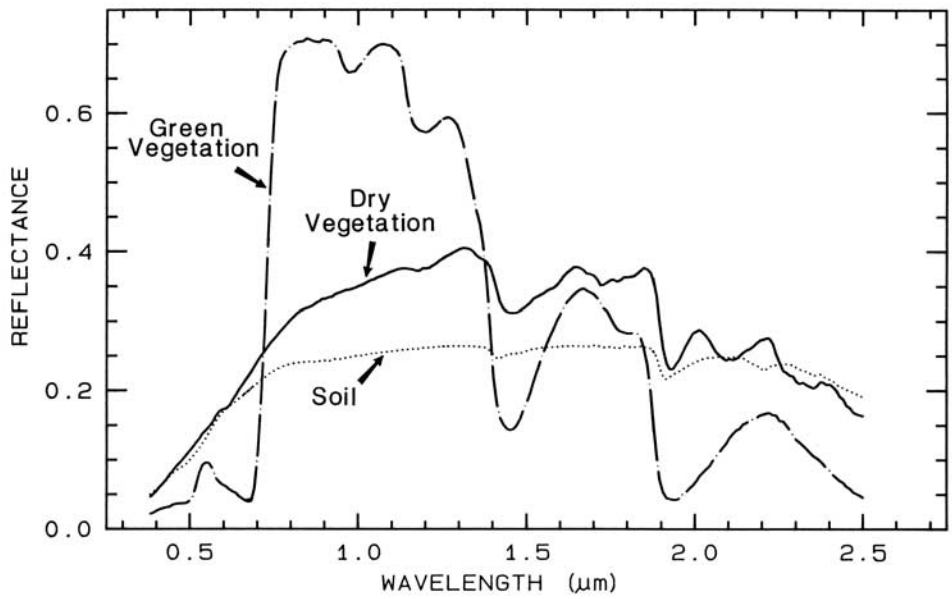

Figure 15. Spectra of green photosynthetic vegetation, dry, nonphotosynthetic vegetation, and a soil containing montmorillonite.

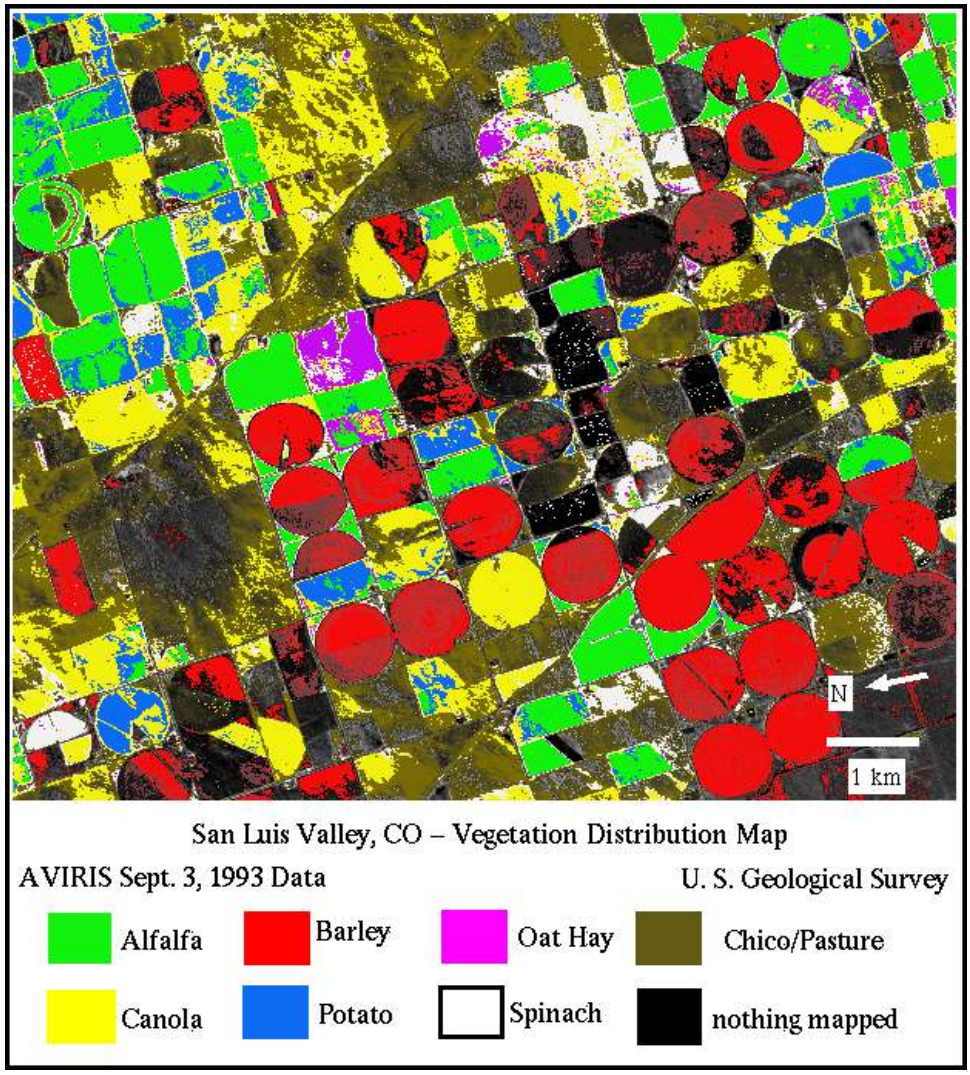

Figure 16a. Spectrally determined vegetation species map for San Luis Valley, Colorado.

due to differences in hydrogen bonding. The reflectance spectrum of dry, nonphotosynthetic vegetation (Figure 15) shows absorptions due to cellulose, lignin, and protein. Some of these absorptions can be confused with mineral absorptions, unless a careful spectral analysis is done. For example, the 2.3-μm feature in dry, nonphotosynthetic vegetation spectra is similar to that of low abundances of calcite.

[135] The Tetracorder system was tested for distinguishing vegetation species using AVIRIS data over farm fields in the San Luis Valley of Colorado. Reference spectra from known species of crops were used to map similar spectral shapes in the AVIRIS data using Tetracorder. Species identification accuracy was greater than 97% based on farm fields of known vegetation types (Figures 16a and 16b) [*Clark et al.*, 1995a, 1995b]. The imaging spectroscopy data also resolves absorptions due to water in the plant leaves (Figure 15), and those absorptions were mapped. The vegetation chlorophyll absorption and the leaf-water absorptions can be combined into a color composite image to indicate relative water content in plants (Figure 17). The results also show that dry nonphotosynthetic vegetation can be mapped with imaging spectroscopy. Vegetation leaf-water maps might indicate plant health and regions of drought for monitoring forests, grasslands, and irrigation of crops, or as indicators of forest fire danger potential, and could be especially effective when data are acquired over a growing season. Recent mapping of conifer forest species in Yellowstone National Park [*Kokaly et al.*, 1998, 2003] have extended these results to the natural environment.

6.4. Water

[136] There are many potential water monitoring possibilities [*Carder and Steward*, 1985; *Carder et al.*, 1993]. We show one example here involving pollution entering a lake. Turquoise Lake, on land administrated by the U.S. Forest Service near the town of Leadville, Colorado, shows nothing out of the ordinary using visual wavelengths (Figure 18a). Landsat TM bands and band ratios show similar results, with no obvious or unique pollution source except for several locations where sediment appears to be entering the from the lake's banks. Imaging spectroscopy can resolve the reflectance maximum at 0.58 μm in phytoplankton-rich water [*Mustard et al.*, 1999] as shown in Figure 18b, but traditional analysis methods provide an ambiguous/cluttered signal. For example, Figure 18c

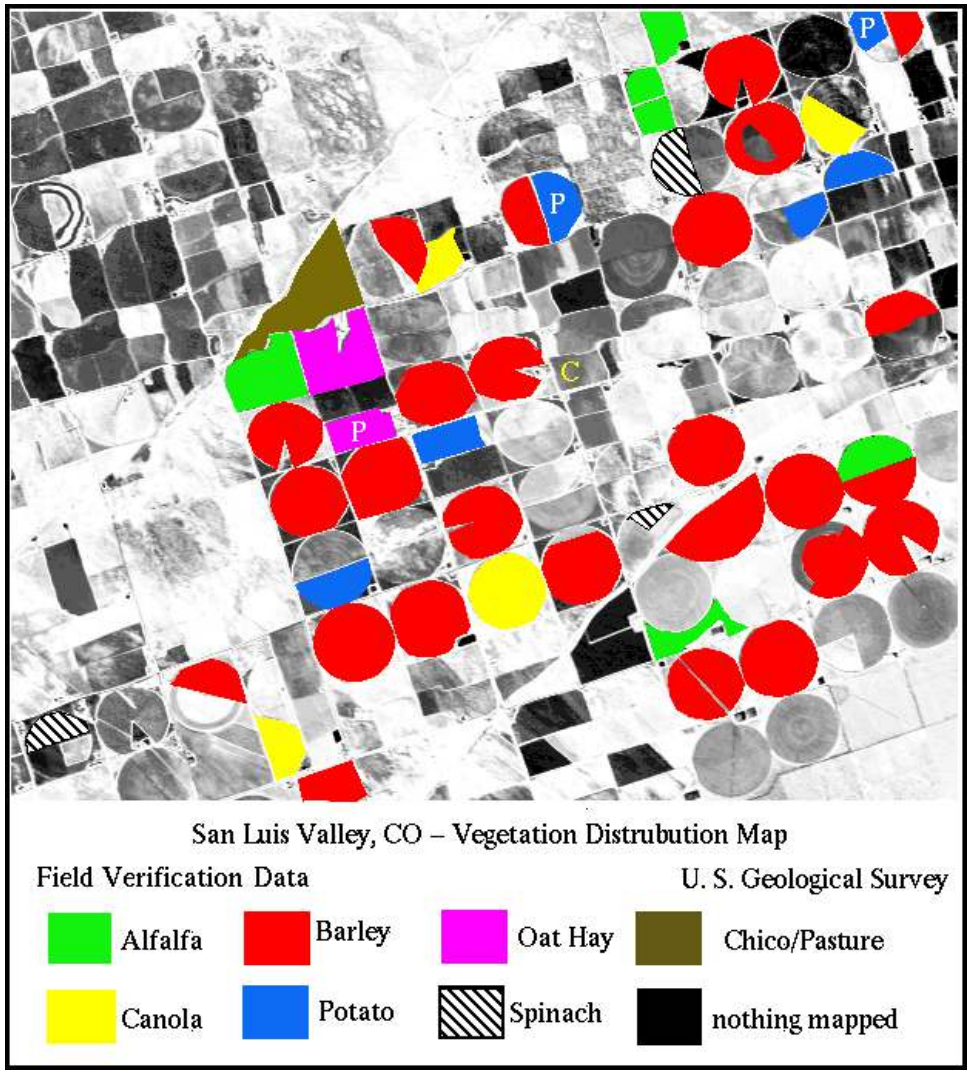

Figure 16b. Verification map for the vegetation species map for San Luis Valley, Colorado (Figure 16a) derived from in situ field identification of crops. Compare the colored fields with the image in Figure 16a. All fields except two were identified correctly, and for those two about half the fields were correctly identified, leading to an average accuracy of 97%. Letter C shows location of AVIRIS calibration site. Letter P shows fields found to be partially correct; all other colored fields were determined to be correctly mapped.

shows a band ratio selected to isolate the feature, but other materials in the scene also show a response in the ratio image, notably vegetation on land. The reflectance maximum can be isolated using the three-point band depth method (as outlined in Figure 8d). However, this too shows response from other materials in the scene (Figure 18d). The Tetracorder imaging spectroscopy map (Figure 18b) correctly isolates the reflectance maximum from phytoplankton-rich water showing a plume originating from a campground where sewer lines are less than 50 m from the shore (Figure 18e). These lines are probably leaking. However, the Forest Service took a sample of the surface water and found no coliform bacteria. Visually, from the lake shore edge, the plume cannot be seen with the human eye. It is likely that contamination is entering the lake through ground water inflow and subsurface testing is warranted to rule out possible leaks. This result indicates that imaging spectroscopy has the potential to be a sensitive environmental monitoring tool for finding concealed point sources of pollution.

6.5. Ice and Snow

[137] Ice is a special case in remote sensing of minerals on the Earth because it is the one mineral that changes location

Table 3. Pyrite and Secondary Minerals[a]

Mineral	Formula
Pyrite	FeS_2
Copiapite	$Fe^{2+}Fe_4^{3+}(SO_4)_6(OH)_2 \cdot 20H_2O$
Jarosite	$(Na,K)Fe_3^{+3}(SO_4)_2(OH)_6$
Goethite	alpha-FeO(OH)
Hematite	alpha-Fe_2O_3

[a]Acid-generating potential is highest with pyrite, decreasing with each lower entry.

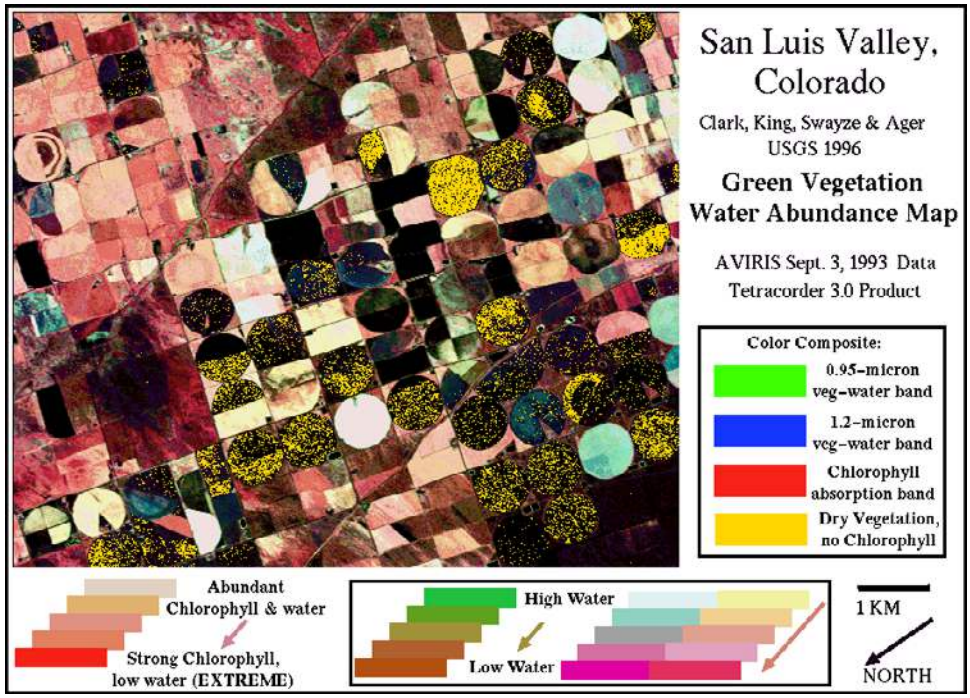

Figure 17. San Luis Valley vegetation water abundance map. In this color composite, areas that are white to bluish have plenty of water in the plant leaves; those areas that appear reddish have possible water deficiencies. Yellow areas are dry, nonphotosynthetic vegetation. Such maps, if done for a region as a function of time, may indicate areas suffering from drought and increased fire danger.

and grain size with weather, and it is probably the most abundant surficial mineral in the solar system, covering many outer solar system surfaces [*Clark et al.*, 1986], as well as portions of Mars and the Earth. The water absorption bands in the near infrared shift to shorter wavelengths from gas to liquid and shift still further from liquid to solid (Figure 19a). Imaging spectrometers can be used to detect that shift and map different phases of water. Water absorptions in vegetation occur at slightly different positions and have different shapes and, combined with the chlorophyll absorption at 0.69 μm, can be used to spectrally separate liquid water, ice, and water in plants.

[138] We applied the differences in position and shapes of water and ice absorption features to the task of mapping melting snow in the San Juan Mountains of Colorado (Figure 19b). The AVIRIS data were acquired in August 1992, after a brief summer snow storm. The snow was frozen at the highest elevations, was partially melted at lower elevations, and was turning to slush at even lower elevations. At tree line, significant wet vegetation was encountered, and finally at the lowest elevations dry, nonphotosynthetic vegetation and green but not wet vegetation are mapped at the bottom of the valleys. These results were confirmed by field

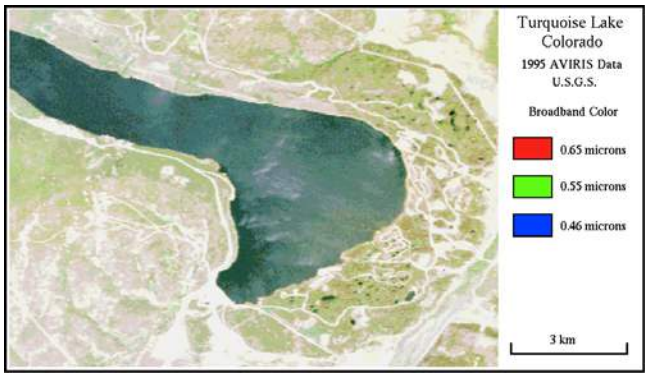

Figure 18a. Turquoise Lake, Lake County, Colorado. Color TM image synthesized from AVIRIS. The image shows several areas of turbidity in the lake but no obvious pollution.

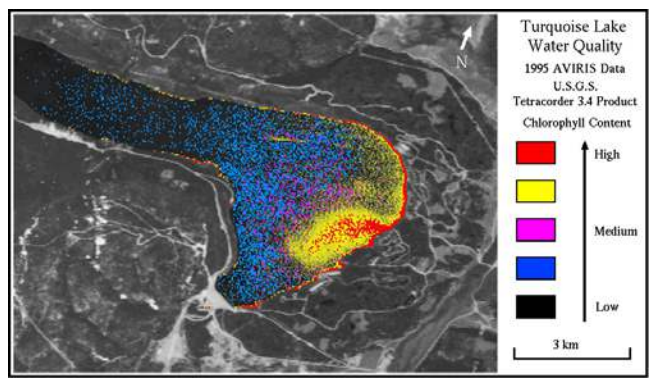

Figure 18b. Spectral map of phytoplankton-rich water shows a plume originating from the shore. The plume probably originates from a low-volume sewage leak near a campground. The Tetracorder result shows detection of phytoplankton-rich water only over the lake and no response from nonwater targets. The Tetracorder spectral matching-decision process enables robust identifications in this situation, whereas simpler analyses show false responses over land (compare Figures 18c and 18d).

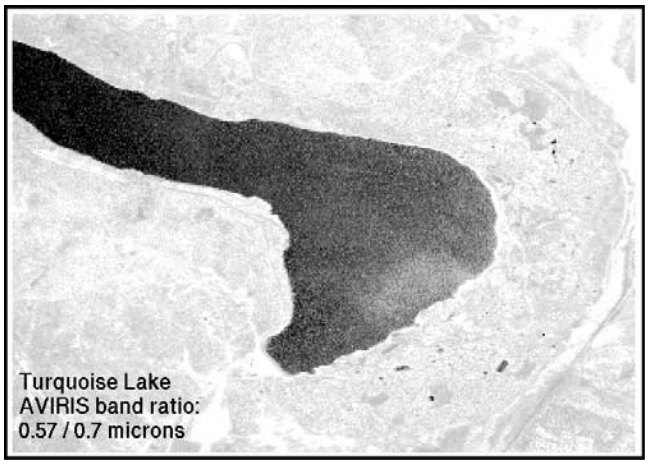

Figure 18c. A ratio image using AVIRIS channels at 0.58 and 0.7 μm. The ratio does not uniquely isolate the reflectance maximum due to phytoplankton-rich water.

work showing relationships in the image were consistent and virtual verification of snow spectra because of limited access to the rough terrain and the time between image acquisition and data analysis. A spectral bandpass of about 25 nm or better, with 12 nm sampling or better, is required to make the spectral distinctions between liquid water, snow, and water in vegetation. The finer discrimination of mixtures of these three possibilities requires the finer sampling and bandpass of a system like AVIRIS (~10 nm sampling and ~10 nm bandpasses). Present broadband remote sensing systems can not distinguish between these cases because the absorption features can not be resolved.

6.6. Atmospheric Gases

[139] Planetary atmospheres also show absorption features in spectra. Visual and near-infrared spectra of the Earth's atmosphere show absorptions due to water, oxygen, carbon dioxide, ozone, and other components. The atmospheric

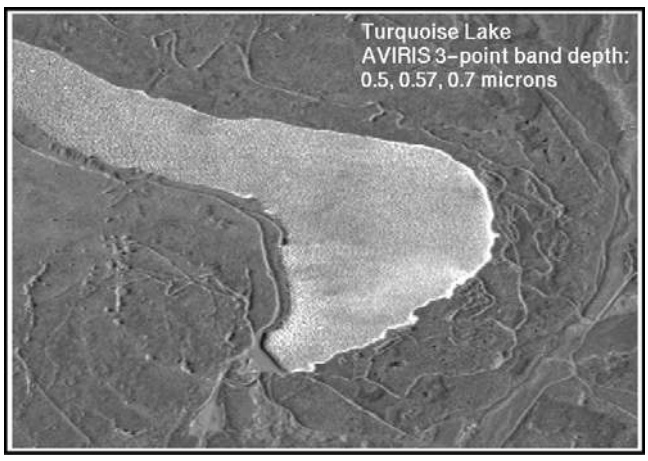

Figure 18d. A three-point band depth image using AVIRIS data at continuum wavelengths 0.5 and 0.7 μm and the reflectance maximum at 0.58 μm. The three-point band depth isolates the phytoplankton-rich water spectral maximum better than a simple band ratio but also shows response from other materials.

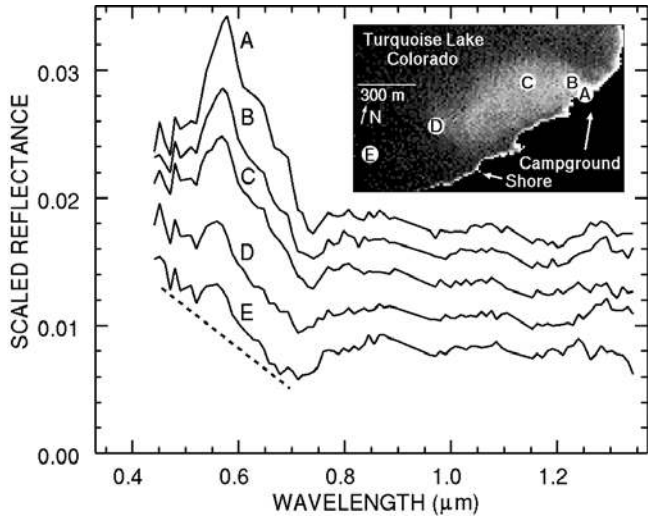

Figure 18e. Spectra from the AVIRIS data over Turquoise Lake. The spectra show a reflectance maximum at 0.58 μm in phytoplankton-rich water with the strongest signature near the shore (a) but decreasing as the plume disperses toward the outlet of the lake (e).

absorptions can be mapped much like surface materials whether for the Earth [e.g., *Green et al.*, 1996], the Jupiter system [e.g., *Carlson et al.*, 1996], or Mars [*Christensen et al.*, 1998]. Applications include mapping local sources of pollution to global mapping of atmospheric gases.

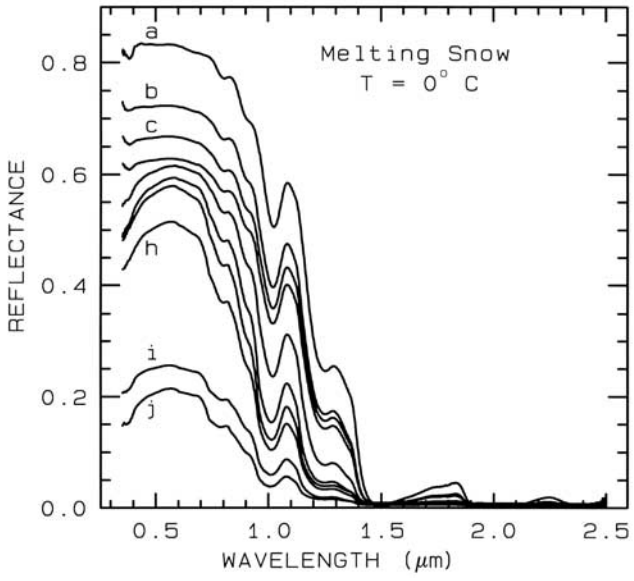

Figure 19a. A series of reflectance spectra of melting snow. The top curve (a) is at 0°C and has only a small amount of liquid water, whereas the lowest spectrum (j) is of a puddle of water about 3 cm deep on top of the snow. Note the increasing absorption at about 0.75 μm and in the short wavelength side of the 1-μm ice band, as more liquid water forms. The liquid water becomes spectrally detectable at about spectrum (e) (not labeled; two curves below c), when the UV absorption increases. Spectra from *Clark* [1999].

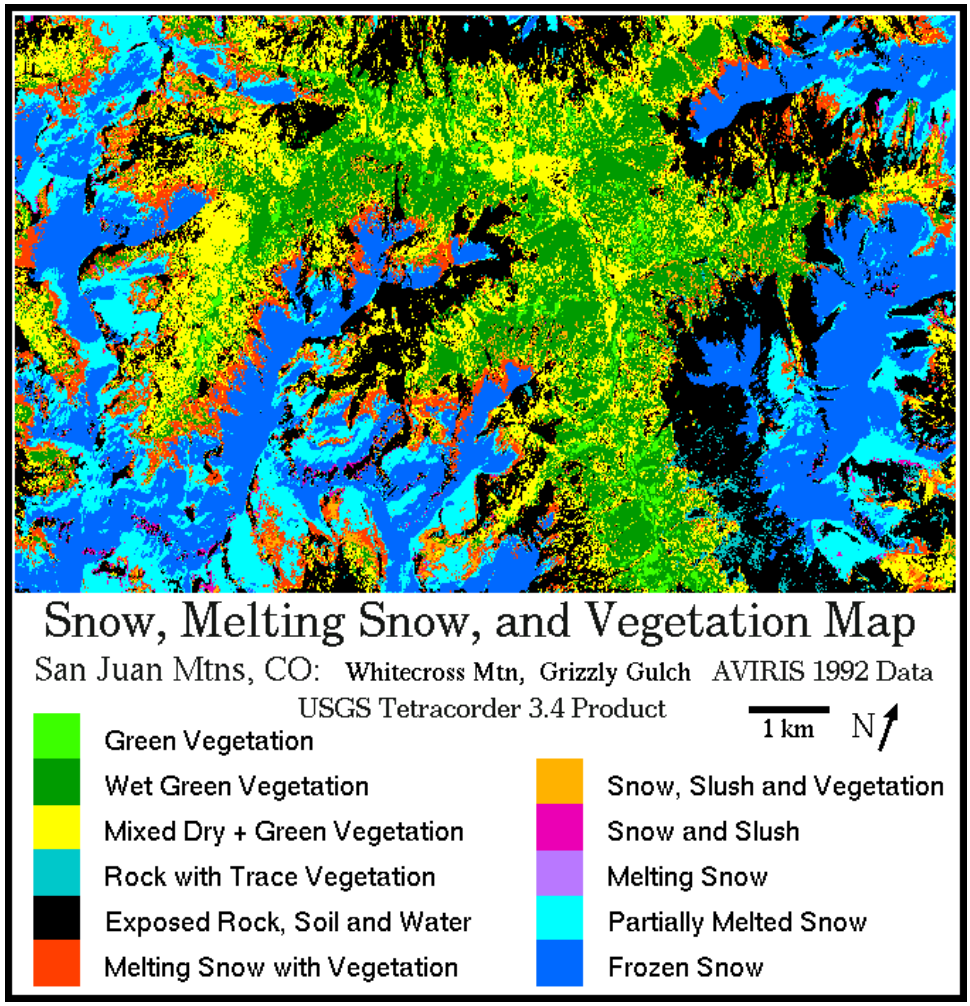

Figure 19b. Snow, melting snow, snow mixed with vegetation, and wet and dry vegetation are shown for a region in the San Juan Mountains of Colorado in August of 1992. The spectral resolution of AVIRIS enables analysis of detailed changes in the liquid-solid water absorption bands to map liquid water versus ice, versus water in plants, and mixtures between them. Such detailed discrimination is not possible with broad-band instruments.

[140] Carbon dioxide is a well-mixed gas on the Earth, and its spectroscopic strength is proportional to its atmospheric path length. The path length from the surface to space is variable due to topographic differences, thus a map of CO_2 feature strength (Figure 20a) shows an inverse correlation to topography (higher elevations = lower CO_2 feature strength). Using control points to derive a correlation of 2-μm CO_2 band depth versus elevation we see a linear trend in this data set covering over 1700 m in elevation difference (Figure 21). The least squares correlation coefficient shows an excellent trend with an R^2 value of over 0.98. The derived equation was applied to the CO_2 band depth image to derive a Digital Elevation Model (DEM). The derived DEM (Figure 20b) correlates well with the USGS DEM (Figure 20c). Some artifacts are due to shadows and low albedo regions where the signal-to-noise ratio in the AVIRIS data was insufficient to compute an accurate CO_2 depth.

[141] The DEM derived from CO_2 absorptions was used to geometrically correct the AVIRIS data. Tests show a factor of 10 improvement in geometric rectification using such a DEM with only four control points, compared to third-order polynomial stretch with 20 control points without using a DEM. The advantage of imaging spectroscopy derived DEMs is that the resulting topography is inherently registered with the spectroscopy data and at the same spatial resolution. Accurate orthorectification allows for local lighting geometries to be accounted for and true reflectance to be derived.

6.7. Other Planetary Applications

[142] The Galileo spacecraft which until recently orbited Jupiter carried the Near Infrared Mapping Spectrometer (NIMS). This instrument has provided data for making maps of surface materials on the Galilean satellites and atmospheric components in Jupiter's atmosphere [*Carlson et al.*, 1996]. Data from NIMS has been used to discover absorption bands in spectra of Ganymede and Callisto [*Carlson et al.*, 1996; *McCord et al.*, 1998]. Tetracorder has been used to map (Figure 22) the water ice and CO_2 absorption features [*Carlson et al.*, 1996]. The CO_2 feature at 4.25-μm is probably due to fluid or gas inclusions, but the host mineral has yet to be identified. The mapping of

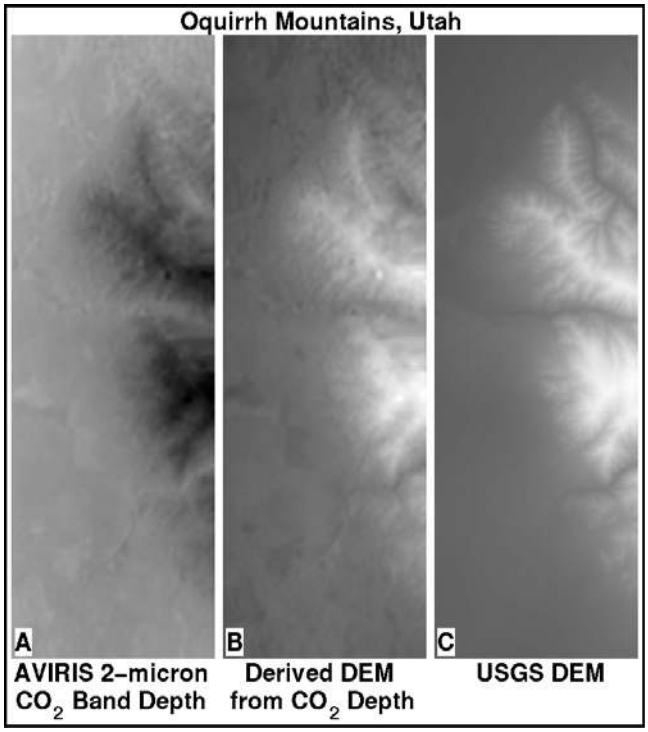

Figure 20. The 2-μm CO_2 absorption strength (a) can be converted to topographic elevation (b). The derived elevations matches the USGS Digital Elevation Model (DEM) (c). The CO_2 absorption strength image (Figure 20a) is brighter for increasing strength. Because the atmospheric path length is smaller with increasing elevation, the absorption strength decreases, becoming darker in the image. The DEMs (Figures 20b and 20c) are brighter for increasing elevation, thus are inversely correlated with the CO_2 strength in (Figure 20a).

the 4.25-μm feature illustrates that a material may be mapped even though we do not yet understand the origin of the material. In this case a spectrum from Ganymede was used for the library reference spectral feature. Note that the 4.25-μm absorption is not a CO_2 ice feature, which occurs at a slightly longer wavelength.

[143] The Mars Global Surveyor (MGS) is currently orbiting Mars with the Thermal Emission Spectrometer (TES), the first thermal infrared imaging spectrometer covering the range 6 to 50 μm with 143 or 286 channels [*Christensen et al.*, 1992, 1998]. MGS is currently in the mapping configuration and TES mapping most of Mars at ~3 km spatial resolution. Absorption bands in the thermal infrared have been used to map minerals on the martian surface similar to the mineral maps illustrated here, including hematite and olivine [*Christensen et al.*, 2000; *Clark and Hoefen*, 2000; *Hoefen and Clark*, 2001; *Hoefen et al.*, 2000]. Tetracorder mid-Infrared expert system rules are being developed for the TES investigation and will be reported in a future paper.

[144] The Cassini mission is currently on its way to Saturn with the Visual and Infrared Mapping Spectrometer (VIMS) covering the 0.4 to 5.1 μm range with 352 spectral channels. The VIMS has obtained data on Venus [*Baines et al.*, 2001] and recently flew by Jupiter where it obtained imaging spectroscopy data on Jupiter, its satellites, rings, and the Io Torus. VIMS will provide imaging spectroscopy coverage in the Saturn system adequate to allow surficial materials to be mapped on the satellites and rings of Saturn and atmospheric components in Saturn's atmosphere.

7. Discussion and Conclusions

[145] The Tetracorder materials identification system takes a spectroscopic approach to interpretation of imaging spectrometer data that was developed essentially to mimic the process a spectroscopist uses for spectral analysis but makes the process more quantitative and much more rapid. The performance of our system has been highly satisfactory to ourselves and our many sponsors, but there are clear areas for improvement in addition to the detailed deficiencies noted. One critical area is quantifying the detection limit for each material identified. To a degree this can be simulated and examined in the laboratory by creating mixtures or analyzing a large number of natural materials and mixtures. This, however, is a general research topic for the spectroscopic science community.

[146] For planetary science applications the system we have developed should be extremely useful when data in the visible and near-IR are returned from planned missions to Mars. Mars is expected to display considerable mineralogical diversity at high spatial resolution. The concepts we have put forth are more challenging to implement in the thermal IR because spectral signatures overlap more and vary in shape more due to grain size variations, but we have demonstrated that by employing a small number of key spectra Tetracorder can mitigate this shortcoming. Fortunately, linear mixing applies much more frequently at these wavelengths.

[147] In producing materials maps, robustness is vital. If a sensor is flown over the same site with minor changes to the instrument spectral sampling, spectral bandpass, and spatial resolution, the materials mapped should still be the same. If the sensor is flown over a geologically different region, but the same minerals exist as in other areas, those minerals should be similarly detected and accurately mapped. Such is

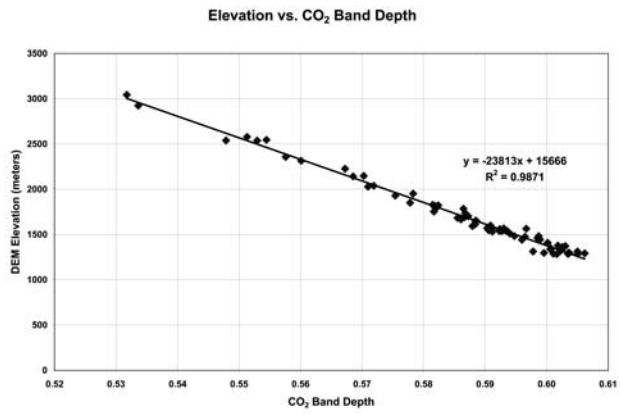

Figure 21. The 2-μm CO_2 absorption strength versus USGS DEM elevation shows a linear trend with an excellent least squares correlation coefficient.

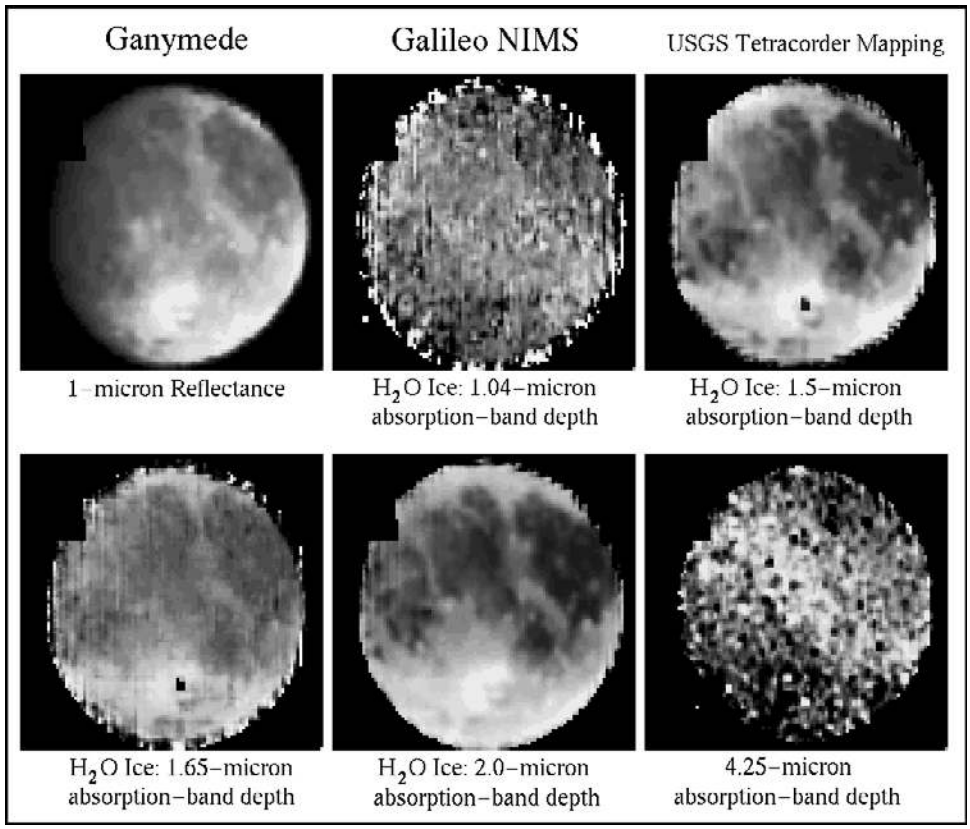

Figure 22. Galileo NIMS spectra of Ganymede were analyzed to show the locations of ice and CO_2 (the 4.25-micron image) that appears to be in fluid or gas inclusions in a yet unidentified mineral [*Carlson et al.*, 1996; *McCord et al.*, 1998]. The CO_2 has its greatest concentration on the equator, decreasing toward the poles. Tetracorder mapping used reference spectra from NIMS data of Jupiter's moon Ganymede, thus the material does not have to be a laboratory reference spectrum for use in Tetracorder.

not the case with some algorithms. Statistically based algorithms (e.g., linear unmixing or those in some commercial image processing packages) produce a different answer based on the input data and on how much the derived material map images are stretched [e.g., *Goetz and Kindel*, 1999; *Boardman*, 1999]. Tetracorder and our expert system rules are more robust because results are independent of spectral data in adjacent pixels.

[148] Consistency in mapped products is important, whether the spectra are of vegetation, minerals, liquid or solid water. The Turquoise Lake results are not a separate analysis over water but a standard part of the Tetracorder analysis using the same Tetracorder rules as those that mapped acid drainage in the Leadville area (Turquoise Lake and Leadville were covered by the same AVIRIS flight). Tetracorder analyzes each spectrum for water, snow, vegetation, minerals, or man-made materials. Diagnostic features and unique spectral characteristics, not statistical parameters, determine what is found. Thus Tetracorder found water and mapped the chlorophyll in the lake water only over Turquoise Lake. There is no masking of the data for land versus water; it uses a completely independent analysis to decide what is present in each pixel. It is the same case for the World Trade Center environmental assessment [*Clark et al.*, 2001]: Tetracorder mapped water versus land correctly and at the same time as asbestos, organics, and other materials. Tetracorder had no prior knowledge or limits as to where the water boundaries were located. The fact that Tetracorder produces robust materials maps that when field checked are correct, from locating water to locating subtle mineralogy in many different environments, attests to the robustness of the spectral analysis approach.

[149] The success of the algorithm relies on a spectral library for Tetracorder to make the correct decisions. We have developed a robust set of expert system rules that as of this writing, uses about 250 reference spectra to identify mineralogy, vegetation, water, ice and snow, environmental materials, and man-made materials. In the future we expect to be testing for hundreds more if not thousands of materials. A goal is to utilize Tetracorder and a refined expert system for mapping of other planetary surfaces equally well. The expert system has been designed with that use in mind, and it is possible to apply Tetracorder to identify spectra from anywhere in the solar system, whether laboratory data, field spectrometer data, aircraft imaging spectroscopy data, spacecraft imaging spectroscopy data, or telescopic spectra of other planets. It can also work with reflectance or emittance data in any wavelength region.

[150] Future enhancements to Tetracorder will include fuzzy logic to replace hard threshold levels and the addition of more algorithms, including unmixing codes that use answers from the first round identification analyses, temperature, and pressure constraints for application to other planets. Similar rules are being derived for the thermal

infrared spectral region to analyze Mars Global Surveyor Thermal Emission Spectrometer data, and a new midinfrared spectral library is in preparation. Galileo NIMS and Cassini VIMS include wavelengths to 5 μm, thus rules for that region are also being developed.

7.1. Availability

[151] Because of the complexity involved in spectroscopic analysis and the necessary sophistication of Tetracorder, expert knowledge of spectroscopy is important to successfully use this algorithm, especially when evaluating the results and when exploring for new materials not already in the expert system rules. The complete system, including source code, command files, and spectral libraries will be available on our web site at http://speclab.cr.usgs.gov.

[152] **Acknowledgments.** Development of the algorithms in this paper was funded by the NASA Planetary Geology and Geophysics program and the U.S. Geological Survey Mineral Resources Program. Early developments were funded by the NASA HIRIS team. Development of the concepts of Tetracorder spectral analysis has benefited from many days of field work by many scientists in many different geologic environments, researching why Tetracorder produced certain results. We have also benefitted from the AVIRIS workshops held at the Jet Propulsion Lab (JPL) and are indebted to Robert Green and the AVIRIS team at JPL. The advanced concepts have been difficult to describe and we are thankful to reviewers for their help in clarifying our paper. We are especially indebted to Paul Lucey, past JGR editor for extensive suggestions on improving the manuscript.

References

Ball, D. W., Defining terms, *Spectroscopy*, *10*, 16–18, 1995.

Boardman, J. W., Precision geocoding of low-altitude AVIRIS data: Lessons learned in 1998, in *Ninth Annual JPL Airborne Earth Science Workshop*, edited by R. O. Green, Jet Propul. Lab., Pasadena, Calif., 1999.

Carder, K. L., and R. G. Steward, A remote sensing reflectance model of a red tide dinoflagellate off West Florida, *Limnol. Oceanogr.*, *30*, 286–298, 1985.

Carder, K. L., P. Reinersman, R. F. Chen, F. Muller-Karger, C. O. Davis, and M. Hamilton, AVIRIS calibration and application in coastal oceanic environments, *Remote Sens. Environ.*, *44*, 205–216, 1993.

Carlson, R., et al., Near-infrared spectroscopy and spectral mapping of Jupiter and the Galilean satellites: First results from Galileo's initial orbit, *Science*, *274*, 385–388, 1996.

Clark, R. N., Spectroscopy of rocks and minerals and principles of spectroscopy, in *Manual of Remote Sensing*, edited by A. N. Rencz, pp. 3–58, John Wiley, New York, 1999.

Clark, R. N., and T. M. Hoefen, Spectral feature mapping with Mars Global Surveyor thermal emission spectra: Mineralogic implications, *Bull. Am. Astron. Soc.*, *32*, 1118, 2000.

Clark, R. N., and P. G. Lucey, Spectral properties of ice-particulate mixtures and implications for remote sensing. I: Intimate mixtures, *J. Geophys. Res.*, *89*, 6341–6348, 1984.

Clark, R. N., and T. L. Roush, Reflectance spectroscopy: Quantitative analysis techniques for remote sensing applications, *J. Geophys. Res.*, *89*, 6329–6340, 1984.

Clark, R. N., and G. A. Swayze, Mapping minerals, amorphous materials, environmental materials, vegetation, water, ice and snow, and other materials: The USGS Tricorder algorithm, in *Summaries of the Fifth Annual JPL Airborne Earth Science Workshop*, *JPL Publ. 95-1*, edited by R. O. Green, pp. 39–40, Jet Propul. Lab., Pasadena, Calif., 1995.

Clark, R. N., F. P. Fanale, and M. J. Gaffey, Surface composition of satellites, in *Natural Satellites*, edited by J. Burns and M. S. Matthews, 437 pp., Univ. of Arizona Press, Tucson, 1986.

Clark, R. N., T. V. V. King, M. Klejwa, G. Swayze, and N. Vergo, High spectral resolution reflectance spectroscopy of minerals, *J. Geophys Res.*, *95*, 12,653–12,680, 1990a.

Clark, R. N., A. J. Gallagher, and G. A. Swayze, Material absorption band depth mapping of imaging spectrometer data using a complete band shape least-squares fit with library reference spectra, in *Proceedings of the Second Airborne Visible/Infrared Imaging Spectrometer (AVIRIS) Workshop*, *JPL Publ. 90-54*, pp. 176–186, Jet Propul. Lab., Pasadena, Calif., 1990b.

Clark, R. N., G. A. Swayze, A. Gallagher, N. Gorelick, and F. Kruse, Mapping with imaging spectrometer data using the complete band shape least-squares algorithm simultaneously fit to multiple spectral features from multiple materials, in *Proceedings of the Third Airborne Visible/Infrared Imaging Spectrometer* (*AVIRIS*) *Workshop*, *JPL Publ. 91-28*, pp. 2–3, Jet Propul. Lab., Pasadena, Calif., 1991.

Clark, R. N., G. A. Swayze, and A. Gallagher, Mapping the mineralogy and lithology of Canyonlands, Utah with imaging spectrometer data and the multiple spectral feature mapping algorithm, in *Summaries of the Third Annual JPL Airborne Geosciences Workshop, Volume 1: AVIRIS Workshop*, *JPL Publ. 92-14*, pp. 11–13, Jet Propul. Lab., Pasadena, Calif., 1992a.

Clark, R. N., G. A. Swayze, C. Koch, A. Gallagher, and C. Ager, Mapping vegetation types with the multiple spectral feature mapping algorithm in both emission and absorption, in *Summaries of the Third Annual JPL Airborne Geosciences Workshop, Volume 1: AVIRIS Workshop*, *JPL Publ. 92-14*, pp. 60–62, Jet Propul. Lab., Pasadena, Calif., 1992b.

Clark, R. N., G. A. Swayze, A. Gallagher, T. V. V. King, and W. M. Calvin, The U.S. Geological Survey Digital Spectral Library: Version 1: 0.2 to 3.0 μm, *U.S. Geol. Surv. Open File Rep., 93-592*, 1340 pp., 1993a. (available at http://speclab.cr.usgs.gov)

Clark, R. N., G. A. Swayze, and A. Gallagher, Mapping minerals with imaging spectroscopy, *U.S. Geol. Surv. Off. Mineral Res. Bull.*, *2039*, 141–150, 1993b.

Clark, R. N., G. A. Swayze, K. Heidebrecht, A. F. H. Goetz, and R. O. Green, Comparison of methods for calibrating AVIRIS data to ground reflectance, in *Summaries of the Fourth Annual JPL Airborne Geosciences Workshop, Volume 1: AVIRIS Workshop*, *JPL Publ. 93-26*, pp. 31–34, Jet Propul. Lab., Pasadena, Calif., 1993c.

Clark, R. N., T. V. V. King, C. Ager, and G. A. Swayze, Initial vegetation species and senescence/stress mapping in the San Luis Calley, Colorado using imaging spectrometer data, in *Proceedings:Summitville Forum '95*, *Colorado Geol. Surv. Spec. Publ. 38*, edited by H. H. Posey, J. A. Pendelton, and D. Van Zyl, pp. 64–69, Colorado Geol. Surv., Denver, Colo., 1995a.

Clark, R. N., T. V. V. King, C. Ager, and G. A. Swayze, Initial vegetation species and senescence/stress mapping in the San Luis Calley, Colorado using imaging spectrometer data, in *Summaries of the Fifth Annual JPL Airborne Earth Science Workshop*, *JPL Publ. 95-1*, edited by R. O. Green, pp. 35–38, Jet Propul. Lab., Pasadena, Calif., 1995b.

Clark, R. N., et al., Environmental studies of the World Trade Center area after the September 11, 2001 attack, *U.S. Geol. Surv. Open File Rep., OFR-01-0429*, 2001. (available at http://speclab.cr.usgs.gov/wtc)

Christensen, P. R., et al., Thermal emission spectrometer experiment: Mars Observer mission, *J. Geophys. Res.*, *97*, 7719–7734, 1992.

Christensen, P. R., et al., Initial results from the Mars Global Surveyor Thermal Emission Spectrometer investigation, *Science*, *279*, 1692–1698, 1998.

Christensen, P. R., et al., Detection of crystalline hematite mineralization on Mars by the Thermal Emission Spectrometer: Evidence for near-surface water, *J. Geophys. Res.*, *105*, 9623–9644, 2000.

Doelling, H. H., Geologic map of Arches National Park and vicinity, Grand County, Utah, *Map 74*, Utah Geol. and Mineral. Surv., Salt Lake City, Utah, 1985.

Farmer, J. D., Hydrothermal systems on Mars: An assessment of present evidence, in *Evolution of Hydrothermal Ecosystems on Earth* (*and Mars?*), edited by G. R. Beck and J. A. Goode, pp. 273–299, John Wiley, New York, 1996.

Farmer, V. C., (Ed.), *The Infra-Red Spectra of Minerals*, 539 pp., Mineral. Soc., London, 1974.

Goetz, A. F. H., and B. Kindel, Comparison of unmixing results derived from AVIRIS, high and low resolution, and HYDICE images at Cuprite, NV, in *Ninth Annual JPL Airborne Earth Science Workshop*, edited by R. O. Green, Jet Propul. Lab., Pasadena, Calif., 1999.

Goetz, A. F., G. Vane, J. E. Soloman, and B. N. Rock, Imaging spectrometry for Earth remote sensing, *Science*, *228*, 1147, 1985.

Green, R. O., D. A. Roberts, and J. A. Conel, Characterization and compensation of the atmosphere for the inversion of AVIRIS calibrated radiance to apparent surface reflectance, in *Summaries of the Sixth Annual JPL Airborne Earth Science Workshop*, *JPL Publ. 96-4*, 135 pp., 1996.

Hoefen, T. M., and R. N. Clark, Compositional variability of Martian olivines using Mars Global Surveyor Thermal Emission Spectra (abstract 2049) [CD-Rom], *Lunar Planet. Sci.*, *32*, 2001.

Hoefen, T. M., R. N. Clark, J. C. Pearl, and M. D. Smith, Unique spectral features in Mars Global Surveyor Thermal Emission Spectra: Implications for surface mineralogy in Nili Fossae, *Bull. Am. Astron. Soc.*, *32*, 1118, 2000.

Hunt, G. R., Spectral signatures of particulate minerals, in the visible and near-infrared, *Geophysics*, *42*, 501–513, 1977.

Huntoon, P. W., G. H. Billingsley Jr., and W. J. Breed, Geologic map of Canyonlands National Park and vicinity, Utah, Canyonlands Nat. Hist. Assoc., Moab, Utah, 1982.

King, T. V. V., and R. N. Clark, Verification of remotely sensed data, in *Remote Sensing for Site Characterization, Methods in Environmental Geography*, edited by F. Kuehn et al., pp. 59–62, Springer-Verlag, New York, 2000.

King, T. V. V., R. N. Clark, C. Ager, and G. A. Swayze, Remote mineral mapping using AVIRIS data at Summitville, Colorado and the adjacent San Juan Mountains, in *Proceedings: Summitville Forum '95*, edited by H. H. Posey, J. A. Pendelton, and D. Van Zyl, *Colorado Geol. Surv. Spec. Publ., 38*, 59–63, 1995a.

King, T. V. V., et al., Environmental considerations of active and adandoned mine lands-Lessons from Summitville, Colorado, *U.S. Geol. Surv. Bull.*, *2220*, 38 pp., 1995b.

King, T. V. V., R. N. Clark, and G. A. Swayze, Application of imaging spectroscopy data: A case study at Summitville, Colorado, in *Remote Sensing for Site Characterization, Methods in Environmental Geology*, edited by F. Kuehn et al., pp. 164–185, Springer-Verlag, NewYork, 2000.

Kokaly, R. F., R. N. Clark, and K. E. Livo, Mapping the biology and mineralogy of Yellowstone National Park using imaging spectroscopy, in *Summaries of the 7th Annual JPL Airborne Earth Science Workshop*, *JPL Publ. 97-21*, edited by R. O. Green, pp. 235–244, Jet Propul. Lab, Pasadena, Calif., 1998.

Kokaly, R. F., D. G. Despain, R. N. Clark, and K. E. Livo, Mapping vegetation in Yellowstone National Park using spectral feature analysis of AVIRIS data, *Remote Sens. Environ.*, *84*, 437–456, 2003.

Livo, K. E., R. N. Clark, F. A. Kruse, and R. F. Kokaly, Characterization of hydrothermally altered rock and hot spring deposits at Yellowstone National Park using AVIRIS data, in *Summaries of the Eighth JPL Airborne Earth Science Workshop*, *JPL Publ. 99-17*, edited by R. O. Green, pp. 259–266, Jet Propul. Lab., Pasadena, Calif., 1999.

Livo, K. E., R. N. Clark, R. F. Kokaly, and F. A. Kruse, Distribution of hydrothermal mineralization and altered rock at Yellowstone National Park, paper presented at the Fourteenth International Conference and Workshops on Applied Geologic Remote Sensing, Environ. Res. Inst. of Michigan, Las Vegas, Nevada, 6–8 November 2000.

Lucey, P. G., and R. N. Clark, Spectral properties of water ice and contaminants, in *Ices in the Solar System*, edited by J. Klinger et al., pp. 155–168, D. Reidel, Norwell, Mass., 1985.

McCord, T. B., et al., Non-water-ice constituents in the surface material of the icy Galilean satellites from the Galileo Near-Infrared Mapping Spectrometer investigation, *J. Geophys. Res.*, *103*, 8603–8626, 1998.

Mustard, J. F., M. L. Staid, and W. Fripp, Atmospheric correction and inverse modeling of AVIRIS data to obtain water constituent abundances, in *Summaries of the Eighth Annual JPL Airborne Earth Science Workshop*, *JPL Publ. 99-17*, edited by R. O. Green, pp. 309–315, Jet Propul. Lab., Pasadena, Calif., 1999.

Pearson, R. M., Environmental geology of operable unit 6 removal action design data California gulch superfund site Leadville, Colorado, U.S. Bureau of Reclamation Rep., Washington, D. C., 1997.

Pieters, C. M., and P. A. Englert, *Remote Geochemical Analysis: Elemental and Mineralogical Composition*, 594 pp., Cambridge Univ. Press, New York, 1993.

Rencz, A. N., *Manual of Remote Sensing*, 707 pp., John Wiley, New York, 1999.

Shock, E. L., Hydrothermal systems as an environment for the emergence of life, in *Evolution of Hydrothermal Ecosystems on Earth* (*and Mars?*), edited by G. R. Beck and J. A. Goode, pp. 40–60, John Wiley, New York, 1996.

Swayze, G. A., The hydrothermal and structural history of the Cuprite mining district, southwestern Nevada: An integrated geological and geophysical approach, Ph.D. thesis, 399 pp., Univ. of Colorado, Boulder, Colo., 1997.

Swayze, G. A., and R. N. Clark, Spectral identification of minerals using imaging spectrometry data: evaluating the effects of signal to noise and spectral resolution using the Tricorder algorithm, in *Summaries of the Fifth Annual JPL Airborne Earth Science Workshop*, *JPL Publ. 95-1*, edited by R. O. Green, pp. 157–158, Jet Propul. Lab., Pasadena, Calif., 1995.

Swayze, G. A., R. N. Clark, S. Sutley, and A. Gallagher, Ground-truthing AVIRIS mineral mapping at Cuprite, Nevada, in *Summaries of the Third Annual JPL Airborne Geosciences Workshop, Volume 1: AVIRIS Workshop*, *JPL Publ. 92-14*, pp. 47–49, Jet Propul. Lab., Pasadena, Calif., 1992.

Swayze, G. A., R. N. Clark, R. M. Pearson, and K. E. Livo, Mapping acid-generating minerals at the California gulch superfund site in Leadville, Colorado using imaging spectroscopy, in *Summaries of the 6th Annual JPL Airborne Earth Science Workshop*, JPL Publ. 96-4, edited by R. O. Green, pp. 231–234, Jet Propul. Lab., Pasadena, Calif., 1996.

Swayze, G. A., et al., Using imaging spectroscopy to map acidic mine waste, *Environ. Sci. Technol.*, *34*, 47–54, 2000.

Swayze, G. A., et al., Effects of spectrometer band pass, sampling, and signal-to-noise ratio on spectral identification using the Tetracorder algorithm, *J. Geophys. Res.*, *108*, doi:10.1029/2002JE001975, in press, 2003.

U.S. Environmental Protection Agency, Advanced Measurement Initiative Workshop Report, *EPA-235-R-98-002*, 22 pp., Washington, D.C., 1998.

R. N. Clark, J. B. Dalton, C. Gent, R. F. Kokaly, K. E. Livo, R. McDougal, S. Sutley, and G. A. Swayze, U. S. Geological Survey, Denver Federal Center, Denver, CO 80225, USA. (rclark@usgs.gov; Dalton@mail.arc.nasa.gov; Raymond@usgs.gov; elivo@usgs.gov; rmcdouga@usgs.gov; ssutley@usgs.gov; gswayze@usgs.gov)